

## ABSTRACT

Title of Document: Tissue and Metabolic Engineering of Biohybrid Artificial Organs  
Chong Wing Yung, Doctor of Philosophy, 2005

Directed By: Professor, Timothy A. Barbari, Department of Chemical and Biomolecular Engineering

In an effort to develop a biohybrid artificial organ, mammalian cells were engineered with several properties to make them adept in secreting therapeutic proteins and surviving low oxygen levels in an encapsulated environment. Three cell lines, C2C12, Jurkat, and HEK293, were investigated for their ability to secrete human interleukin 2 (hIL2), which can serve as an anti-cancer agent. An intracellular fluorescent protein marker was independently expressed using an internal ribosome entry site sequence so that hIL2 remained active and free for secretion. DsRed fluorescent protein markers were used since red light is known to be transmissible through mammalian tissue. Transient transfection of all three cell lines proved that internal red fluorescence measurements were indeed linearly correlated with the concentration of hIL2 secreted. To increase the survivability of encapsulated cultures, cells were engineered with an anti-apoptotic gene, *bcl-2 $\Delta$* , placed under the control of a hypoxia sensitive promoter. This protective system was found to lessen both hypoxia induced necrosis and apoptosis. To complete the biohybrid system, a

novel hydrogel (mTG-Gel), utilizing microbial transglutaminase (mTG) to enzymatically crosslink gelatin, was developed as a biocompatible cellular scaffold for encapsulating the engineered cells. These gels were stable at physiological temperature (37 °C) and could be tailored for enzymatic stability. Specifically, HEK293 cells that were metabolically engineered with all the previous characteristics were encapsulated in 4% mTG-Gels. *In situ* analysis of DsRed fluorescence showed that cells overlaid with mTG-Gel exhibited reductions in fluorescence with increasing height of gel. Human IL2 diffusion through the hydrogel into overlaying media was found to exhibit the expected dependence on the square of the gel thickness. Diffusion cells were used to determine an effective diffusion coefficient for hIL2, which compared well to that obtained from the gel-overlay cell culture experiments.

TISSUE AND METABOLIC ENGINEERING OF  
BIOHYBRID ARTIFICIAL ORGANS

By

Chong Wing Yung

Dissertation submitted to the Faculty of the Graduate School of the  
University of Maryland, College Park, in partial fulfillment  
of the requirements for the degree of  
Doctor of Philosophy  
2005

Advisory Committee:  
Professor Timothy A. Barbari, Chair  
Professor William E. Bentley  
Professor William A. Weigand  
Associate Professor Peter Kofinas  
Professor Siba K. Samal

© Copyright by  
Chong Wing Yung  
2005

## **Dedication**

I dedicate the culmination of my learning to my parents:  
Ying Kwan Yung and Li Tsuin Hong Yung

## **Acknowledgements**

I would like to acknowledge all the friends that I have grown to love and respect at the University of Maryland. Thank you for all the wonderful intellectual discussions about life and science. I cherish your friendships, and for these I feel that I am not alone.

I would like to give thanks to my advisors, Tim Barbari and Bill Bentley, for their dedication to my research and development of my intellectual spirit. You have taught me the meanings of scientific rigor, patience, and humility. I am honored to be your student.

Finally, I would like to give thanks to my sisters and parents for their continual support and encouragement throughout my life. You have filled me with goodness and confidence, and are the foundation of my achievements. There are no words to express my fortune to be in this family.

## Table of Contents

1. Introduction .....	1
1.1 Research Motivation .....	1
1.2 Eukaryotic Protein Expression System .....	4
1.2.1 Transcriptional Regulations .....	4
1.2.2 Translation of mRNA .....	4
1.2.3 Monocistronic vs. Polycistronic Translation .....	5
1.2.4 Internal Ribosome Binding Site (IRES) Bicistronic System .....	5
1.2.5 Antibiotic Resistance and Cell Selection: .....	5
1.2.6 Secreteable Protein Processing [37] .....	6
1.2.6.1 Sorting Signals and the Endoplasmic Reticulum .....	6
1.2.6.2 Glycosylation and Post-Translational Modification .....	7
1.3 Fluorescent Protein Markers .....	8
1.3.1 Green Fluorescent Protein (GFP) .....	9
1.3.1.1 Biochemical and Physical Properties .....	9
1.3.1.2 GFP Variants for Mammalian Applications .....	10
1.3.2 New Red Fluorescent Protein (RFP) Markers .....	12
1.3.2.1 DsRed – <i>Discosoma</i> sp (sea coral) .....	12
1.3.2.2 HcRed – <i>Heteractis crispa</i> (sea anemone) .....	14
1.4 Biohybrid Artificial Organs .....	14
1.4.1 Cell Source .....	15
1.4.2 Molecular Diffusion and Device Design .....	15
1.4.3 Immuno-Protection .....	18
1.5 Hypoxia .....	20
1.5.1 Mammalian Oxygen Homeostasis .....	20
1.5.2 Molecular Biochemistry .....	21
1.5.3 Normal Physiological Causes .....	22
1.5.4 Conditions in Encapsulation that Cause Hypoxia .....	22
1.5.5 Hypoxia-Induced Cell Death and Bcl-2 $\Delta$ Protection .....	23
1.6 Cell Lines .....	24
1.6.1 C2C12 .....	24
1.6.2 HEK293 .....	24
1.6.3 Jurkat .....	25
1.7 Human Interleukin 2 (hIL2) .....	25
1.8 Cellular Scaffolds and Gelatin Hydrogels .....	26
2. Integrated Non-Invasive System for Quantifying Secreted Human Therapeutic hIL2 .....	28
2.1 Introduction .....	28
2.2 Materials and Methods .....	29
2.2.1 Cell Culture - Passaging and Maintenance .....	29
2.2.2 Vector Constructs .....	30
2.2.3 Transfections .....	33
2.2.4 ELISA .....	34
2.2.5 Flow Cytometry .....	34

2.2.6	Fluorescence Microscopy .....	36
2.3	Results and Discussion .....	37
2.3.1	Correlating DsExDR with Intracellular hIL2 .....	37
2.3.2	Correlating DsExDR with Secreted hIL2 from Attachment Cells .....	39
2.3.3	Correlating DsExDR with Secreted hIL2 from Suspension Cells .....	40
2.3.4	Examining IRES – mediated Co-expression of DsExDR and hIL2 Proteins .....	41
2.4	Conclusions .....	45
2.5	Acknowledgements .....	46
3.	Counteracting Apoptosis and Necrosis with Hypoxia Responsive Expression of Bcl-2 $\Delta$ .....	47
3.1	Introduction .....	47
3.2	Materials and Methods .....	49
3.2.1	Cell Culture Media and Maintenance .....	49
3.2.2	Construction of Recombinant Plasmids .....	49
3.2.3	Transfections .....	52
3.2.4	Hypoxic Chambers .....	53
3.2.5	Flow Cytometry of EYFP Recombinant Proteins .....	55
3.2.6	Viability Assay .....	55
3.2.7	Apoptosis Assay .....	56
3.2.8	Fluorescence Microscopy .....	57
3.3	Results and Discussion .....	57
3.3.1	Differential Hypoxic Induction of Protein Production .....	57
3.3.2	Transient Expression of Heterologous Proteins under Hypoxic Condition .....	61
3.3.3	Bcl-2 $\Delta$ Protection of Cells under Hypoxic Stress .....	63
3.4	Conclusions .....	64
3.5	Acknowledgements .....	65
4.	Biocompatible Cellular Scaffold for Encapsulating Cells .....	67
4.1	Introduction .....	67
4.2	Materials and Methods .....	69
4.2.1	Maintenance of Cell Cultures .....	69
4.2.2	Cell Encapsulation and Culture .....	69
4.2.3	In Situ Cell Proliferation Assay .....	70
4.3	Results and Discussion .....	71
4.4	Conclusions .....	75
5.	Transglutaminase Crosslinked Gelatin Hydrogels as Tissue Engineering Scaffolds .....	76
5.1	Introduction .....	76
5.2	Material and Methods .....	76
5.2.1	Transglutaminase Crosslinked Gelatin Hydrogels .....	76
5.2.2	Thermal and Proteolytic Degradation of mTG Crosslinked Hydrogels .....	77
5.3	Results and Discussion .....	78



5.3.1	Thermal and Proteolytic Stability of mTG-Gels.....	78
5.3.2	Tuneable Degradability of HybriGels.....	81
5.4	Conclusions.....	85
6.	Diffusion of hIL2 from Encapsulated Cells.....	87
6.1	Introduction.....	87
6.2	Materials and Methods.....	88
6.2.1	Maintenance of Cell Cultures.....	88
6.2.2	mTG-Gel Formation.....	88
6.2.3	Plasmid Constructs.....	89
6.2.4	Cell Transfection and Encapsulation.....	91
6.2.5	Fluorescence Microscopy and ELISA.....	93
6.2.6	Diffusion Cell Experiments.....	94
6.3	Results and Discussion.....	97
6.3.1	Therapeutic Protein Secretion by Encapsulated HEK293.....	97
6.3.2	Mathematical Modeling of hIL2 Release.....	103
6.3.3	Obtaining the Fluxes and Diffusion Coefficient of hIL2 Secreted by HEK293.....	106
6.3.4	Measuring Diffusion Coefficient of hIL2 in mTG-Gel.....	111
6.4	Conclusions.....	112
7.	Summary.....	113
7.1	Integrated Non-Invasive System for Quantifying Secreted Human Therapeutic hIL2.....	113
7.2	Counteracting Apoptosis and Necrosis with Hypoxia Responsive Expression of Bcl-2 $\Delta$ .....	114
7.3	Biocompatible Cellular Scaffold for Encapsulating Cells.....	115
7.4	Transglutaminase Crosslinked Gelatin Hydrogels as Tissue Engineering Scaffolds.....	115
7.5	Diffusion of hIL2 from Encapsulated Cells.....	116
8.	Bibliography.....	117

## List of Tables

Table 1.1	Spectroscopic properties of fluorescent proteins. ....	13
Table 3.1	Transfection Protocol for C2C12 in 6- and 12-well tissue culture plates. ....	53
Table 5.1	Thermal and enzymatic degradation rates for various forms of hydrogels.....	82
Table 6.1	hIL2 flux determined from the thinnest overlay (0.16 cm) must be rescaled by the level of DsExDR fluorescence found in the thicker overlays.....	110

## List of Figures

Figure 1.1	Three dimensional representation of $\beta$ -can and $\alpha$ -helix structure of GFP.....	10
Figure 1.2	Excitation (A) and emission (B) spectra of fluorescent proteins.....	13
Figure 1.3	Rate of insulin secretion as a function of oxygen partial pressure in perfused rat islets [56].....	16
Figure 1.4	Oxygen penetration profiles for spheres (A) and slab (B) of various diameters [56].....	17
Figure 1.5	Oxygen penetration profiles for spheres (A) and slabs (B) surrounded by an avascular diffusion barrier [56].....	18
Figure 1.6	Cellular and humoral immune responses experienced by implanted cells.....	19
Figure 2.1	The bicistronic vector, pF2, contains an internal ribosome entry site (IRES) gene sequence, which allows for the independent production of secretable hIL2 and DsExDR red fluorescent marker proteins.....	32
Figure 2.2	Destabilized DsRed-Express fluorescence in mammalian cells was measured using a FACS Calibur flow cytometer (FSC = 1.00, SSC = 394, FL2 = 683 for Jurkat cells and FSC = 0.485, SSC = 288 and FL2 = 538 for HEK293 and C2C12 cells). Histograms were obtained only after gating live cells from dead ones using a FSC-SSC dot plot within 10,000 cell samples.....	36
Figure 2.3	HEK293 and C2C12 attachment cells were transfected with pF2 (0, 0.2, 0.5, 0.8, 1.2, 1.6, and 2.0 mg-DNA per $2 \times 10^5$ cells) for the bicistronic expression of Destabilized DsRed-Express (DsExDR) red fluorescent protein and secretion of human interleukin-2 (hIL2). Both cell lines secreted large amounts of hIL2 on the order of nanograms per million cells (A, D). The presence of hIL2 within HEK293 cells was also measured. These cells lines were able to express similar quantities of the intracellular red fluorescent protein (B, E). The elevated concentration of DsExDR at the highest levels of transfection resulted in decreases of fluorescence measurements in both cell lines. This was indicative of self-quenching. Strong linear correlations between the two proteins were observed in both cell lines when the last data points were omitted (C, F). A linear correlation of DsExDR with intracellular hIL2 was also present in HEK293 cells. Jurkat cells were transfected with five higher concentrations of the bicistronic plasmid pF2 (1.1, 1.7, 2.6, 3.4, and 5.1 mg-DNA per $2 \times 10^5$ cells). This cell line secreted hIL2 concentrations that were three orders of magnitude lower than the previous cells (G). This may be due to two factors	

	that are inherent to Jurkat cells. The first is the notoriously low transfection efficiency of this line, evident by observation under fluorescence microscopy and the lack of DsExDR self-quenching at the highest pF2 transfection level (H). The second is the presence of natural regulatory mechanisms for controlling the secretion of hIL2, which is an intrinsic product of T-cells. A linear correlation was found among all concentrations of secreted hIL2 and DsExDR fluorescence in Jurkat cells (I). .....	38
Figure 2.4	The functionality of using the IRES bicistronic expression system among the three cell lines (Jurkat, C2C12, and HEK293) can be compared by plotting the expression of DsExDR and secretion of hIL2, each normalized by the respective data point at which the recommended transfection level was made (Jurkat = 1.1 mg, C2C12 & HEK293 = 0.8 mg). A slope of unity indicates that both proteins are accumulating at equal rates. Jurkat cells have the most balanced accumulation rate, while C2C12 and HEK293 cells accumulated slightly more fluorescent protein per hIL2 secreted. ....	42
Figure 3.1	The hypoxic incubation system is composed of individual hypoxic chambers placed upon a rocker platform within a CO <sub>2</sub> incubator. Each chamber is connected to its own gas tank via a bubble column, which humidifies and warms the incoming air. The gas environment within each chamber is determined by the premixed composition of the compressed gas cylinders. Mix gas flows at 0.5 L/min. The chambers and bubble columns are each 1L in volume. Dissolve oxygen content in tissue cultures plates with 1mL of media is monitor by a Clark-type dissolved oxygen probe and OM4 Oxygen Meter (Microelectrodes).....	54
Figure 3.2	Kinetic measurements of dissolved oxygen content within a 1mL mock culture were made to ensure that cells were exposed to the intended hypoxic environments. A 0 % O <sub>2</sub> gas mixture was directed into a rocking hypoxic chamber (0.5 L/min, 37 oC), which contained the mock culture. Steady state was reached in approximately 1 hour. ....	54
Figure 3.3	C2C12 cells transfected with pO2Ybp and p5HRE-d2EGFP were compared for their ability to hypoxically induce fluorescent protein production. Cells were exposed to five oxygen concentrations (0.0, 0.5, 1.0, 2.0, 5.0, 21.0 %) and assayed after an 18 hour incubation. C2C12 cultures transfected with pO2Ybp produced enhance yellow fluorescent protein (EYFP) in a similar fashion to those transfected with p5HRE-d2EGFP produced destabilized enhance green fluorescent protein (d2EGFP). EYFP	

	fluorescence, however, was higher than EGFP at every O <sub>2</sub> concentration. This is most likely due to the short, 2-hour half-life of the destabilized EGFP. Both transfections indicated that a decrease in O <sub>2</sub> content is able to exponentially induce fluorescence. ....	58
Figure 3.4	C2C12 cells were transfected with either pCYp, pCYbp, pO2Yp, or pO2Ybp expression vectors and incubated for 30 hrs under various hypoxic conditions (0.0, 0.5, 1.0, 2.0, 5.0, or 21.0 % O <sub>2</sub> plus 5% CO <sub>2</sub> , and a balance of N <sub>2</sub> ) beginning at 24 hours post-transfection (hpt). Cells that were transfected with the hypoxia sensitive promoters showed increased fluorescence with a decrease in O <sub>2</sub> concentration. Cells that contained the CMV promoter, however, displayed an opposite trend despite their overall higher levels of fluorescence at all oxygen concentrations. This decrease in fluorescence was indicative of metabolic stress due to hypoxia. In all C2C12 culture, it was clear that the presence of Bcl-2Δ was helpful to the cells' protein production capabilities. ....	60
Figure 3.5	C2C12 cells were transfected with either pCYp, pCYbp, pO2Yp, or pO2Ybp expression vectors and monitored for 24 hrs when grown under a 2% O <sub>2</sub> hypoxic environment beginning at 24 hpt. All transfections, besides pO2Yp, showed an increase in EYFP fluorescence within the 24 hours. Although this phenomenon was expected for cells containing hypoxia inducible promoters, those without were apparently unencumbered within the exposure period. All myoblasts that were able to express Bcl-2Δ were able to produce more EYFP than their deficient counterparts. This indicated the production advantage of having the anti-apoptotic protein. Myoblasts that were transfected with pO2Yp, had neither the <i>bcl-2Δ</i> gene, nor the brute capability of the CMV promoter, and thus lagged in EYFP production as time progressed.....	62
Figure 3.6	The protective nature of Bcl-2Δ against hypoxia can be more accurately accessed through measurements of necrosis and apoptosis in the host. C2C12 cells that were transfected with either pO2Ybp and pO2Yp were exposed to five hypoxic environments (0.0, 0.5, 1.0, 2.0, 5.0, or 21.0 % O <sub>2</sub> plus 5% CO <sub>2</sub> , balance N <sub>2</sub> ) for 30 hours beginning at 24 hpt. Myoblasts that were able to express Bcl-2Δ were able to sustain both a higher level of viability, as well as lowered levels of apoptosis. Thus, Bcl-2Δ was successful in not only enhancing protein production, but also the long term health of the host cells under hypoxic stress. ....	64

Figure 4.1	In situ monitoring of proliferation for gelatin encapsulated cells was attempted with both SYTO-16 and Hoechst 33342 nucleic acid dyes. SYTO-16 staining produced a non-linear relationship, while Hoechst 33342 staining generated a linear correlation of $5.05 \times 10^5$ cells/RFU ( $r^2 = 0.98$ ). This calibration curve was generated from HEK293 cells encapsulated in 60 $\mu$ L of 4% mTG-Gel in 96-well plate using a 4 hr incubation period. ....	71
Figure 4.2	HEK293 cells (2,000 cells/well) were encapsulated in the mTG crosslinked gelatin hydrogels (60 $\mu$ L/well) were initially seeded into 96-well plates with white walls and clear bottoms. Hoechst 33342 staining (4 hr incubation) showed that encapsulated cells were growing in clusters, and proliferating at a linear rate of approximately $0.03 \text{ day}^{-1}$ ( $r^2 = 0.95$ ). ....	72
Figure 4.3	HEK293 cells stained with Hoechst 33342 nuclear dye can be seen proliferating while they are encapsulated in mTG crosslinked gelatin hydrogels. Cells formed spherical clusters and proliferated linearly with time. ....	72
Figure 4.4	Encapsulated HEK293 cells were released by masticating the mTG-Gels followed by a 20 minute incubation with a 0.25% Trypsin + 0.03% EDTA solution at 37 oC. Released cells appeared as clusters (A), as well as singlets (B). Both of these forms of released cells were able to re-attach to tissue culture plates under normal incubation conditions (37 oC, 8% CO <sub>2</sub> ).....	74
Figure 5.1	Exposure of the three hydrogels (T-Gel, mTG-Gel, and HybriGel) in a 37 °C bath of DPBS showed that only the uncrosslinked T-Gel was susceptible to thermal degradation.....	78
Figure 5.2	Although 4% mTG-Gels were thermally stable, they were slightly less resistant to proteolysis by trypsin. HybriGels were developed by first thermally cooling gelatin and then crosslinking with a 10% mTG overlay. The resultant hydrogel was both thermally stable and as proteolytically resistant as the T-Gels.....	79
Figure 5.3	Gelatin hydrogels formed with initial cooling, to create a physical gel, before crosslinking with mTG were found to be consistently more resistant to proteolysis as compared to hydrogels that were crosslinked before cooling (mTG-Gels). An explanation may be that thermal cooling allows gelatin to first self-organize into a tight network of polypeptides through hydrogen bonding. Once gelatin has formed this network, there are more potential junction points where crosslinking can occur, creating a denser permanent hydrogel. mTG-Gels, however, were unable to form this tight network since mTG is immediately crosslinking gelatin	

	polypeptides. The result is a less tightly packed hydrogel with a larger mesh size, which may be more susceptible to proteolytic attack.....	80
Figure 5.4	The proteolytic degradation rate of HybriGels was found to be adjustable based on the amount of gelatin in the hydrogel (4, 10, 15, and 25%). A disproportionate drop in degradation rate between 4% and 10% HybriGels may indicate that below a critical mesh size the trypsin may be limited to the surface of denser gels. ....	83
Figure 5.5	A study to elucidate the mechanism by which trypsin degrades 10% HybriGels. Proteolysis occurs mainly by surface erosion. ....	84
Figure 5.6	Swelling studies were done to determine how proteolytic degradation rates would be affected by water content. 10% and 15% HybriGels that were pre-soaked in DPBS overnight (*) were found to be more susceptible than their non-soaked counterparts.....	85
Figure 6.1	Transient DsRed fluorescence in HEK293 cells transfected with the pF2 expression vector, and overlaid with three mTG-Gel thicknesses.....	98
Figure 6.2	Transient DsRed fluorescence in HEK293 cells transfected with the pF3 expression vector, and overlaid with three mTG-Gel thicknesses.....	98
Figure 6.3	HEK293 cells were transfected with the pF2 expression vector, and overlaid with three mTG-Gel thicknesses. hIL2 was measured in the media that was covering the mTG-Gel overlays. Rates have units of ng/hr-10 <sup>6</sup> cells.....	101
Figure 6.4	HEK293 cells were transfected with the pF2 expression vector, and overlaid with three mTG-Gel thicknesses. hIL2 was measured in the media that was covering the mTG-Gel overlays. Rates have units of ng/hr-10 <sup>6</sup> cells.....	101
Figure 6.5	HEK293 cells were transfected with the pF3 expression vector, and overlaid with three mTG-Gel thicknesses. HIL2 was measured in the media that was covering the mTG-Gel overlays. Rates have units of ng/hr-10 <sup>6</sup> cells. ....	102
Figure 6.6	HEK293 cells were transfected with the pF3 expression vector, and overlaid with three mTG-Gel thicknesses. HIL2 was measured in the media that was covering the mTG-Gel overlays. Rates have units of ng/hr-10 <sup>6</sup> cells. ....	102
Figure 6.7	Normalized hIL2 accumulation and time were plotted to reveal a transition from transient to steady state diffusion of hIL2. An analysis of the steady state flux, indicated by the linear regression (circled points) shows that HEK293 transfected with pF2 were producing hIL2 at a rate of 0.94 pg/cm <sup>2</sup> hr. ....	108

Figure 6.8	Analysis of the steady state flux (circled points), show that HEK293 cells transfected with pF3 were producing hIL2 at double the rate (1.83 pg/cm <sup>2</sup> hr) of cells transfected with pF2. ....	108
Figure 6.9	Comparison of data with simulated hIL2 accumulation using diffusion coefficients obtained from steady state analysis and fluxes scaled by DsExDR fluorescence for each overlay thickness.....	110
Figure 6.10	Well inserts filled with three thicknesses of 4% mTG-Gels were used as diffusion cells to measure the diffusion coefficient of hIL2. ....	112



# 1. Introduction

## 1.1 Research Motivation

Biohybrid artificial organs combine the usage of living cells along with synthetic materials for the treatment of serious and chronic human ailments. Encapsulation therapy has already been used for treating several human diseases, including chronic pain [1] and Amyotrophic Lateral Sclerosis (ALS) or Lou Gehrig's disease [2]. In order to further expand the application of this technology, however, several technical challenges must yet be surmounted. The objectives of this research are to address three major challenges found in creating a viable biohybrid artificial organ: (i) Design an *in situ* method for detecting therapeutic proteins secreted from encapsulated engineered cells; (ii) Lessen the level of necrosis and apoptosis induced by hypoxia, and (iii) Develop a biocompatible cellular scaffold and encapsulation material for the metabolically engineered cells.

To explore the first of these considerations, cells will be engineered to secrete human interleukin-2 (hIL2), as a model therapeutic protein. hIL2 is a polypeptide hormone and is a natural component of the body's immune system. This molecule normally functions to simulate the differentiation of enhanced cytotoxic cells, which have been shown to be effective in fighting cancer and AIDS. In order to gauge how reliably hIL2 can be secreted in an encapsulated device, it may also be important to have an indicator for tracing its production. The indicator, however, should be self-contained, as well as detectable even when the device is implanted subdermally. To address this issue, the usage of a self-fluorescing protein marker may be an ideal candidate for tracing therapeutic protein production and secretion. DsRed is one of

such proteins, and is unique in that it emits red fluorescent light, which is translucent through tissues. Thus, the co-expression of DsRed may provide a self-sufficient, and yet non-invasive means, for detecting hIL2 production in a transplanted device.

The second challenge that will be studied is the issue of inadequate oxygen supplies inside a biohybrid artificial organ. This problem is especially critical for devices that may be implanted for months and ideally, years, while cells can tolerate deficient oxygen levels for only a few days at best. When the metabolic demand of oxygen exceeds levels that are available, cells experience a physiological state known as hypoxia, which has been shown to diminish engineered therapeutic protein production and cell viability. Several extracellular approaches that focus on increasing the flux of oxygen have been taken to mitigate this issue in biohybrid organs. Strategies include inducing vascularization around the implant [3], electrochemically generating oxygen by decomposing water around the membrane [4], as well as using synthetic oxygen carriers [5, 6].

An alternative approach of counteracting hypoxia is to obstruct apoptosis and necrosis signaling pathways, which are used to induce cell death. Bcl-2 $\Delta$  is an anti-apoptotic agent, which has been shown to enhance a cell's resistance to both hypoxia-induced apoptosis and necrosis [7-9]. Encapsulated cells that are producing hIL2 can also be engineered to produce this protein as a protective agent against hypoxia. Furthermore, the *bcl-2 $\Delta$*  gene can be designed to be expressed only under low oxygen conditions. This functionality can be achieved by placing the gene under the control of a hypoxia sensitive promoter [10, 11]. In analogy to the production of the model therapeutic protein, a yellow fluorescent marker can be expressed for indicating the

level of Bcl-2 $\Delta$  production and indirectly, the oxygen concentration experienced by the encapsulated cells.

The third challenge of this work is to develop a biomaterial that can serve as a cellular scaffold, as well as a substance for encapsulating the engineered cells. For this purpose, gelatin was selected as the foundational biomaterial due to its native role as the major building block of extracellular matrices [12-14]. Using gelatin offers a high biocompatibility towards encapsulated cells and host tissue alike, alleviating the issues of pyrogenicity and immuno-rejection [12]. Since physical hydrogels are susceptible to melting at physiological temperatures a permanently crosslinked hydrogel is more desirable as a scaffold or encapsulation material. Although uv-light and chemical crosslinker are typically used for this purpose, they typically elicit cytotoxic side-effects that detract from their efficacy [15-20]. To overcome this compromise between physiological stability and compatibility, a biological enzyme that has the natural function of crosslinking proteins may be used with gelatin hydrogels.

Transglutaminase is one of such innocuous and ubiquitous proteins that are naturally used among many plant and animal species to create permanent peptide bonds between individual proteins [21, 22]. A form of this enzyme, microbial transglutaminase (mTG), was selected as the crosslinker of choice due to its biochemical stability and wide approval for use in the food industry [21, 23]. Enzyme crosslinked gelatin hydrogels are thus not only thermally stable but also have tunable proteolytic degradation properties, allowing the matrix to serve as either a cellular scaffold that can decompose with time, or a permanent encapsulation material that will protect engineered cells from degradation or attack by the host's immune system. An

additional property that makes gelatin hydrogel even more amenable to this project is that the matrix is optically clear, which would then permit more light transmission that is pertinent to the first phase of this project.

## **1.2 Eukaryotic Protein Expression System**

### *1.2.1 Transcriptional Regulations*

Gene expression in eukaryotes is highly complex, as compared to prokaryotic cells, containing many more regulatory mechanisms at both the transcriptional and translational levels. Differences begin with eukaryotes having three separate RNA polymerases (I, II, III) rather than just one found in prokaryotes. Regulation differs in two important aspects from the typical bacteria. First, eukaryotic RNA polymerases require several general transcription factors to assemble on the promoter gene sequence prior to transcription. Second, gene regulatory proteins bound to multiple enhancer/repressor sequences, which can be thousands of nucleotides away from the promoter, are often used to control mRNA polymerization. Even after an mRNA is synthesized, it must undergo many extensive modifications, such as the addition of a 5'-Cap (7-methylguanosine), and 3'-polyA tail (polyadenine) or possibly splicing before it can become fully functional. In most mammalian cells, only approximately 1% of all DNA sequences are transcribed into functional mRNAs.

### *1.2.2 Translation of mRNA*

Mature mRNA expression is subject to post-transcriptional controls. These methods, although less prevalent than transcriptional controls, are crucial to the expression of most genes. Eukaryotic cells typically utilize the functionalities of the 5'-Cap and 3'-polyA tail to modulate mRNA activity and stability.

### *1.2.3 Monocistronic vs. Polycistronic Translation*

As opposed to bacterial mRNAs, which have Shine-Dalgarno sequences, eukaryotic mRNAs utilize the 5'-Cap to bind a small ribosomal subunit for initiating translation. Ribosomal subunits that bind begin scanning the nucleotide sequence for the first AUG start codon. Although there are rare incidences of “leaky scanning” in eukaryotes, where a second or third start codon is recognized, the first AUG typically determines the reading frame and start site for translation. This form of expression is called monocistronism. Bacterial mRNAs often contain several ribosomal binding sites, giving rise to several proteins from one transcript. Thus prokaryotes are polycistronic.

### *1.2.4 Internal Ribosome Binding Site (IRES) Bicistronic System*

Some eukaryotes and viral mRNAs employ an alternative 5'-cap independent mechanism for initiating translation. This form of protein expression initiates with ribosomes binding to an internal ribosome entry sites (IRES). It is believed that IRES systems are used in crucial genes sequences in case there is a disruption to the availability of initiation factors, which are required for the normal cap-dependent translation machinery. Disruption can be due to stress [24-26], apoptosis [27, 28], or G2-M cell cycle transitions [29]. The IRES gene sequence derived from encephalomyocarditis virus (EMCV) is typically used to create bicistronic mRNA in a variety of cell cultures, such as C2C12, NIH 3T3, CHO, HeLa, and COS-7 [30].

### *1.2.5 Antibiotic Resistance and Cell Selection:*

Protein synthesis requires a smooth spatial and temporal coordination of DNA, RNA, and regulatory proteins. This network of molecules is intricately complex and offers many opportunities for disruptions. Certain antibiotics, which are naturally

produced by one organism in defense towards another, exploit this complexity. Antibiotics that are used for cell selection in mammalian cell culture are typically inhibitors of protein synthesis. Three antibiotic selection agents used in various constructs in this proposal include hygromycin, geneticin (G418), and puromycin. The first two antibiotics are aminoglycosides and act by binding to the 30S ribosomal subunits, thereby preventing them from participating in the ribosome complex. Puromycin is an aminoneucleoside. It functions as an aminoacyl t-RNA analog, and competes with endogenous tRNAs during peptide synthesis, causing translation to prematurely terminate [31-36]. Cell cultures that contain genes that can produce enzymes to deactivate the antibiotics are immune to these effects. This form of resistance selection method is important in creating permanent stable cell lines in mammalian cultures.

### *1.2.6 Secreteable Protein Processing [37]*

#### *1.2.6.1 Sorting Signals and the Endoplasmic Reticulum*

All mRNA in eukaryotic cells, other than those manufactured in the mitochondria and plastid, are expressed by free or membrane-bound ribosomes found in the cytosol. The final destination of a protein depends on which type of sorting signal it has. Proteins have several possible sites for distribution, including the nucleus, mitochondria, plastids (plants), peroxisomes, and endoplasmic reticulum (ER). Proteins that are to be excreted extracellularly are mediated from the ER to the Golgi network and secretory vesicles, which are used to deliver payloads to the exterior of a cell.

There are at least two forms of sorting signals for proteins. A signal peptide is typically a 15-60 continuous amino acid sequence found on either the amino (N) or carboxyl (C) -terminus of a protein. The immunoglobulin (Ig)  $\kappa$ -chain secretion leader sequence, used in the vector constructs, is of this form, which contains a 63 amino acid sequence on the N-terminus [38, 39]. C-terminal signal peptides, such as KDEL (Lys-Asp-Glu-Leu), are used for retaining proteins in the lumen of the ER. The second, more sophisticated, sorting signal is the signal patch. This recognition site is three dimensional, and is formed when separate peptide sequences come together in a folded protein. This type of signal is not typically used by secreted proteins.

In mammalian cells, the transport of proteins into the ER commonly occurs through a co-translational process, where proteins are translocated as they are synthesized. Co-translation ensures that secreted proteins, which typically are meant to have hydrolase activity, are never in contact with the cytosol. Although post-translational translocation is also known to occur, it is usually found in yeast ER and bacterial plasma membranes.

#### *1.2.6.2 Glycosylation and Post-Translational Modification*

As a protein is translated and translocated into the lumen of the ER, it is still bound to the membrane by its secretion signal. A signal peptidase is required to cleave the N-terminal sorting signal before the protein can be released. Before a protein is freed, however, it may receive several forms of modifications. Sulfhydryl groups are catalytically attached to cysteine residues, which form disulfide bonds between different regions of a polypeptide. This modification helps the protein attain its predetermined, three-dimensional form. Exposed asparagine (N) residues are also

processed by the addition of prefabricated blocks of oligosaccharides, which may be trimmed later. This N-linked glycosylation is exclusive to eukaryotes, and helps give a protein a rigid structure and resistance to degradation. Protein folding is sometimes further assisted by chaperone proteins found in the ER.

Secretory proteins that enter the ER are automatically shuttled to the Golgi complex for further processing. Incomplete or misfolded proteins, however, are retained and recycled. As particular glycoproteins enter the Golgi, N-linked oligosaccharides may be further trimmed or augmented. Certain OH-groups on serine or threonine side chains may also receive O-linked glycosylation.

As a secretable protein awaits its final destination out of a cell, it has one of two possible paths for secretion. All cells contain a constitutive secretory pathway, which is the default route. Cells that specialize in secreting products on demand, such as hormones, neurotransmitters, and digestive enzymes, utilize a regulated secretory pathway. The sorting signal used by this pathway is not well known, but is believed to be a signal patch. Thus, the secretion pathway taken may be more dependent on the protein rather than the cell type.

### **1.3 Fluorescent Protein Markers**

Bioluminescence is a relatively rare trait in nature, but can be found in many phylogenetically different groups [40] such as bacteria, dinoflagellates (plankton), cnidarians (jellyfish), and fireflies [40, 41]. In these organisms, the biochemical and physiological mechanisms for emitting light are distinct and are not evolutionarily conserved.



Natural functions for bioluminescence fall into three classes: defensive (distract or frighten predators), offensive (lure prey), and communication (courtship and mating) [42, 43]. Among the various molecules used in bioluminescence, fluorescent proteins are unique in that they are able to emit light when stimulated by exogenous radiation. Green fluorescent protein (GFP), found in various coelenterates, is of particular value as a biological marker, since it is able to fold and fluoresce independent of any cofactors or enzymatic substrates.

### 1.3.1 *Green Fluorescent Protein (GFP)*

Green fluorescence in *Aequorea victoria* jellyfish was first reported by Davenport and Nichol in 1955 [44]. Shimomura and colleagues later purified the protein extract in 1962 [45]. Interest in green fluorescent protein, however, did not begin to explode until thirty years later when the gene was cloned and expressed by Prasher and Chalfie [42]. Since that time, GFP has been expressed in a wide variety of prokaryotic and eukaryotic organism for innumerable applications.

#### 1.3.1.1 *Biochemical and Physical Properties*

Most of the attributes of GFP were discovered from studies on *Renilla reniformis* (sea pansy) and *Aequorea victoria* (hydrozoan jellyfish), although there are at least twenty other naturally occurring GFPs that have been studied. All known forms have a molecular weight around 27 kDa, with an acidic, compact, and globular  $\beta$ -can structure (Figure 1.1). GFP derived from jellyfish is unique in that it is preferentially monomeric in dilute solutions, where others form dimers.

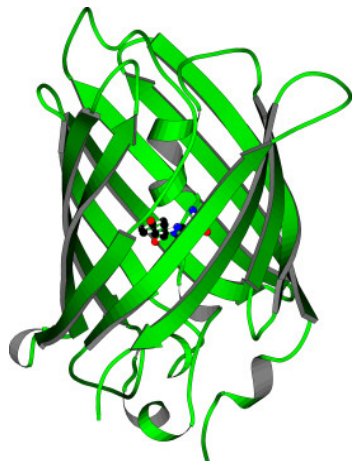


**Figure 1.1** Three dimensional representation of  $\beta$ -can and  $\alpha$ -helix structure of GFP.

The  $\beta$ -can is composed of eleven beta-strands, which surround and protect the chromophore that is in the center. The top and bottom of the can are sealed by short loop regions and distorted alpha helices. This unique structure creates surprising chemical stability, offering protection to typical fluorescence quenching agents such as acrylamide, halides, and molecular oxygen. The full length protein contains 238 amino acids, and has a C-terminal sequence of His-Gly-Met-Asp-Glu-Tyr-Lys [46]. This tail, unlike the bulk of the protein, is somewhat susceptible to proteolytic attacks by carboxypeptidases, proteinase K, and pronase [47]. The wild-type GFP has two excitation peaks, a major peak at 395nm, and a minor peak at 475nm [48]. The molar extinction coefficients are respectively 27,600 and 14,000  $M^{-1}cm^{-1}$  [49]. The normal emission peak is at 508nm. GFP has a fluorescence quantum efficiency of 0.72-0.78 [50].

#### *1.3.1.2 GFP Variants for Mammalian Applications*

The physical and biochemical simplicity of GFP, as well as its resistance to proteolytic, thermal, and pH-dependent degradation makes the molecule an ideal marker. Over the course of usage, many variants have been optimized for expression

and detection under mammalian cell systems. A common mutant is S65T-GFP, which has a fluorescence signal several times stronger than the wild-type by substituting Ser65 with Thr [51]. Other multiple amino acid, red-shifted variants, such as EGFP, were designed to be brighter and have an excitation peak match that of an argon laser, which is commonly used with fluorescent activated cell sorters (FACS). EGFP, currently licensed by Clontech Laboratories, Inc., has excitation and emission peaks at 488nm and 507nm, respectively. The variant is optimized for mammalian expression by the addition of a Kozak consensus translation initiation site at the beginning of the gene [52], the deletion of potentially inhibitory sequences, and containing 190 silent mutations using preferred human codons [53, 54]. Besides being easier to express, the final protein is 35 times more intense than the wild-type [55-60]. Several other variants and their properties, such as ECFP, and EYFP (to be used in this study), which are offered by Clontech, are listed in Table 1.1.

GFP and its variants from *A. victoria* have since been expressed as fusion products in many mammalian cell types including BHK, CHO, COS, GH3, HeLa, NIH 3T3, cc12, NRK, PTK1, and C2C12 mouse cells [50, 52, 61, 62]. Applications are varied, including time-lapse imaging, double-labeling, photobleaching, subcellular distribution, protein function and expression experiments. Advancements in microscopy, spectroscopy, and imaging instruments are already offering more sensitive and accurate detection of this reporter protein. Future novel applications will depend on the further optimization of GFP expression and spectral properties [63, 64].

### 1.3.2 *New Red Fluorescent Protein (RFP) Markers*

Since the inception of fluorescent protein markers, many variants with different spectral properties have been created for multi-labeling purposes. The creation of red fluorescent GFP mutants, however, has been elusive. Relatively recent studies have shown that GFP can be made to emit red light. However, this requires photoactivation of the fluorescent molecule under conditions of low oxygen with a laser [65]. More recently, researchers have sought a solution to this problem by using chromophores found in two other oceanic organisms, the common sea corals and anemones.

#### 1.3.2.1 *DsRed – *Discosoma sp* (sea coral)*

DsRed fluorescent protein is derived from the sea coral, *Discosoma sp*. The chromoprotein extracted from the coral is not naturally fluorescent, but simply red. The characteristic of fluorescence is created through a combination of random and site-directed mutagenesis techniques [66, 67]. Although this molecule only has 26-30% of its amino acid sequence resembling GFP, the two fluorophores share many similar biochemical features. Like GFP, DsRed contains a 11-stranded  $\beta$ -can structure with central  $\alpha$ -helices sealing the ends [68]. The red fluorescent protein also does not require any additional cofactors or substrates for proper folding, and is spectroscopically stable under a wide range of pH (5-12) [69]. Differences include its necessity to form tetramers rather than monomers for fluorescence, and its fluorescence is sensitive to mild detergents, such as sodium dodecyl sulfate (SDS). An early version of this marker, DsRed1, had the tendency to form large insoluble aggregates and was slow to fold. DsRed2 is the latest variant developed at Clontech, which contains three mutations for faster appearance of fluorescence (< 24 hr), and three others for lessening

aggregation. This improved molecule has excitation and emission peaks at 561 and 587nm, respectively (Table 1.1). It is also the first red fluorescence protein marker marketed to complement GFP variants for multi-labeling experiments (Figure 1.2).

**Table 1.1** Spectroscopic properties of fluorescent proteins [70, 71].

Fluor. Protein	Ex/Em Max (nm)	Extinction Coeff ( $M^{-1}cm^{-1}$ )	Quantum Yield
DsRed2	561 / 587	43,800	0.55
DsRed-Express	557 / 579	31,000	0.42
HcRed1	588 / 618	20,000	0.015
EGFP	488 / 508	55,000	0.60
EYFP	514 / 527	84,000	0.61
ECFP	434 / 477	26,000	0.40

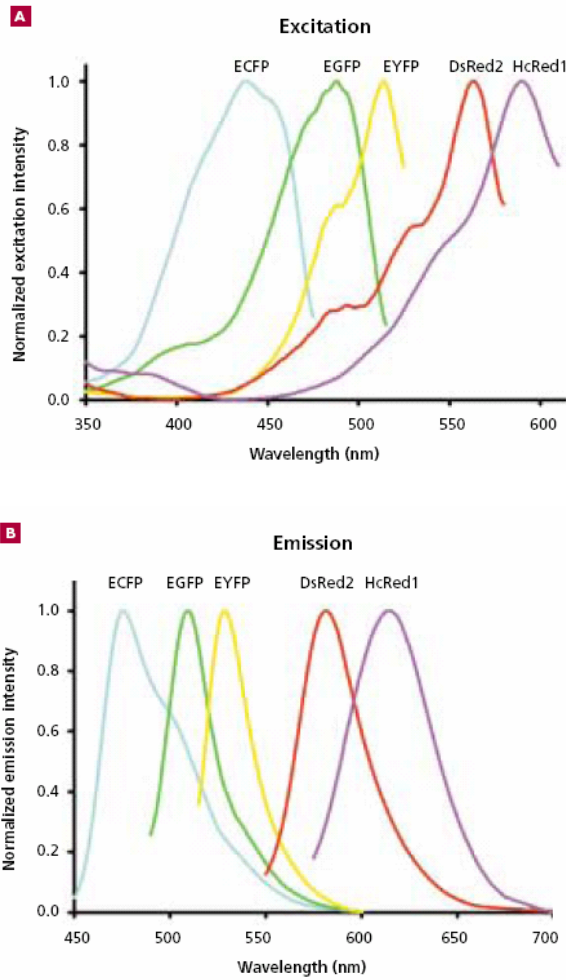


**Figure 1.2** Excitation (A) and emission (B) spectra of fluorescent proteins [Clontech] [71].

### 1.3.2.2 HcRed – *Heteractis crispa* (sea anemone)

The most applicably advanced red fluorescent protein marker is HcRed, which is extracted from the sea anemone, *Heteractis crispa*. Similar to DsRed, this new protein was generated by mutating a naturally non-bioluminescent chromophore. HcRed, however, does not form aggregates nor tetramers for fluorescence. The fluorophore is stable as a dimer, and thus requires less units of protein to fluoresce as brightly as DsRed. The maximum excitation and emission peaks are also at longer wavelengths of 488 and 615nm, respectively, referred to as far-red fluorescence. The advantages of these wavelengths include the use of less energetic or damaging light for excitation, and higher transmittance of red light.

## 1.4 Biohybrid Artificial Organs

Biohybrid artificial organs are implantable biomedical devices, engineered to incorporate live cells or tissue within a synthetic immuno-isolation barrier. Development of these devices began in the 1970's with experimental implantations, such as those using Langerhan's islets for the treatment of diabetes. Biohybrid organs are distinguished from traditional implants in that both allogenic and xenogenic cells can be safely used. Cells may also be genetically engineered to resist harsh environmental conditions or produce particular proteins that are not native to the cell type. Besides considering the type of cells to be encapsulated, other major design challenges include maintaining high viability, and providing protection for the cells from the immune system.

#### *1.4.1 Cell Source*

The choice of cells used for encapsulation will typically determine the density required, since different cell types have different metabolic activities and secretion rates. Applications for treating the central nervous system require only low concentrations of neuroactive compounds due to their natural potency. The number of cells required for such applications appears to be  $10^6$ - $10^7$ , which is equivalent to a volume of 1-10  $\mu\text{L}$ , and is easily accommodated in an encapsulation device [69]. Treatment of diabetes, however, may require larger quantities of therapeutics and cells. It is estimated that  $10^9$  cells or nearly a 1 mL volume is necessary for provide enough of the therapeutic compound [72]. Devices with large volumes prove difficult to implant due to an increase in the diffusional distance for nutrients and oxygen to travel to all encapsulated cells.

#### *1.4.2 Molecular Diffusion and Device Design*

In order to maintain cell viability, an encapsulation device must provide adequate freedom for nutrients and oxygen to diffuse inward and metabolic wastes to leave. While nutrients such as glucose and macromolecules like albumin, growth factors, and transferrin may be needed for cell survival, the adequate supply of oxygen is the most critical factor for maintaining cell viability. In an encapsulated cell mass, a necrotic core of cells usually develops for devices with a diameter larger than 150  $\mu\text{m}$  [73]. Although necrosis may still occur for well oxygenated cells with high metabolisms, the lack of oxygen (hypoxia) is usually the leading cause of death or lowered cellular functionalities. Perfused rat islets have been shown to have secretion rates of insulin of 100, 50, and 2% compared, to normoxic conditions (140 mmHg), as

the partial pressure of oxygen is dropped to 60, 27, and 5 mmHg, respectively (Figure 1.3) [72].

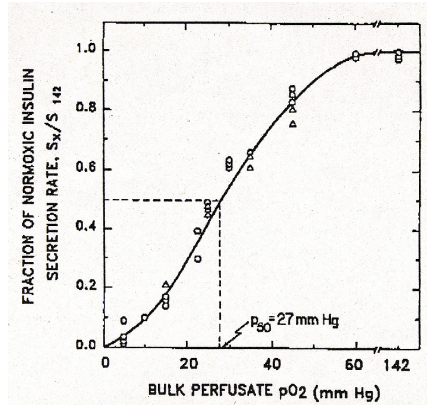


**Figure 1.3** Rate of insulin secretion as a function of oxygen partial pressure in perfused rat islets [74, 75].

Several geometric configurations have been designed for balancing cell mass and performance with oxygen requirements. Intravascular arteriovenous shunts are the most technically advanced, and have been extensively tested on large animals [76]. These devices, however, require major surgical procedures for integration into the vascular system of the host, and are subject to the dangers of blood clots. Thus, there is motivation for developing extravascular devices that can circumvent these difficulties.

There are three main geometric configurations used for extravascular designs. Spherical microcapsules have a typical diameter range of 500 to 800  $\mu\text{m}$ . The production method for this configuration results in the encapsulation of a very low volume fraction of cells, and offers an advantage in mass transfer. Tubular devices, such as hollow fibers, share similar advantages with microcapsules and additionally, are more readily retrievable. Islets encapsulated in tubular diffusion chambers with an internal diameter of 2.2 mm have shown viable tissue near the inner surface. Larger tubes with a 4.8 mm internal diameter, however, indicate a large core of necrotic cells



due to oxygen depletion [72]. Planar chambers formed by parallel membranes are the third type of design. These devices were initially used to study immune rejection of transplantations. Planar configurations, however, typically elicit a larger immune response than the other geometric forms.

Using a theoretical model for oxygen diffusion and consumption, described by Michaelis-Menten kinetics, spheroids offer the least diffusional resistance to oxygen. The following parameters were used in a simulation by Colton CK, 1995 [72]: the maximum oxygen consumption rate,  $V_{\max} = 3 \times 10^{-8} \text{ mol/cm}^3\text{-s}$ ; Michaelis constant,  $K_m = 0.44 \text{ mmHg}$ ; effective oxygen diffusion coefficient  $D = 1.6 \times 10^{-5} \text{ cm}^2/\text{s}$ ; and Bunsen solubility coefficient  $a = 1.02 \text{ } \mu\text{M/mmHg}$ . The surface oxygen partial pressure was taken as  $pO_2 = 40 \text{ mmHg}$ , which is the typical value found in microvasculatures. Figure 1.4 indicates that for a slab with a thickness of  $150 \mu\text{m}$ , the oxygen level is completely depleted at the center plane. However, the oxygen environment in the sphere does not become anoxic until the diameter is increased to  $250 \mu\text{m}$ .

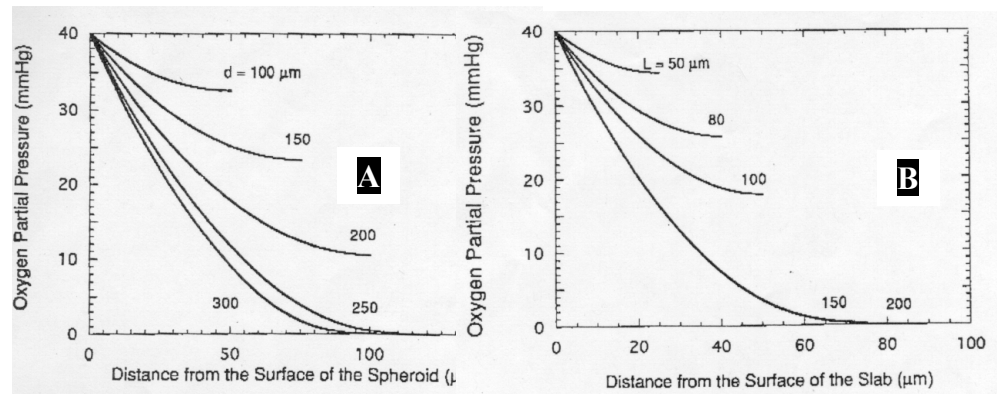


**Figure 1.4** Oxygen penetration profiles for spheres (A) and slab (B) of various diameters [72].

In situations where avascularization occurs, and the oxygen source is further removed from the encapsulated cells, the spheroid is clearly advantageous over the planar conformation (Figure 1.5).

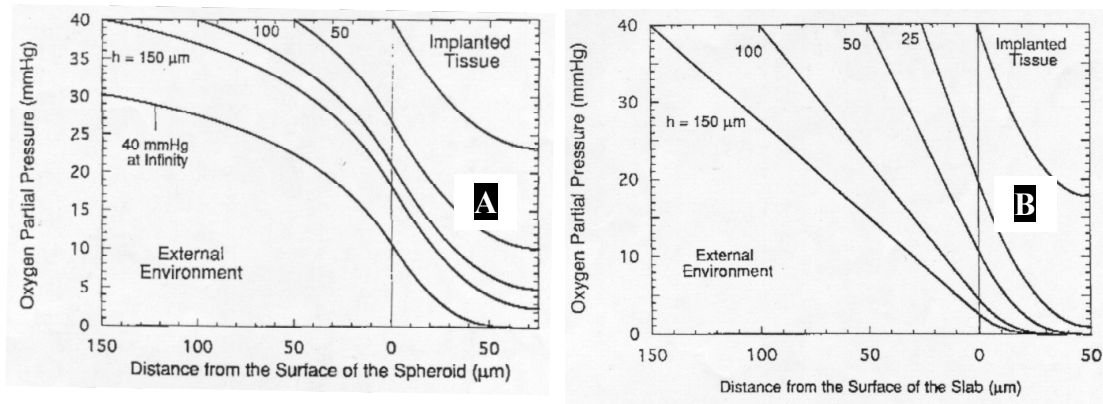


**Figure 1.5** Oxygen penetration profiles for spheres (A) and slabs (B) surrounded by an avascular diffusion barrier [77].

### 1.4.3 *Immuno-Protection*

The primary objective of an immuno-isolation barrier in a biohybrid artificial organ is to provide protection for transplanted cells from the immune system of the host. An immune response can be triggered by three possible sources, cell surface antigens, secreted proteins, and cell debris from dead cells. Recognition of antigens by the host organism can signal cellular and humoral immune responses (Figure 1.6).

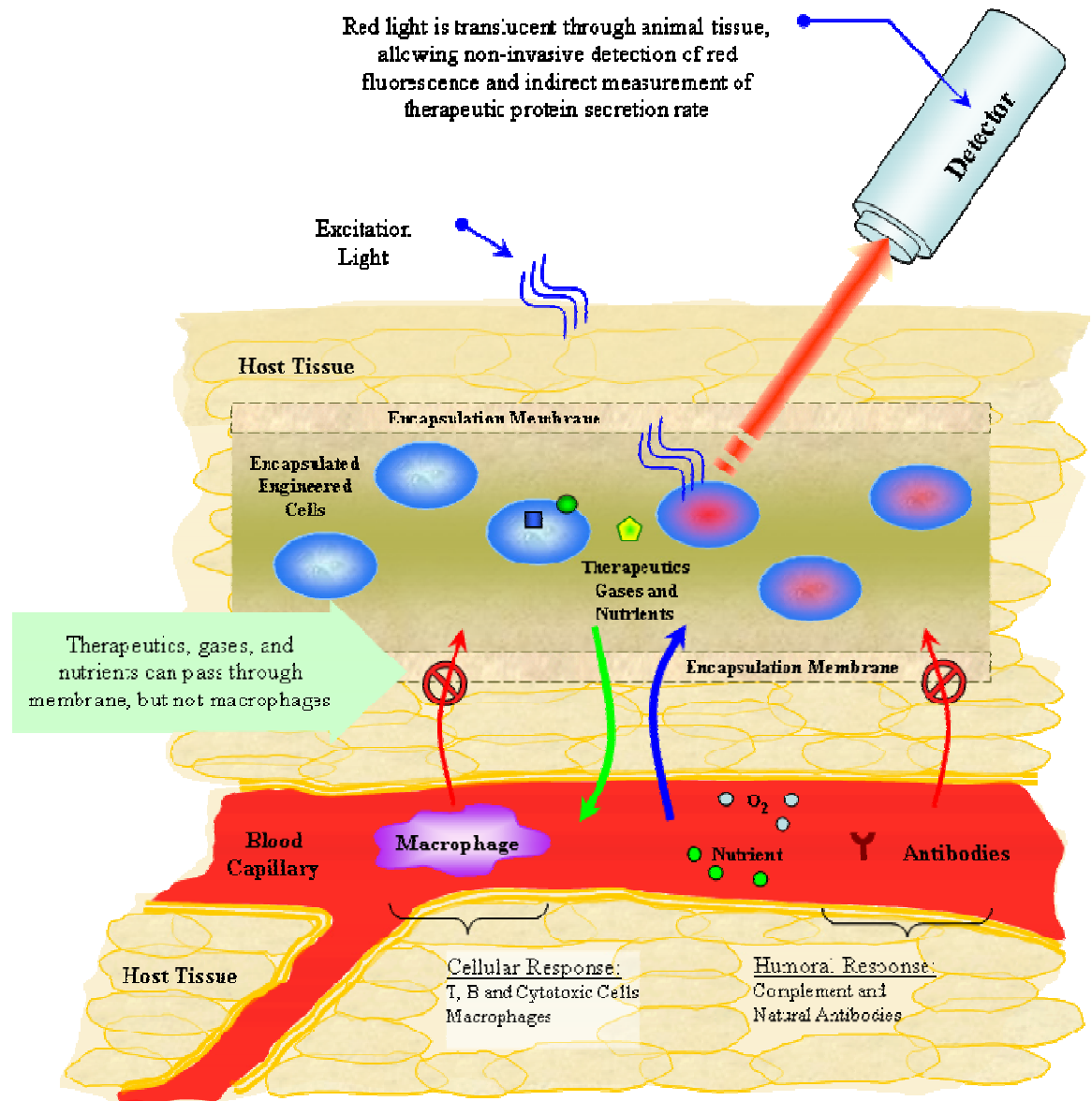


**Figure 1.6** Cellular and humoral immune responses experienced by implanted cells.

Cellular responses include the activation of macrophages, cytotoxic cells, and other immune cells. Preventing these cells from passing through the membrane is relatively easy since their sizes are on the same order as the encapsulated cells. Macrophages, however, have the added ability to secrete low molecular weight reactive metabolites. These oxygen and nitrogen intermediates may include free radicals,

hydrogen peroxides, and nitric oxides, which kill surrounding cells non-discriminately. The humoral response also poses a serious threat to transplanted cells since lymphokines, cytokines, and antibodies are small and may be able to pass through the membrane barrier.

## **1.5 Hypoxia**

Oxygen is one of the most critical molecules used by aerobic organisms since it is the terminal electron acceptor in metabolic pathways. The ability of organisms to adapt to low oxygen conditions, or hypoxia, is crucial to survival. In mammals, oxygen homeostasis is maintained meticulously at both the systemic and cellular levels.

### *1.5.1 Mammalian Oxygen Homeostasis*

Oxygen concentrations in the body are monitored by chemoreceptors in the arterial and pulmonary neuroepithelial bodies. Low concentrations of oxygen transduce an increased number of nerve signals to the brain, which in turn increase both respiratory and circulatory rates of an animal [78]. On the intracellular level, hypoxia induces the expression of many genes that help adapt cells to the lowered availability of oxygen. Erythropoietin (EPO) expression increases the production of red blood cells, and is utilized to expand the oxygen carrying capacity of blood. Transferrin provides the transport of iron, which is necessary for heme proteins [79]. Vascular endothelial growth factors (VEGF) are over-expressed to promote the formation of new blood vessels [80]. Nitric oxide and carbon monoxide, which are generated from inducible nitric oxide synthase (iNOS) [81] and heme oxygenase 1 (HO-1) [82], respectively, help reduce vascular tone so that blood can flow more freely. Cell metabolisms are

also optimized as GLUT-1 expression enhances the uptake of glucose, and elevated amounts of glycolytic enzymes allow cells to increase anaerobic ATP synthesis.

### *1.5.2 Molecular Biochemistry*

The molecular mechanism for sensing oxygen is centered on the protein called the hypoxia-inducible factor 1 (HIF-1). This transcriptional activator is triggered by many upstream signal transduction pathways and is, in turn, responsible for inducing downstream target gene expression that are used to regulate oxygen homeostasis. Effectors of this central activator are not limited to hypoxia, but also include nitric oxide, cytokine, and growth factor signaling, embryonic development, and pathological stresses.

HIF-1 is a heterodimer, composed of an HIF-1 $\alpha$  subunit (120 kDa) and an HIF-1 $\beta$  subunit (91-94 kDa). It was first recognized as an oxygen sensor by its ability to bind and activate erythropoietin gene expression. Purification and microsequencing of the protein indicates that the second subunit is identical to a previously identified aryl hydrocarbon receptor nuclear translocator (ARNT) protein, whereas HIF-1 $\alpha$  is a newly recognized protein. Under normal physiological conditions, both subunits are constitutively expressed. HIF-1 $\alpha$  level, however, is continually controlled by ubiquitination, which marks it for proteasomal degradation. Under hypoxic conditions, where cells are exposed to O<sub>2</sub> levels below 6%, the level of expression exponentially increases [83].

The amino (N)-terminal half of HIF-1 $\alpha$  (1-390 amino acids, AA) is determined to be necessary and sufficient for dimerization with HIF-1 $\beta$  and DNA binding. The carboxyl (C)-terminal half contains two transactivation domains (531-575, 786-826

AA) and one regulation domain. The actual molecular mechanism that mammalian cells use to sense and transduce oxygen levels for regulating HIF-1 $\alpha$  expression and activity is still unclear. Many mechanisms have been postulated [84-88], but recent studies indicate that reactive oxygen species (ROS), such as hydrogen peroxides, are either directly or indirectly responsible for regulating HIF-1 $\alpha$  pathways [89].

### *1.5.3 Normal Physiological Causes*

Hypoxic conditions can be caused by a wide variety of environmental or physiological stimuli. Increased metabolism from exercise is a common cause, while exposure to high altitudes or embryonic development can also trigger hypoxia-induced pathways. Pathological infections, vascular diseases, and cancer are also common causes.

### *1.5.4 Conditions in Encapsulation that Cause Hypoxia*

Several geometric configurations for encapsulating foreign cells for implantation have been investigated. These include spherical microencapsulations, planar diffusion chambers, and tubular hollow fibers. Regardless of the configuration, the transport of molecular oxygen from the host tissue into the encapsulated cells faces several diffusional barriers. These include the surrounding host tissue (particularly if an avascular fibrotic wall develops), the immuno-isolation membrane, and the mass of foreign cells themselves. In the relatively stagnant environment of an encapsulated device, it is typical to find a central core of cells deprived of necessary oxygen concentrations.

### 1.5.5 Hypoxia-Induced Cell Death and Bcl-2 $\Delta$ Protection

Hypoxic stress can induce cell death by both necrosis and apoptosis. The propensity towards either pathway is highly dependent on the cell type [90]. The first pathway, however, is typically the result of severe and prolonged exposure to a stimulus such as the deprivation of oxygen. Characteristics of necrosis are cell membrane disruption, mitochondrial swelling, and loss of cytosolic structures. Apoptosis, also known as programmed cell death, is a more gradual and organized process characterized by chromatin condensation, DNA cleavage, cell size shrinkage, and cell membrane blebbing.

Bcl-2 belongs to a family of regulatory proteins that have the ability to prevent or delay apoptosis. Its activity was first described by Vaux *et al.* in 1988 as being able to protect cells from apoptosis induced by deprivation of the hormone IL3 [91]. It was later discovered that Bcl-2 could prevent apoptosis induced by other factors, including serum deprivation, heat shock, chemotherapy agents, ethanol, and hypoxia [89, 92-95]. More recently, Bcl-2 has also been shown to inhibit necrosis induced by hypoxia and inhibition of mitochondrial respiration [96].

Since the discovery of Bcl-2, other members of this family of regulatory proteins have been discovered. Members include proteins that are anti-apoptotic (Bcl-2, Bcl-xL, Bcl-w) and pro-apoptotic (Bax, Bak, Bik, and Bid). A commonality among the members is four Bcl-2 homologous domains, BH (1-4), which may all be present, but not all active in a single protein. Activity of BH3 has been shown to be necessary for the efficacy of pro-apoptotic members [96-98], while BH1, 2, and 4 are required for anti-apoptotic effects [9, 99]. Recent studies also indicate that a nonconserved region of peptides between BH3 and BH4, encoding an unstructured loop, is responsible for

attenuating the anti-apoptotic effects of Bcl-2 and Bcl-xL. Bcl-2 $\Delta$  is a deletion mutant of the human Bcl-2 protein, made by deleting amino acids 32-80. In comparisons to the full-length protein, the deletion mutant showed enhanced ability to inhibit apoptosis. It is postulated that this loop region is a negative regulatory domain used for post-translational modifications of Bcl-2 proteins [2].

## **1.6 Cell Lines**

### *1.6.1 C2C12*

The C2C12 is a murine myoblast cell line, subcloned from the skeletal leg muscle cells of an adult C3H mouse. The original culture was ordered from American Type Cell Culture (ATCC; CRL-1772, MD, USA). C2C12 cells are not carcinomas and are undifferentiated. These cells were selected for use in this project due their previous demonstration of endogenous HIF-1 activity, and its ability to stimulate hypoxic response elements of transfected genes. C2C12 cells engineered to secrete human erythropoietin have been successfully encapsulated in hollow microporous fibers for implantation in mouse animal models [100-103].

### *1.6.2 HEK293*

The human embryonic kidney cell lined, Flp-In<sup>TM</sup> HEK293, is an attachment dependent strain that was obtained from Invitrogen Corporation. This particular clone was modified from the basal cell line, CRL-1573 (ATCC)[104], to express zeocin resistance and contains a single stably integrated Flp Recombinase Target (FRT) site within its genome[105]. When Flp-In HEK cells are used in conjunction to FRT expression vectors and the Flp recombinase enzyme, the likelihood of obtaining a recombination event is not only dramatically higher, but also specific to the FRT



site[106, 107]. Thus, selecting a stable isogenic cell line is greatly facilitated compared to traditional random recombination techniques. Cells that have properly integrated the expression vector at the FRT site will exhibit hygromycin resistance, zeocin sensitivity, loss of  $\beta$ -galactosidase activity, and expression of gene of interest.

### *1.6.3 Jurkat*

Jurkat cells are a suspension cell line derived from human T-cell leukemia, TIB-152 (ATCC) [108]. This strain of cells was originally obtained from Invitrogen, and is also a Flp-In modified clone. Although Jurkat cells are attachment independent, they can still be grown in tissue culture flasks. Advantages of using a suspension cell line are its ease of handling during passage, transfection, and cell sampling. Jurkat cells, however, tend to have a poor transfection efficiency and protein production capabilities.

## **1.7 Human Interleukin 2 (hIL2)**

Interleukin-2 (IL2) is a polypeptide hormone and belongs to a class of molecules called cytokines. The term cytokine was first used to describe molecules produced by and influencing only the immune system in an autocrine manner. It was later discovered that these hormones have a far reaching paracrine effect.

Interleukin-2 is perhaps the most extensively studied lymphokine. It has profound influences in the development, expansion, and activation of T cells, natural killer (NK) cells, and B-cells [109]. The glycoprotein is produced by activated T lymphocytes. It has a molecular weight of 15-18 kDa depending on the pattern of glycosylation [110-112]. Incubation of human peripheral blood lymphocytes with IL2 for 4-7 days induces the generation of lymphokine activated killer (LAK) cells, which are generated from NK cells. LAK cells are shown to mediate enhanced cytotoxic

activity against NK-resistant tumor cell lines and freshly isolated tumor cells with little effect on normal cells [101, 113]. IL2 is also responsible for augmenting the release of other cytokines including IFN- $\gamma$ , GM-CSF, TNF- $\alpha$ , and TNF- $\beta$ , to form a network of responses to infections [100]. The critical role of IL2 in activating cytotoxic cells has led to clinical trials for the treatment of cancer [114, 115] and AIDS [1], and is thus a relevant choice as a model therapeutic protein for production in the encapsulated device.

## **1.8 Cellular Scaffolds and Gelatin Hydrogels**

In engineering artificial tissues and organs, the incorporation of a cellular scaffold is crucial for providing a physical support matrix for cells to attach and grow on once implanted into a host. Hydrogels are the most commonly used scaffolds due to their high water content ( $\geq 30\%$  by weight) and structural similarity to macromolecular-based components in the body [13]. This type of support matrix can be formed from both synthetic polymers, such as poly (lactide-co-glycolide) (PLG), poly (glycolic acid) (PGA), and copolymers (PLGA) or natural biopolymer, such as collagen, hyaluronate, fibrin, alginate, and chitosan [12]. Synthetic polymers often give more flexibility for tailoring the gelling mechanism and mechanical properties of the hydrogel, but face a challenge in coaxing cells to adhere and typically elicit immunogenic responses from the host. Scaffolds made with natural polymers are often times more biocompatible with host tissues, as well as encapsulated cells, and have adequate physical strengths. Of all natural biopolymers used in tissue engineering, collagen is the most widely utilized due to its natural and dominant role as the building block of mammalian extracellular matrices[12]. Collagen, however, is expensive to produce and contains

much variability among production lots. The basic protein element of collagen is gelatin, and is relatively inexpensive. Gelatin can be derived from collagen by simple acidic decomposition (producing gelatin A) or alkaline treatment (producing gelatin B). This biomaterial has similar biocompatibility properties as collagen, and has also been used to deliver growth factor, as well as promote vascularization of regenerative tissues. A shortcoming of physical gelatin hydrogels is that it is thermally reversible under physiological temperatures (37°C). To overcome this disadvantage, however, it is possible to permanently crosslinking the gelatin peptides with a crosslinker. Although this crosslinking is traditionally done with uv-light or chemical crosslinkers (e.g. glutaraldehyde or diphenylphosphoryl azide) [20, 116, 117] these elements themselves raise an issue of cytotoxicity, which detracts from their overall applicability . An alternative method for creating a permanent gelatin hydrogel is to use a natural biological enzyme to form covalent peptide bonds among the gelatin proteins. A microbial transglutaminase (mTG) is one of such enzymes, which is also highly biocompatible as it is approved for use in many food manufacturing processes in various countries, including the United States [21]. However, the further characterization of the biocompatibility and degradability of mTG crosslinked hydrogels when they are applied as cellular scaffolds still remains unexplored. This reach seeks to elucidate these properties of these hydrogels, and advance its application in tissue engineering.

## **2. Integrated Non-Invasive System for Quantifying Secreted Human Therapeutic hIL2**

### **2.1 Introduction**

Biohybrid artificial organs are implantable biomedical devices, engineered to incorporate live cells within a synthetic immuno-isolation barrier. Development of these devices began in the 1970's with experimental implantations, such as those using Langerhan's islets for the treatment of diabetes. Since then, encapsulation therapy has been used for ameliorating other persistent ailments, including chronic pain [2] and amyotrophic lateral sclerosis (ALS) or Lou Gehrig's disease [100-103]. Cancer, which is the second leading cause of mortality in the United States, is one of such chronic diseases that may be a target for treatment with biohybrid implants. Human interleukin-2 (hIL2) is a natural polypeptide hormone, which has a key role in activating a network of immune responses within the body [100]. The critical role of hIL2 has led to clinical trials for the treatment of several deadly diseases, including cancer [114, 115] and AIDS [118, 119]. The clinical efficacy of hIL2 makes it an appropriate therapeutic protein for development of usage in biohybrid organs.

The objective of this portion of the work was to engineer mammalian cells to secrete hIL2 as a potential anti-cancer therapeutic, in a manner ultimately suitable for encapsulation behind an immuno-protective membrane. In order to gauge the productivity of cells performing in this capacity, it is ideal to have a reporter system that can accurately and non-invasively indicate the differential secretion of hIL2. To meet these criteria, a destabilized form of the DsRed-Express fluorescent protein, DsExDR, was selected for co-expression with hIL2. This fluorescent protein emits

red light (emission maximum is 579 nm), which is translucent through tissue [120], and is hypothesized to discreetly trace hIL2 secretion. Additionally, this low toxicity protein has a quick maturation and degradation rate (half-life is ~12 hours) to produce a finer differential signal as compared with other fluorescent proteins. Although expressing DsExDR in fusion with hIL2 may offer the closest correlation between the two proteins (1:1), an internal ribosome entry site (IRES) enables the respective genes to be translated independently from a single monocistronic mRNA. Thus, with appropriate translocation signals, the therapeutic protein can be secreted without secretion of the marker. Three cell lines (C2C12, HEK293, Jurkat) were transfected with this bicistronic construct and tested as potential hosts for producing hIL2. The specific intracellular red fluorescence, as measured by flow cytometry, was correlated with ELISA measurements for secreted hIL2.

## **2.2 Materials and Methods**

### *2.2.1 Cell Culture - Passaging and Maintenance*

Three mammalian cells lines, C2C12, HEK293, and Jurkat, were used in this work. C2C12 is a murine myoblast subcloned from the skeletal leg muscle of an adult C3H mouse (American Type Cell Culture, ATCC). This cell line is attachment dependent and has been shown to efficiently produce exogenous interleukin-2 [121]. HEK293 is a human embryonic kidney cell line, which was selected for comparison based on its high transfection and protein production efficiencies [108]. This particular strain, Flp-In™-293 (Invitrogen), contains an Flp-In Recombinase Target (FRT) sequence in its genome. When used in combination with an expression vector that also contains an FRT sequence, a stable polyclonal cell line can be selected in

approximately two weeks with hygromycin (200-400 µg/mL). This cell line is also attachment dependent, but is readily detached with minimal trypsinization (3-5 min, 37°C). The Jurkat cell line, Flp-In™-Jurkat (Invitrogen) also contains an FRT sequence within its genome. These cells grow in a suspended form and are derived from human T-cells [122].

All cell lines were cultured in Dulbecco's Modified Eagle's Media containing glucose (4.5 g/L), GlutMAX™ I (3.97 mM), and 10% fetal bovine serum (FBS, Sigma). Media for both FRT cell lines also contained zeocin (100 mM) in order to maintain the stability of their FRT insertions. Cells were subcultured every two to three days in 75cm<sup>2</sup>-tissue culture flasks (Costar) as the population approached 80-90% confluency. Attachment cells were passaged by first removing the old media, and rinsing the flask with Dulbecco's Phosphate Buffer Solution without Ca<sup>2+</sup> or Mg<sup>2+</sup> (DPBS-cm, Invitrogen). Washed cells were then incubated in 1.5 mL of a 0.25% Trypsin with 0.03% EDTA solution (Sigma) for 5-10 minutes in a 37°C, 8% CO<sub>2</sub> incubator. The Jurkat suspension cells did not require trypsinization, and a fraction of the previous culture was simply aliquoted into a new flask during passaging. All cells were passaged with a 1:4 to 1:10 split ratio, and supplemented with fresh complete media up to 12 mL for further growth.

### 2.2.2 *Vector Constructs*

The expression vector used in this study, pF2, contains an assembly of four gene elements: the human interleukin-2 (*hIL2*) gene, its Ig-κ secretion signal, an internal ribosome entry site (IRES), and a Destabilized DsRed-Express (DsExDR) fluorescent protein marker. The secretable *hIL2* (*ShIL2*) fragment was first derived

from a previously constructed vector called pSIEG. This vector was made by PCR extraction of the *hIL2* gene from pBlueBacHis2-GFPuv/hIL2 [51], using the following primers: 5'-AAT GTC GAC AAA TGG CAC CTA CTT CAA GTT CTA CAA A-3' and 5'-ATT ACC GGT TTC TTG TCA TCG TCA TCT CAA GTT AGT GTT GAG ATG ATG CTT TG-3'. The first primer contained a Sal I restriction site, and the second primer has enterokinase (EK) and Age I restriction sites. The blunt PCR fragment was first ligated to pCR-Blunt II-TOPO (pCR) (Invitrogen) before digesting with Sal I and Age I restriction enzymes. The digested fragment was then ligated into the corresponding unique cloning sites of pEGFP1-N1 (Clontech). Hind III and Not I were then used to restrict the *hIL2-EK-EGFP* fusion gene for ligation into pSecTag2A/hygro (Invitrogen) in order to add on the Ig- $\kappa$  secretion signal.

The following primers were used to extract *ShIL2* from pSIEG: 5'-GAA GAT CTG CCG CCA CCA TGG AGA CAG ACA CAC TCC TGC TAT-3' and 5'-GGA TCC GCG TTA TCA AGT TAG TGT TGA GAT GAT GCT TTG ACA AAA-3'. The first primer contained a Bgl II restriction site and a Kozak consensus sequence, which was used to further increase translation efficiency in eukaryotic cells [122, 123]. The second primer introduced a BamH I restriction site. A pCR plasmid was again used as an intermediary cloning vector. The secretable *hIL2* gene was excised with Bgl II and BamH I and then ligated into pIRES2-DsRed2 (Clontech) in order to pick up the IRES bicistronic element. The vector constructed thus far is called pShIRDs, and was initially used in a transient experiment to gauge the optimal time point for detection of red fluorescence.

The *ShIL2-IRES* fragment was then extracted by PCR and ligated to pDsRed-Express-DR (Clontech) in order to add on the red fluorescent protein marker gene. The following primers: 5'-GAA GAT CTG CCG CCA CCA TGG AGA CAG ACA CAC TCC TGC TAT-3' 5'-TCC CCG CGG GGA TGT GGC CAT ATT ATC ATC GTG TTT TTC AAA G-3' were used. The first primer was the same as the one used in the previous cloning procedure. The second primer contained a *Sac* II restriction site. pCR was again used as an intermediary cloning vector. The final expression vector, pF2, was constructed by digesting the *ShIL2-IRES-DsExDR* fragment from pCR using *Bgl* II and *Sac* II restriction enzymes and ligating it to the respective unique sites on the host vector, pSecTag/FRT/V5-His-TOPO (Invitrogen) (Figure 2.1).

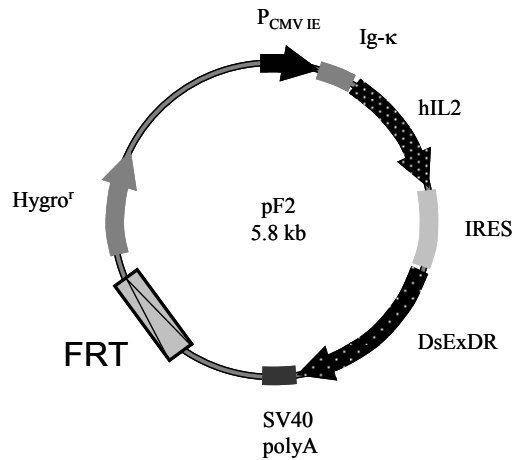


**Figure 2.1** The bicistronic vector, pF2, contains an internal ribosome entry site (IRES) gene sequence, which allows for the independent production of secretable hIL2 and DsExDR red fluorescent marker proteins



### 2.2.3 *Transfections*

Procedures for transfecting the HEK239 and C2C12 attachment dependent cell lines were developed for 24-well tissue culture plates (Costar) in a suspended form. Cells were passaged, at most, two days before transfection so that they would remain in a non-confluent, growing state at the moment of harvest. For collection, cultures were trypsinized (1.5 mL Trypsin/EDTA, 5 min, 37°C), centrifuged (500 x g, 5 min, 25°C (RT)) and resuspended to yield  $2 \times 10^5$  cells/well using 0.5 mL/well of complete media without antibiotics. DNA and LipofectAmine 2000 (LF2000) (Invitrogen), were independently mixed with OptiMEMI (Invitrogen) in 5 mL polystyrene tubes and incubated for 5 min at RT. The two solutions were then combined and incubated for 20 min before proportional volumes were aliquoted to respective wells to obtain 0, 0.2, 0.5, 0.8, 1.2, 1.6, and 2.0 µg-DNA/well concentrations.

Transfections of Jurkat suspension cells were developed in 6-well plates. Cells were collected by the same procedure as before, and inoculated at a density of  $3.5 \times 10^5$  cells/well using 1.5 mL/well of complete media without antibiotics. The concentrations used in the transfections were 2.0, 3.0, 4.5, 6.0, and 9.0 µg -DNA/well. If these values were normalized by the same number of cells used in the HEK293 and C2C12 experiments, the concentrations would be equivalent to 1.1, 1.7, 2.6, 3.4, and 5.1 µg -DNA/well. These higher concentrations of DNA were used due to the low transfection efficiency of Jurkat cells.

In all cases, the transfection volumes were the same and the samples taken for protein analysis were at 24 hrs post-transfection.

#### 2.2.4 *ELISA*

Supernatant samples containing secreted hIL2 from the attachment cell lines were collected from each well and centrifuged at 2000 x g for 5 min to remove cells that are suspended in the media. Supernatants from Jurkat cells were collected by centrifugation at 500 x g in order to preserve the cells for flow cytometry. Supernatant samples were immediately transferred to a -80°C freezer until assayed. To collect intracellular hIL2 samples, cells were lysed by adding 100 µL of M-Per (Pierce-Endogen). The samples were allowed to incubate for 10 min with gentle shaking at RT before centrifugation at 14,000 x g for 15min. Measurements for the concentrations of both secreted and intracellular hIL2 were made with an OptEIA Human IL-2 ELISA Kit II (BD Pharmingen). Human IL2 standards were made by serially diluting a 500 pg/mL hIL2 stock provided in the kit. A highly linear correlation was obtained with eight concentrations, including a zero ( $r^2 > 0.98$ ). Standards were assayed in duplicates as instructed by the manufacturer, while supernatant samples were always assayed in triplicate. The calculation for the final concentrations of hIL2 secreted takes into account the different culture volumes due to the transfection procedure.

#### 2.2.5 *Flow Cytometry*

Attachment cell samples were collected by first detaching them from the wells with Trypsin/EDTA (300 µL /well). A fresh aliquot of DPBS-cm, with 10% FBS (300 µL /well) was added to each to neutralize the Trypsin before centrifuging at 500 x g for 5 min. The supernatant was then carefully aspirated and the cell pellet gently resuspended in 300 µL of DPBS-cm. Half of each of these cell suspensions was used

for ELISA assays of intracellular hIL2, and the other half for flow cytometry. These samples were then supplemented with 150  $\mu$ L of DPBS- $\text{Ca}^{2+}$ ,  $-\text{Mg}^{2+}$ , with 7.4% paraformaldehyde to fix the cells. Samples were kept in a 4°C refrigerator until they were ready for the flow cytometer. Red fluorescence of C2C12, HEK293, and Jurkat cells was measured by a FACSCalibur™ (BD Biosciences, Immunocytometry) flow cytometer equipped with a 15 mW, 488 nm, air-cooled argon-ion laser and three color detectors (FL1=530/30, FL2=585/42, FL3=670LP), which was kindly provided by D.M. Mosser (University of Maryland, College Park). FL2 was used for the detection of Destabilized DsRed-Express fluorescent proteins. The cytometer was used with the following settings: FSC = 1.00, SSC = 394, FL2 = 683 for Jurkat cells and FSC = 0.485, SSC = 288 and FL2 = 538 for HEK293 and C2C12 cells. Ten thousand cells were analyzed in each sample. Fluorescence measurements were made only on live cells, which were gated by the upper right quadrant of an FSC-SSC dot plot. Histogram plots of the live cells were then used to determine the number of cells and their corresponding fluorescence intensities that were above background (Figure 2.2).

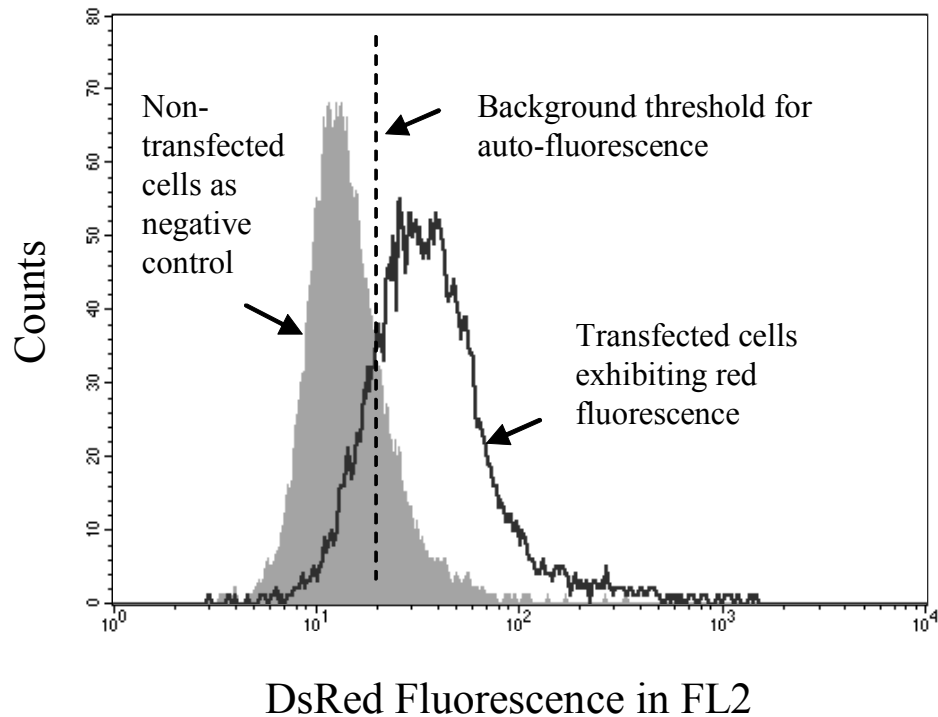


**Figure 2.2** Destabilized DsRed-Express fluorescence in mammalian cells was measured using a FACS Calibur flow cytometer (FSC = 1.00, SSC = 394, FL2 = 683 for Jurkat cells and FSC = 0.485, SSC = 288 and FL2 = 538 for HEK293 and C2C12 cells). Histograms were obtained only after gating live cells from dead ones using a FSC-SSC dot plot within 10,000 cell samples.

All fluorescence data were reported in Total Relative Fluorescent Units (RFU), which is defined as the product of the number of cells and the mean fluorescence intensity above background. This unit more accurately reflects the total number of fluorescence molecules within a cell sample and was used for correlations to hIL2 secretion levels.

### 2.2.6 Fluorescence Microscopy

Fluorescent cells were observed using an Olympus BX60 fluorescent microscope equipped with a DsRed2 filter cube (Exciter HQ540/40x, Dichroic Q570LP BS, Emitter HQ600/50m EM). Cell cultures were removed from flasks by

either trypsinizing attached cells or by simply pipetting out suspension cultures. Samples were washed and resuspended in DPBS-cm in order to minimize the background autofluorescence of the media. Cells were then placed on a microscope slide with a cover slip before imaging.

## **2.3 Results and Discussion**

### *2.3.1 Correlating DsExDR with Intracellular hIL2*

Before exploring the utility of red fluorescent markers as indicators of secreted hIL2 concentrations, it was necessary to see if the bicistronic vector would produce both proteins and if useful correlations between fluorescence and intracellular hIL2 concentrations could be obtained. Similar internal correlations, using fusional constructs between hIL2 and GFP, have been successfully obtained [124, 125]. To examine the bicistronic construct in this work, the cell line with the highest transfection efficiency, HEK293, was selected for trial studies. Transfections were performed in 24-well tissue culture plates using 0.2, 0.5, 0.8, 1.2, 1.6, and 2.0  $\mu\text{g}$  of the pF2 vector for every  $2 \times 10^5$  cells in each well. Non-transfected cells were used as negative controls for both hIL2 and DsExDR expressions. ELISAs of the intracellular fraction showed that hIL2 concentrations increased linearly with transfection DNA level when transfected with up to 1.6  $\mu\text{g}$  of pF2 plasmid (Figure 2.3A). The intracellular hIL2 concentration, however, became saturated when 2.0  $\mu\text{g}$

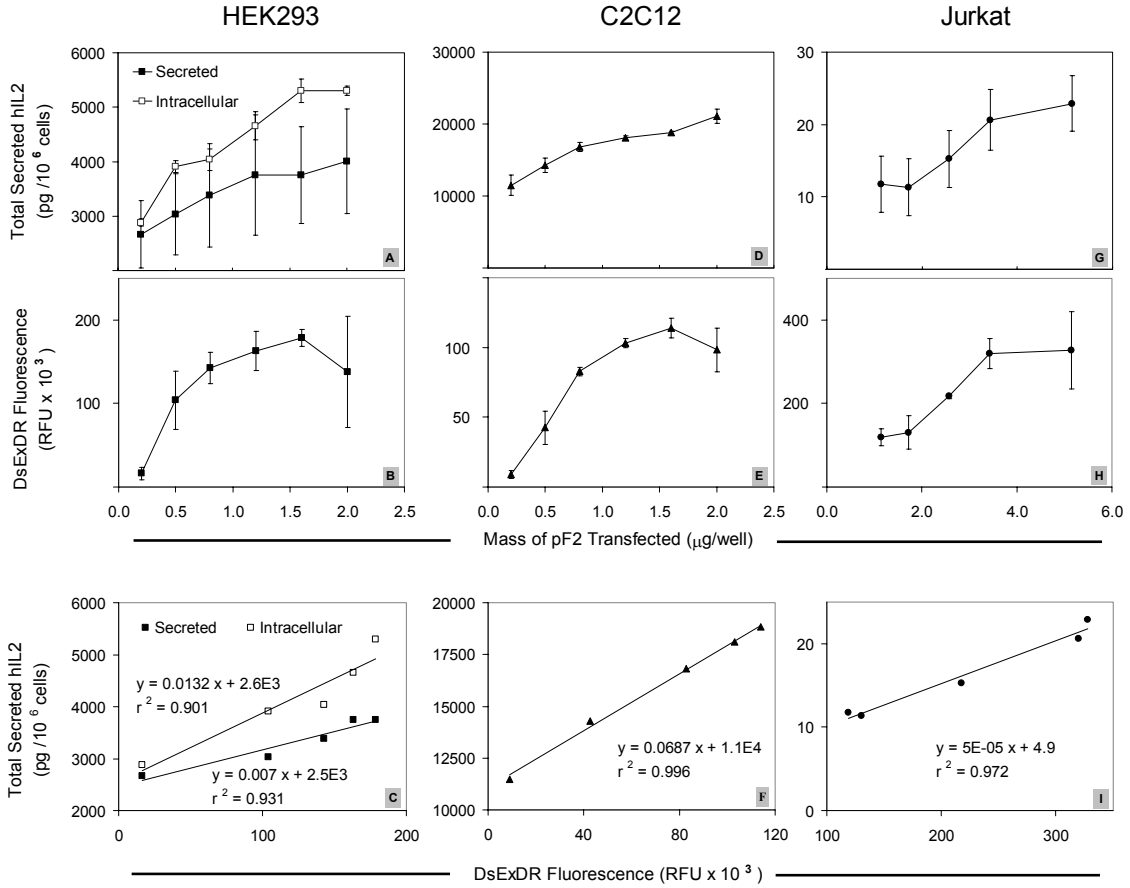


**Figure 2.3** HEK293 and C2C12 attachment cells were transfected with pF2 (0, 0.2, 0.5, 0.8, 1.2, 1.6, and 2.0 mg-DNA per 2 x 10<sup>5</sup> cells) for the bicistronic expression of Destabilized DsRed-Express (DsExDR) red fluorescent protein and secretion of human interleukin-2 (hIL2). Both cell lines secreted large amounts of hIL2 on the order of nanograms per million cells (A, D). The presence of hIL2 within HEK293 cells was also measured. These cells lines were able to express similar quantities of the intracellular red fluorescent protein (B, E). The elevated concentration of DsExDR at the highest levels of transfection resulted in decreases of fluorescence measurements in both cell lines. This was indicative of self-quenching. Strong linear correlations between the two proteins were observed in both cell lines when the last data points were omitted (C, F). A linear correlation of DsExDR with intracellular hIL2 was also present in HEK293 cells. Jurkat cells were transfected with five higher concentrations of the bicistronic plasmid pF2 (1.1, 1.7, 2.6, 3.4, and 5.1 mg-DNA per 2 x 10<sup>5</sup> cells). This cell line secreted hIL2 concentrations that were three orders of magnitude lower than the previous cells (G). This may be due to two factors that are inherent to Jurkat cells. The first is the notoriously low transfection efficiency of this line, evident by observation under fluorescence microscopy and the lack of DsExDR self-quenching at the highest pF2 transfection level (H). The second is the presence of natural regulatory mechanisms for controlling the secretion of hIL2, which is an intrinsic product of T-cells. A linear correlation was found among all concentrations of secreted hIL2 and DsExDR fluorescence in Jurkat cells (I).

of DNA was used. Measurements of DsExDR fluorescence showed a similar trend (Figure 2.3B). The highest concentration of pF2 transfected, however, resulted in a drop in total fluorescence rather than a plateaued value as found in intracellular hIL2 measurements. While untested, it is speculated that this is due to aggregation and self-quenching of DsExDR proteins in high density [108]. A linear correlation between the intracellular hIL2 concentration and DsExDR fluorescence can be seen when the highest DNA concentration datum is omitted ( $r^2 = 0.901$ ) (Figure 2.3C). These results show that DsExDR is a suitable biomarker for hIL2 production and suggests that it should be tested as a measure for extracellular hIL2.

### *2.3.2 Correlating DsExDR with Secreted hIL2 from Attachment Cells*

The examination of correlations between red fluorescence and hIL2 measurements was continued by examining secreted hIL2 from the HEK293 cells, as well as an additional attachment dependent cell line, C2C12. Transfections with pF2 vectors were performed in 24-well plates of constant volume (0.5 mL). These cultures were transfected with DNA concentrations identical to the previous intracellular hIL2 study: 0.2, 0.5, 0.8, 1.2, 1.6, and 2.0  $\mu\text{g-DNA}$  per  $2 \times 10^5$  cells in each well. ELISAs of supernatant samples derived from HEK293 cultures and sampled after 24 hrs showed a linear rise in the amount of hIL2 secreted beginning from the lowest level of DNA transfected (Figure 2.3A). The relationship between red fluorescence and secreted hIL2 concentrations also followed a strong linear correlation ( $r^2 = 0.931$ ) for all DNA concentrations below 2.0  $\mu\text{g}$  in HEK293 cells (Figure 2.3C).

The C2C12 cells exhibited a similar trend in hIL2 secretion as was observed for the HEK293 cells. It is noteworthy, however, that the amount of secreted hIL2 from C2C12 cells was approximately four times higher than that from HEK293 cells for every concentration of transfected pF2 (Figure 2.3D). DsExDR fluorescence measurements in C2C12 cells displayed a rising trend to a maximum followed by a slight decrease at the highest DNA concentration, which was analogous to the behavior found in HEK293 cells (Figure 2.3E). The datum derived from this highest DNA concentration was again omitted from regression analysis and the correlation between DsExDR fluorescence and hIL2 secretion followed a strong linear relationship ( $r^2 = 0.996$ ) (Figure 2.3F).

### 2.3.3 *Correlating DsExDR with Secreted hIL2 from Suspension Cells*

Jurkat cells were similarly transfected with the pF2 bicistronic vector to examine if the previous results can be extended to suspension type cells. Jurkat cultures were transfected with five higher concentrations of pF2 due to their lower transfection efficiencies (1.1, 1.7, 2.6, 3.4, and 5.1  $\mu\text{g-DNA}$  per  $2 \times 10^5$  cells), in 6-well tissue culture plates. The transfected Jurkat cultures exhibited little hIL2 secretion below the second lowest concentration of DNA used. Significant hIL2 secretion only began at the 1.7  $\mu\text{g}$  transfection concentration (Figure 2.3G). The level of hIL2 secretion approached a limit when 5.1  $\mu\text{g}$  of pF2 was used. The total level of protein secreted from the Jurkat cells was three orders of magnitude lower than the attachment cells (1-15  $\text{pg}/10^6$  cells vs. 10  $\text{ng}/10^6$  cells). This could be due to both a lower transfection efficiency for Jurkat cells, and the likelihood that Jurkat cells temper or otherwise regulate hIL2 secretion. As much as one order of magnitude can



be attributed to the difference in transfection efficiency of Jurkat cells (~10%) and those of C2C12 and HEK293 (~80%), which was observed by fluorescence microscopy. The low level of transfection efficiency in Jurkat cells was also evident by the absence of DsExDR self-quenching at high plasmid concentrations. The remaining orders of magnitude can be associated with the restricted secretion rates of hIL2 from Jurkat T-cells, which are natural producers of hIL2 and have many regulatory mechanisms for controlling hIL2 secretion [126]. Intracellular analyses of hIL2 were not performed to confirm this hypothesis.

The total fluorescence measurements showed a pattern of DsExDR expression that was similar to hIL2 secretion (Figure 2.3H). Unlike the previous two cell lines examined, Jurkat cells did not exhibit a quenching of fluorescence intensity at the highest level of DNA transfection. A linear regression of all values resulted in a linear correlation ( $r^2 = 0.972$ ) (Figure 2.3I). This positively demonstrated that red fluorescence measurements could also be used to deduce the amount of hIL2 secreted by suspension cell lines.

#### 2.3.4 Examining IRES – mediated Co-expression of DsExDR and hIL2 Proteins

It was of interest to see whether the secreted hIL2 was correlated one to one with DsExDR, as would be expected for a direct fusion protein expressed intracellularly [72]. To accomplish this, we plotted normalized DsExDR fluorescence levels against normalized hIL2 secretion concentrations (Figure 2.4). For each cell line, the point of normalization was based upon the optimal DNA concentration recommended for transfection by the manufacturer, Invitrogen (Jurkat = 1.1  $\mu\text{g}$ , C2C12 & HEK293 = 0.8  $\mu\text{g}$ , per  $2 \times 10^5$  cells). A slope of unity indicates a

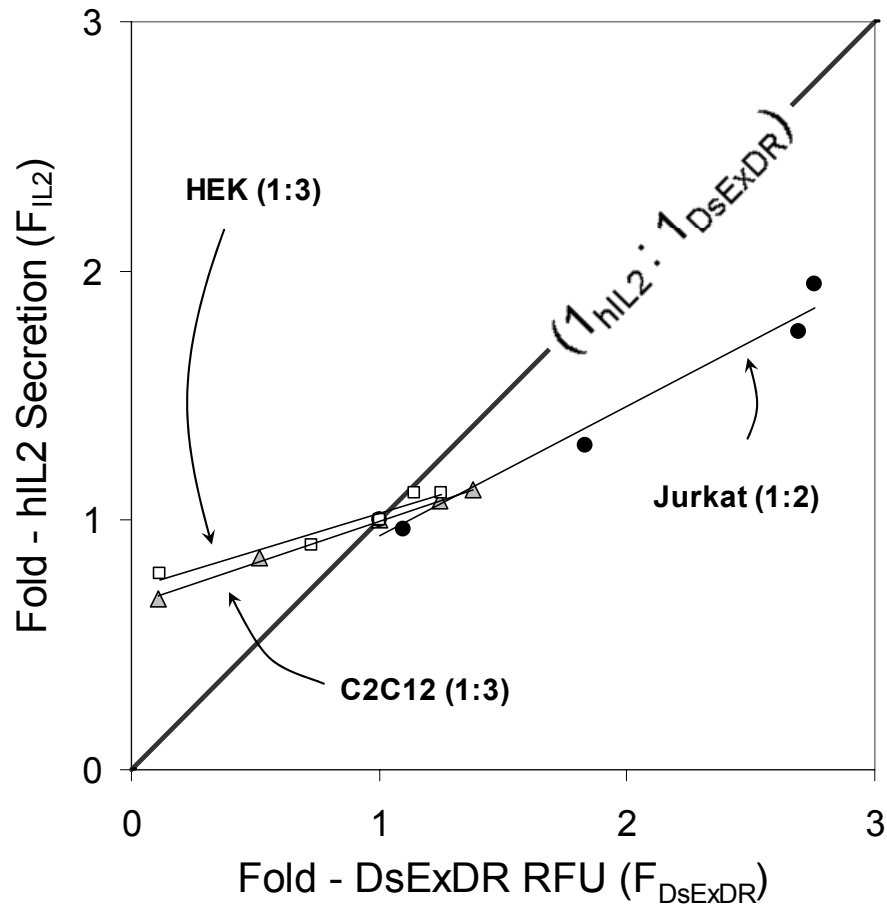


**Figure 2.4** The functionality of using the IRES bicistronic expression system among the three cell lines (Jurkat, C2C12, and HEK293) can be compared by plotting the expression of DsExDR and secretion of hIL2, each normalized by the respective data point at which the recommended transfection level was made (Jurkat = 1.1 mg, C2C12 & HEK293 = 0.8 mg). A slope of unity indicates that both proteins are accumulating at equal rates. Jurkat cells have the most balanced accumulation rate, while C2C12 and HEK293 cells accumulated slightly more fluorescent protein per hIL2 secreted.

1:1 correspondence for accumulated proteins. That is, for every DsExDR expressed and accumulated, an hIL2 protein was also expressed and secreted. As discussed earlier, the highest level of hIL2 secretion was found in C2C12 and HEK293 cells, while Jurkat cells secreted comparatively much less hIL2. When examining the normalized correlations among the cell lines, however, the Jurkat cells achieved a more balanced accumulation of both hIL2 and DsExDR molecules (1:2), as seen by a slope of 0.52 in Figure 2.4. C2C12 and HEK293 cells, though higher producers overall, accumulated slightly smaller proportions of hIL2 with respect to DsExDR (1:3). In general, the bicistronic plasmid, pF2, was successful in effecting a consistent and comparable accumulation of both marker and therapeutic proteins in three distinct mammalian cell lines.

Observations based on Figures 2.3 and 2.4 indicated that the latter two cell lines, C2C12 and HEK293, were intrinsically more efficient in protein expression, such that even low amounts of transfected DNA were sufficient for actuation. Because of these elevated efficiencies, the highest level of DNA transfected (2.0  $\mu\text{g}$ ) caused DsExDR, an internally accumulated protein, to reach a saturation limit, at least with respect to its fluorescence signal. hIL2, which is secreted from the cells, is unbound by the internal constraints or capacities of the cells, and continued to accumulate in the supernatant. Although this phenomenon created a divergence in the relationship between the amount hIL2 secreted and the DsExDR fluorescence at the highest DNA transfection level, the bicistronic system functioned quite well at all lower transfection levels (0.2 to 1.6  $\mu\text{g}$ ). Thus, applications of the pF2 vector can utilize a wide range of transfection concentrations in order to take advantage of the

bicistronic marker. Jurkat cells, which were not as efficient in secreting hIL2 as the previous cell lines, equally approached a limitation in hIL2 secretion and DsExDR expression at the highest DNA concentration (5.1  $\mu\text{g}$ ). In this case, modulating the level of transfected DNA produced a proportionally similar response in both hIL2 secretion and DsExDR accumulation.

It is noteworthy that linear correlations were obtained for all three cell lines (Figures 2.3, 2.4). A simple scaling analysis of the marker half-life ( $t_{1/2}$ ), assuming linear production and first order degradation rates for a continuously expressing stable cell line, shows that a measurement made at any time beyond steady state ( $\tau \equiv t/t_{1/2} \sim 6$ ) is equal to the quantity of protein expressed within a time frame of the immediate  $[t_{1/2}/\ln(2)]$  hours. In the case of DsExDR, which has a reported half-life of  $\sim 12$  hr, a measured fluorescence signal is then representative of how much protein, such as hIL2, was expressed in approximately the last 17 hr. The value of using a destabilized marker becomes more apparent when this bicistronic system is used in applications such as medical devices, where measurements will indicate how much therapeutic was secreted within the last 17 hr rather than over the life time of the device. Furthermore, a 17-hr window is a relatively short period when compared to the lifetime of an implant, which may be on the order of months. This in essence gives a much more responsive indication of the therapeutic production rate, as compared to reporter systems that may utilize a stable marker. As the half-life of a marker protein decreases, so does this window of representation, which in effect gives an even more discrete measurement of a system's therapeutic protein secretion rate. However, a marker protein should also not have too short of a half-life, lest it may not

accumulate enough molecules to produce a detectable fluorescent signal. Because DsExDR has an appreciable turnover rate, though long enough to accumulate a detectable signal, and also preserves the linearity of the response to hIL2 secretion, it is suggested that it is indeed highly suitable for indicating the secretion levels of a co-expressed therapeutic.

Due to the effectively discrete and linear attributes of the DsExDR signal, it is reasonable to believe that this marker is a good platform for non-invasively detecting natively secreted proteins. The generality of this approach was also demonstrated by pF2's functionality in three distinct cell lines, which varied in species, as well as attachment requirements. Such findings are thus valuable for applications such as traditional bioreactor designs, biohybrid artificial organs and regenerative tissue engineering.

## **2.4 Conclusions**

Three common mammalian cells lines, HEK293, C2C12, and Jurkat were transfected with a bicistronic vector, which enabled expression of a DsExDR red fluorescent protein marker and secreted hIL2. Both DsExDR and hIL2 were expressed from all three cell lines. The level of secreted hIL2, per total cell number, was significantly higher in C2C12 cells than in the other two. The levels expressed in Jurkat cells were by far the lowest among the three. It was found that DsExDR fluorescence was a good indicator of intracellular hIL2 in HEK293 cells. Further, it was found that DsExDR fluorescence was linearly correlated with secreted hIL2 from all three cell lines. Finally, by plotting protein levels on a normalized basis, it was determined that the Jurkat cell line had the most balanced accumulation of DsExDR

protein molecules and hIL2 molecules, with a 1:2 ratio. Though HEK293 and C2C12 cell lines had approximately 1:3 DsExDR to hIL2 accumulation ratios, they were also not far from equalized production, and may also be suitable hosts for the bicistronic system developed here. These results thus show promise for further developing *in-situ* and non-invasive methods of monitoring therapeutic protein secretion in various applications such as tissue engineering.

## **2.5 Acknowledgements**

Sincere thanks to David M. Mosser and Wenxia Song (Department of Cell Biology and Molecular Genetics (CBMG), University of Maryland, College Park) for providing the usage of the FACSCalibur flow cytometer.

### **3. Counteracting Apoptosis and Necrosis with Hypoxia Responsive Expression of Bcl-2 $\Delta$**

#### **3.1 Introduction**

Biohybrid artificial organs are implantable medical devices designed to secrete therapeutic proteins from encapsulated cells, typically mammalian in origin. In this encapsulated environment, cells often encounter a deficiency in the availability of oxygen [127] resulting in hypoxia. Since mammalian cells can only tolerate hypoxia for only a few days at best [89], necrosis and apoptosis quickly ensue. The propensity towards either cell death pathway, however, is highly dependent on the cell type [3]. The first pathway is typically the result of severe and prolonged exposure to stimuli such as oxygen deprivation. Characteristics of necrosis are cell membrane disruption, mitochondrial swelling, and loss of cytosolic structures. Apoptosis, also known as programmed cell death, is a more gradual and organized process, marked by chromatin condensation, DNA cleavage, cell size shrinkage, and cell membrane blebbing. Several extracellular strategies have been designed to deliver more oxygen to the encapsulated cells. These include inducing vascularization around the implant [4], electrochemically generating oxygen by decomposing water [5, 6], as well as using synthetic oxygen carriers [90]. An alternate method of helping cells survive hypoxia may be intracellular in nature, involving the metabolic engineering of encapsulated cells to become intrinsically more resistant to oxygen deprivation.

Bcl-2 belongs to a family of regulatory proteins that have the ability to prevent or delay apoptosis. Its activity was first described by Vaux *et al.* in 1988 as

being able to protect cells from apoptosis induced by deprivation of the hormone IL3 [91]. It was later discovered that Bcl-2 could prevent apoptosis induced by other factors, including serum deprivation, heat shock, chemotherapy agents, ethanol, and hypoxia [89, 92-95]. More recently, Bcl-2 has also been shown to inhibit necrosis induced by hypoxia and inhibition of mitochondrial respiration [96]. Since the discovery of Bcl-2, other members of this family of regulatory proteins have been discovered. Members include proteins that are anti-apoptotic (Bcl-2, Bcl-xL, Bcl-w) and pro-apoptotic (Bax, Bak, Bik, and Bid) in nature. A commonality among the members is four Bcl-2 homologous domains, BH (1-4), which may all be present but not all active in a single protein. Activity of BH3 is necessary for efficacy of pro-apoptotic members [96-98], while BH1, 2, and 4 are required for anti-apoptotic effects [9, 99]. Recent studies also indicate that a nonconserved region of peptides between BH3 and BH4, encoding an unstructured loop, is responsible for attenuating the anti-apoptotic effects of Bcl-2 and Bcl-xL. Bcl-2 $\Delta$  is a deletion mutant (residues 32-80) of the human Bcl-2 protein, yielding a variant devoid of this loop, a putative negative regulatory domain used for post-translational modifications [7-9]. In comparison to the full-length protein, the deletion mutant shows enhanced ability to inhibit apoptosis [10, 128].

The objective of this work is to investigate how Bcl-2 $\Delta$  can be used to relieve hypoxic stress. To test the effects of Bcl-2 $\Delta$  on the levels of protein production, necrosis, and apoptosis, a mouse myoblast cell line, C2C12, was transfected to express a yellow fluorescent protein (EYFP) with or without Bcl-2 $\Delta$  under the control of a strong constitutive CMV promoter. To prevent continual or unnecessary over-



production of this protein, however, the regulation of its expression was then placed under the control of a hypoxia sensitive promoter, 5HRE-hCMVmp. These vectors allowed cells to differentially express either EYFP or EYFP-Bcl-2 $\Delta$  based on the level of oxygen that is sensed. These vectors were ultimately designed for use in encapsulated cells such that they can conserve their metabolic energy and produce Bcl-2 $\Delta$  only when necessary.

## **3.2 Materials and Methods**

### *3.2.1 Cell Culture Media and Maintenance*

A murine myoblast cell line, C2C12, was used for all experiments. C2C12 was subcloned from the skeletal leg muscle cells of an adult C3H mouse, and was obtained from American Type Cell Culture (ATCC; CRL-1772, MD, USA). The myoblasts are non-carcinomas and remain undifferentiated. Cells were cultured in Dulbecco's Modified Eagle's Medium (DMEM, Invitrogen) supplemented with 1.5 g/L of NaHCO<sub>3</sub> and 5% fetal bovine serum (FBS, Sigma). Regular maintenance of the cells required subculturing every two days in 75 cm<sup>2</sup> tissue culture flasks as the population approached 80-90% confluency. To detach the cells, spent media was first aspirated, and the culture rinsed with Dulbecco's Phosphate Buffer Solution (DPBS) without Ca<sup>2+</sup> and Mg<sup>2+</sup> (DPBS-cm) (Invitrogen). Rinsed cells were then incubated in a 0.25% Trypsin with 0.03% EDTA solution (Sigma) for 5 minutes at 37 °C. Cells were passaged at a 1:10 split ratio, with 12 mL of fresh media.

### *3.2.2 Construction of Recombinant Plasmids*

Four plasmids were constructed in order to test the ability of the Bcl-2 $\Delta$  protein to be differentially induced under low oxygen conditions, as well as

counteract the ensuing apoptotic and necrotic cellular events. All plasmids contained the gene for an enhanced yellow fluorescent protein (EYFP), which served as a marker for promoter induction and protein expression. The first two plasmids (Figure 3.1) utilized the strong constitutive cytomegalovirus (CMV) promoter, which was part of the backbone vector, pIRESpuro3 (Clontech). The first construct, pCYp, contains only the EYFP gene. This gene was obtained through a polymerase chain reaction (PCR) from a plasmid, dubbed pCYbn, which was generously donated by M.J. Betenbaugh (Johns Hopkins University), using the following primers: 5'- AGA TCC GCT AGC GCT AC -3' and 5'- GTA GCG CTA GCG GAT CT -3'. These primers respectively included the NheI and EcoRI restriction enzyme sites. The PCR product was digested at these restriction sites and ligated into the corresponding sites in pIRESpuro3. The second plasmid constructed was pCYbp, which contained an EYFP-bcl2- $\Delta$  fusion gene. This fusion was obtained by directly digesting NheI and EcoRI sites in the pCYbn plasmid, and ligated into pIRESpuro3.

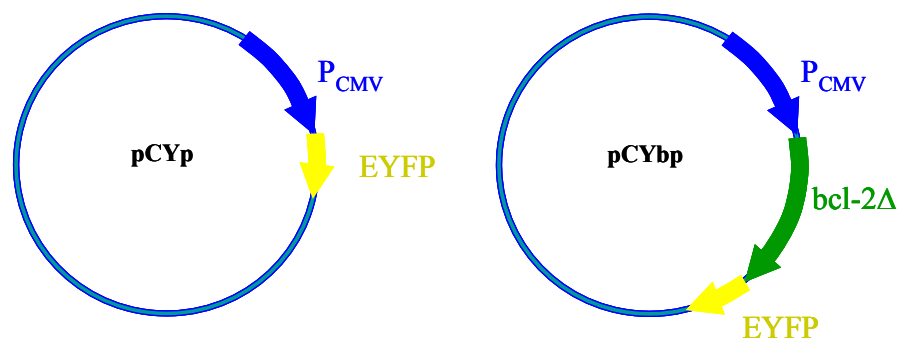


**Figure 3.1** Two plasmids, pCYp and pCYbp, contain strong constitutive CMV promoters, which permit the continual expression of protein in transfected cells. The first vector, pCYp, serves as a negative control for the effects of Bcl-2 $\Delta$  with respect to pCYbp.

The last two plasmids, pO2Yp and pO2Ybp, (Figure 3.2) were built as analogs to the first two plasmids with only a difference in the promoter used. These vectors were constructed by replacing the CMV promoters with a hypoxia-inducible promoter, 5HRE-hCMVmp (5HRE), found in the p5HRE-d2EGFP vector generously provided by J.M. Brown (Stanford University) [129]. This promoter contains five hypoxia responsive elements (HRE) fused upstream of a human cytomegalovirus minimal promoter, and is induced only under low oxygen conditions. In each case of building the last two plasmids, the original CMV promoters were first excised through digestion of the flanking restriction enzymes sites, NruI and NheI, and replaced with 5HRE-hCMVmp. The hypoxia-inducible promoter was obtained through PCR of p5HRE-d2EGFP using the following primers: 5'- TAA TTC GCG ACA TAT GGG TAC CGA GCT TTT CT -3' and 5'- GCA ATG CTA GCG AAT GCC AAG CTT CTA GT -3'. These primers respectively included the NruI and NheI restriction sites.

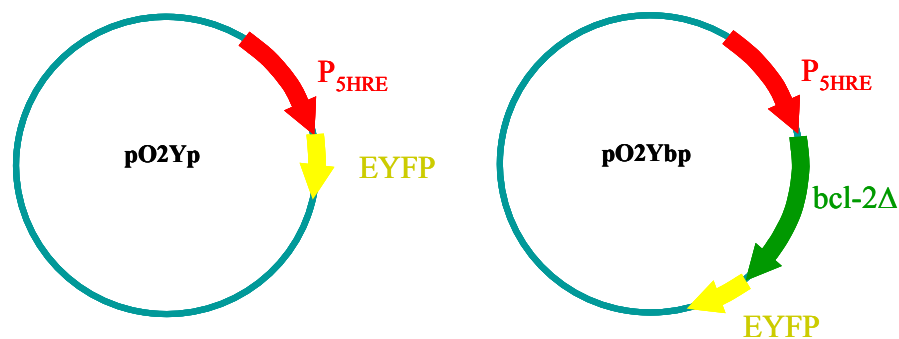


**Figure 3.2** Hypoxic induction of protein expression is achieved with the p5HRE-hCMVmp promoter, which is composed of five tandem hypoxia responsive elements (5HRE) fused to a human CMV minimal promoter (hCMVmp). The pO2Yp vector serves a negative control to pO2Ybp with respect to Bcl-2Δ.

### 3.2.3 *Transfections*

C2C12 myoblasts were transfected in both 6- and 12-well tissue culture plates (Costar) in an attached state (Table 3.1). Cells were passaged at most two days before inoculation so that they remain in a non-confluent, growing state. Cultures were harvested by trypsinization (0.5 – 1.0 mL/well of Trypsin/EDTA, 5 min, 37°C) and resuspended in fresh complete media at a concentration of  $6 \times 10^4$  cells/mL. 6-well plates were inoculated with 1mL/well of this cell solution while 12-well plates were inoculated with 0.5 mL/well. Inoculated plates were incubated for 12 hours before transfection to ensure attachment of cells. Upon transfection, a media exchange was performed on all wells, whereby the respective volumes of complete media were replaced by a serum-free media, OptiMEMI (Invitrogen). Antibiotics were never used during routine passaging nor during transfection. Transfections were accomplished by using a cationic lipid reagent, LipofectAmine Plus (Invitrogen). DNA was first combined with Plus reagent in a solution of OptiMEMI. This mixture incubated for 15min at room temperature and was added to a second vial containing LipofectAmine in a solution of OptiMEMI. Specific amounts for transfecting either 6-well or 12-well plates are detailed in Table 3.1. This final mixture was also allowed to incubate for 15min at RT for the DNA-Lipid complexes to form, and then pipetted into each well drop-wise such that it did not disturb the attached C2C12 cells.

**Table 3.1** Transfection Protocol for C2C12 in 6- and 12-well tissue culture plates.

Format	Plasmid ( $\mu\text{g}$ )	Plus ( $\mu\text{L}$ )	OptiMEMI ( $\mu\text{L}$ )	LipofecAmine ( $\mu\text{L}$ )	OptiMEMI ( $\mu\text{L}$ )
6-well	1.2	6	100	3.4	100
12-well	0.7	5	50	2.0	50

### 3.2.4 Hypoxic Chambers

In order to simulate the various hypoxic conditions needed to induce apoptosis, as well as promoter response, cell culture plates were placed in individual hypoxic chambers within a CO<sub>2</sub> incubator. Each chamber was connected to its own particular mixture of gas. As the gas enters the incubator, it is first passed through a 1 liter fine bubble column, where it is humidified and heated before entering the individual hypoxic chambers. Each chamber was fashioned from a 1-L plastic tray with a non-hermetic lid. As the gas enters the chamber, it fills and saturates the headspace before exiting. Gas exchange was facilitated by placing all hypoxic chambers on a rocker platform (Boekel). The entire experimental assembly is depicted in Figure 3.3. A kinetic measurement of the dissolved oxygen concentration in a mock culture, which contained 1 mL of complete media, showed that steady state was reached at approximately one hour for a 0% O<sub>2</sub> gas mixture flowing at 0.5 L/min (Figure 3.4). Dissolved oxygen was measured using a Clark-type dissolved oxygen probe with an OM4 Oxygen Meter (Microelectrodes).

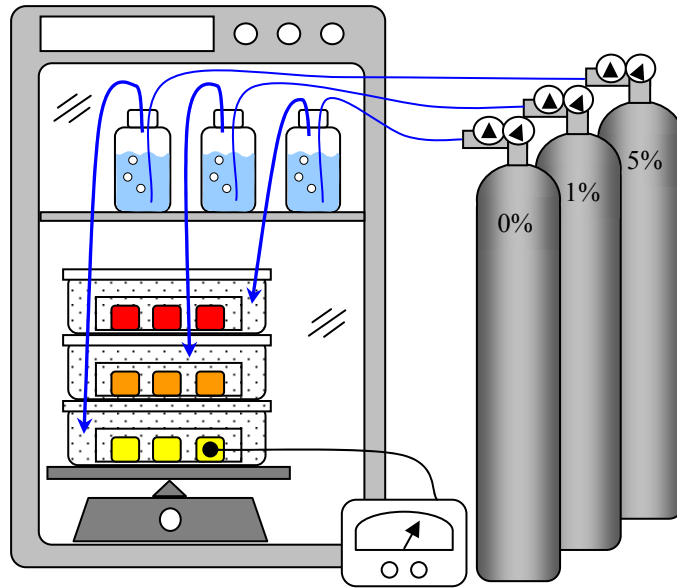


**Figure 3.3** The hypoxic incubation system is composed of individual hypoxic chambers placed upon a rocker platform within a CO<sub>2</sub> incubator. Each chamber is connected to its own gas tank via a bubble column, which humidifies and warms the incoming air. The gas environment within each chamber is determined by the premixed composition of the compressed gas cylinders. Mix gas flows at 0.5 L/min. The chambers and bubble columns are each 1L in volume. Dissolve oxygen content in tissue cultures plates with 1mL of media is monitor by a Clark-type dissolved oxygen probe and OM4 Oxygen Meter (Microelectrodes).

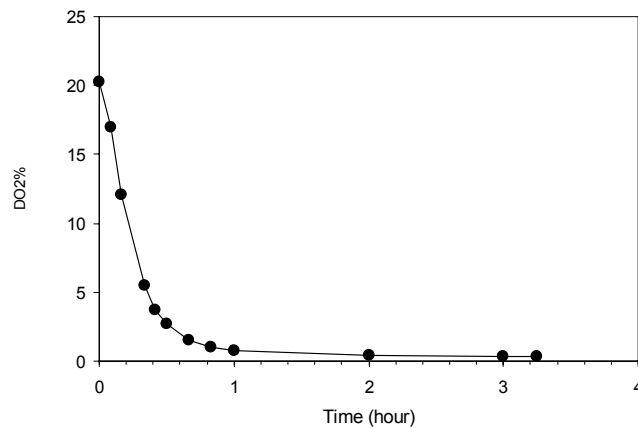


**Figure 3.4** Kinetic measurements of dissolved oxygen content within a 1mL mock culture were made to ensure that cells were exposed to the intended hypoxic environments. A 0 % O<sub>2</sub> gas mixture was directed into a rocking hypoxic chamber (0.5 L/min, 37 oC), which contained the mock culture. Steady state was reached in approximately 1 hour.

### 3.2.5 *Flow Cytometry of EYFP Recombinant Proteins*

The choice of using EYFP as a fusion partner to Bcl-2 $\Delta$  enabled the tracing of its production by means of flow cytometry. When EYFP was produced alone, its fluorescence serves as an indicator of overall cell productivity. Cell samples were collected by aspirating the culture media and rinsing with DPBS-cm. To detach the cells, wells were filled with either 300  $\mu$ L of Trypsin/EDTA for 6-well plates or with 500  $\mu$ L of Trypsin/EDTA for 12-well plates. Samples were incubated for 5 min at 37°C before centrifuging (500  $\times$  g, 5min) and fixing the cells in 300  $\mu$ L of DPBS-cm + 3.7% paraformaldehyde (DPBS-cmf). Samples were stored in 5mL polystyrene culture tubes at 4°C until they were ready for analysis. All analyses were performed with a FACSCalibur (Becton Dickinson, Immunocytometry) three-color flow cytometer (FL1=530/30, FL2=585/42, FL3=670LP) equipped with a single Argon laser (488nm), generously provided by D.M. Mosser (University of Maryland, College Park). Ten thousand cells were analyzed in each sample. The detectors were used with the following settings: FSC = 1, SSC = 350, and FL1 = 380 to 412.

### 3.2.6 *Viability Assay*

Cell viability was determined by a dye exclusion assay using 7-amino-actinomycin D (7-AAD) (Beckton Dickinson, Pharmingen). Cells samples were collected by centrifuging the combined supernant media and trypsinized cells. This ensures that any cells that may have died and detached from the wells were taken into consideration for viability measurements. Samples were then resuspended in DPBS-cm + 5% FBS (DPBS-cms) in order to neutralize any trypsin that may have remained. 100  $\mu$ L of a 10  $\times$  dilution of 7-AAD in DPBS-cms was added to each sample, and

allowed to incubate for 10min in the dark at room temperature. Formaldehyde was not used in this procedure. Samples were immediately placed on ice and analyzed after collection. Fresh cells that were not transfected were processed in the same way to serve as a negative control for 7-AAD. The FACSCalibur flow cytometer with an FL3 = 400 setting was used to detect the viability dye.

### 3.2.7 *Apoptosis Assay*

The level of apoptosis in the cell samples was assessed with an anti-caspase-3 apoptosis kit (BD Pharmingen). Cells were collected similarly to the viability assay. Samples were resuspended in a cold Cytofix/Cytoperm (500  $\mu$ L) solution for 20 min on ice, in order to fix the cells, as well as to permeate the membranes for the subsequent antibody staining. Cells were washed with a Perm/Wash Buffer (PWB) (500  $\mu$ L, RT) before 120  $\mu$ L of the anti-caspase-3 antibody solution was added to each sample. This was allowed to incubate for 30 min at RT before the samples were washed twice with cold PWB (4  $^{\circ}$ C). Final samples used for flow cytometry analyses were resuspended in PWB. The antibody, which was conjugated to phycoerythrin (PE) was detected on FL2 = 493. As a positive control, cells were incubated for 4 hours with a 6  $\mu$ M (final concentration) solution of camptothecin (Sigma), which is a potent inducer of apoptosis [10]. Since all transfected cells produced EYFP, which has some overlapping emissions from FL1 into FL2, it was necessary to have one complete set of samples that were not stained with the conjugated antibody to serve as a background fluorescence reading for all apoptosis data.



### 3.2.8 *Fluorescence Microscopy*

EYFP fluorescence was helpful as an indicator for successful transfection of cells. Fluorescence was verified with an Olympus BX60 fluorescent microscope equipped with a UMN-B filter cube (Exciter BP470-490, Dichroic DM500, Emitter BA515 LP). Cell cultures were removed from tissue culture plates by trypsinization and washed with DPBS-cm in order to minimize the background autofluorescence of media. Cells were then placed on a microscope slide with a cover slip before imaging.

## 3.3 **Results and Discussion**

### 3.3.1 *Differential Hypoxic Induction of Protein Production*

In order to verify the sensitivity of the 5HRE promoter within the vector constructs to hypoxic induction, C2C12 cells transfected with either p5HRE-d2EGFP or pO2Ybp were compared for their levels of fluorescent protein production under five oxygen conditions. Cells inoculated in 6-well plates were placed in individual hypoxic chambers with gas mixtures containing either 0.0, 0.5, 1.0, 2.0, 5.0, or 21.0 % O<sub>2</sub> plus 5% CO<sub>2</sub>, and a balance of N<sub>2</sub>. Cells were first incubated under ambient oxygen conditions for 36 hours post-transfection (hpt) before they were exposed to the various oxygen conditions for another 18 hours. Under these environments, the level of protein induction from the highest to lowest oxygen concentrations were respectively 3.2 and 2.5 fold for each of the plasmids (Figure 3.5).

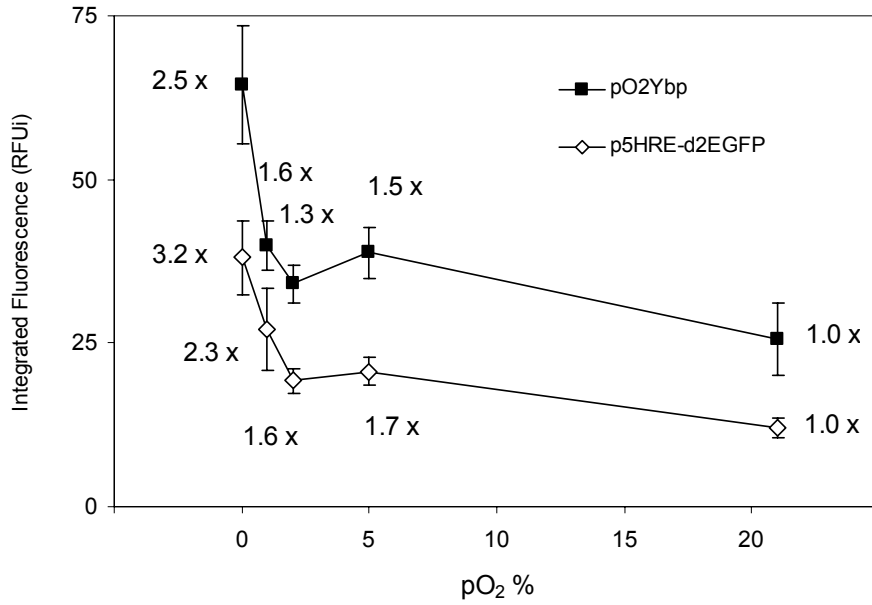


**Figure 3.5** C2C12 cells transfected with pO<sub>2</sub>Ybp and p5HRE-d2EGFP were compared for their ability to hypoxically induce fluorescent protein production. Cells were exposed to five oxygen concentrations (0.0, 0.5, 1.0, 2.0, 5.0, 21.0 %) and assayed after an 18 hour incubation. C2C12 cultures transfected with pO<sub>2</sub>Ybp produced enhance yellow fluorescent protein (EYFP) in a similar fashion to those transfected with p5HRE-d2EGFP produced destabilized enhance green fluorescent protein (d2EGFP). EYFP fluorescence, however, was higher than EGFP at every O<sub>2</sub> concentration. This is most likely due to the short, 2-hour half-life of the destabilized EGFP. Both transfections indicated that a decrease in O<sub>2</sub> content is able to exponentially induce fluorescence.

The fluorescence in cells transfected with pO2Ybp was consistently higher than those transfected with p5HRE-d2EGFP at every oxygen level despite their similar quantum yields (61% and 60%, respectively). This difference was most likely due to the fact that the latter plasmid expressed a destabilized form of EGFP, with a half-life of only two hours rather than over 24 hours as is the case with EYFP. The decrease in the partial pressure of oxygen did not induce a linear response in the level of fluorescence, but was more exponential in nature. This trend was supported by previous studies made with the 5HRE promoter [69, 130, 131]. Furthermore, there appeared to be a slightly higher than expected rise in fluorescence at the 5.0% O<sub>2</sub> level, resulting in a non-monotonic rise in the otherwise exponential trend for both d2EGFP and EYFP induction. This phenomenon may reflect the evolutionarily optimized state for cellular metabolism, since the 5% O<sub>2</sub> gas environment more closely simulated natural mammalian physiological conditions [12].

Upon verifying that the hypoxia inducible promoter was functioning properly within pO2Ybp, we compared how each of the four constructed vectors responded to variations in oxygen partial pressure. Cells inoculated in 6-well plates were placed in individual hypoxic chambers with gas mixtures containing either 0.0, 0.5, 1.0, 2.0, 5.0, or 21.0 % O<sub>2</sub> plus 5% CO<sub>2</sub>, and a balance of N<sub>2</sub> for 30 hours starting from 24 hpt. C2C12 transfected with pO2Yp showed similar trends in expression of EYFP as those transfected with pO2Ybp (Figure 3.6).

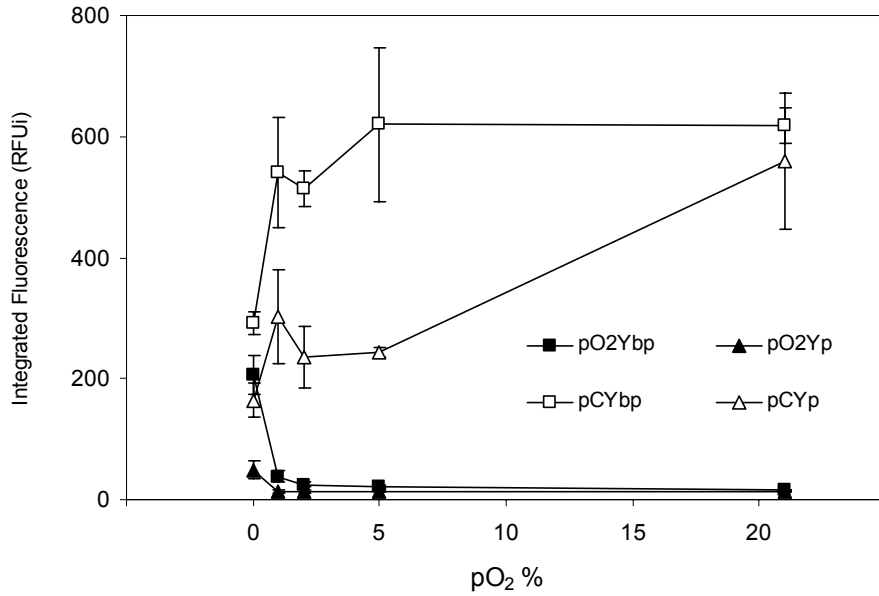


**Figure 3.6** C2C12 cells were transfected with either pCYp, pCYbp, pO2Yp, or pO2Ybp expression vectors and incubated for 30 hrs under various hypoxic conditions (0.0, 0.5, 1.0, 2.0, 5.0, or 21.0 % O<sub>2</sub> plus 5% CO<sub>2</sub>, and a balance of N<sub>2</sub>) beginning at 24 hours post-transfection (hpt). Cells that were transfected with the hypoxia sensitive promoters showed increased fluorescence with a decrease in O<sub>2</sub> concentration. Cells that contained the CMV promoter, however, displayed an opposite trend despite their overall higher levels of fluorescence at all oxygen concentrations. This decrease in fluorescence was indicative of metabolic stress due to hypoxia. In all C2C12 culture, it was clear that the presence of Bcl-2 $\Delta$  was helpful to the cells' protein production capabilities.

The characteristic bump at the 5% O<sub>2</sub> condition, however, was not as apparent. Nevertheless, the culture that expressed Bcl-2Δ showed a consistently higher level of protein production at all oxygen concentrations. This difference became even more dramatic as the oxygen level decreased and hypoxia-induced apoptosis came into effect. Thus, the presence of Bcl-2Δ apparently gave these cells a metabolic advantage. Myoblasts that were transfected with pCYbp and pCYp, showed an overall higher level of fluorescence compared to the hypoxia sensitive transfectants. As expected, the CMV promoter allows a significant level of protein production despite limited oxygen availability. Thus, despite the strength of the promoter, the trend in production suffered as the level of oxygen also decreased. Similar to the relationship among cells transfected with the 5HRE promoter, Bcl-2Δ conferred a metabolic advantage to the cells transfected with pCYbp over those with pCYp.

### 3.3.2 *Transient Expression of Heterologous Proteins under Hypoxic Condition*

C2C12 myoblasts were transfected with the four constructed plasmids, pCYp, pCYbp, pO2Yp, and pO2Ybp, were monitored over a 24 hour period to study their transient behavior under hypoxic conditions. Cells were placed under a 2% O<sub>2</sub> gas mixture environment for 24 hours post-transfection (hpt), and monitored ever 8 hours thereafter. Myoblasts that contained the plasmids with the CMV promoter had significantly higher fluorescence intensities compared to those containing the 5HRE promoter (Figure 3.7).

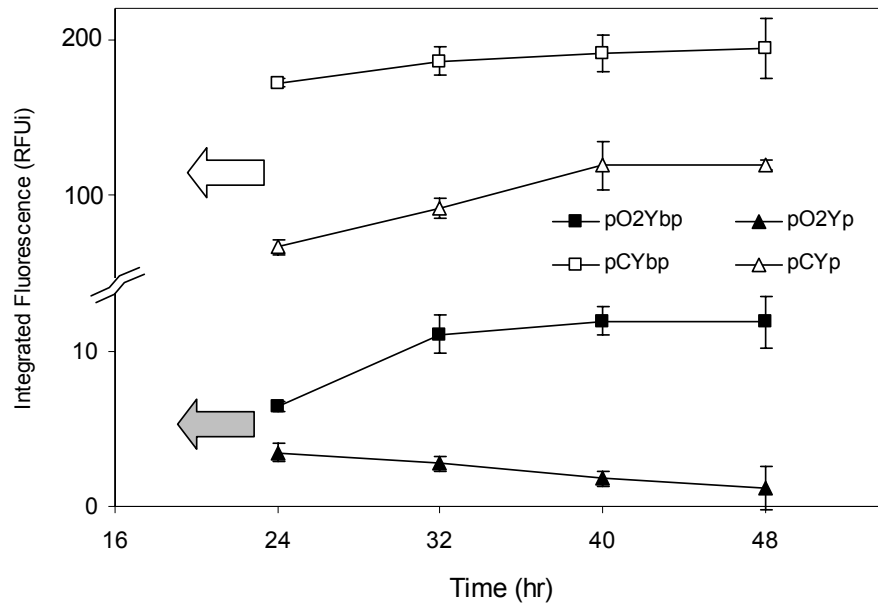


**Figure 3.7** C2C12 cells were transfected with either pCYp, pCYbp, pO2Yp, or pO2Ybp expression vectors and monitored for 24 hrs when grown under a 2% O<sub>2</sub> hypoxic environment beginning at 24 hpt. All transfections, besides pO2Yp, showed an increase in EYFP fluorescence within the 24 hours. Although this phenomenon was expected for cells containing hypoxia inducible promoters, those without were apparently unencumbered within the exposure period. All myoblasts that were able to express Bcl-2Δ were able to produce more EYFP than their deficient counterparts. This indicated the production advantage of having the anti-apoptotic protein. Myoblasts that were transfected with pO2Yp, had neither the *bcl-2Δ* gene, nor the brute capability of the CMV promoter, and thus lagged in EYFP production as time progressed.

Within each pair of promoter constructs, the cells that contained the Bcl-2Δ gene produced more fluorescence in comparison to those without. All plasmids beside pO2Yp showed an increase in EYFP production as a function of time, up to 48 hpt. This phenomena in cultures that did not have the hypoxia inducible promoter indicated that the strength of the CMV promoter was not hindered by the 2% O<sub>2</sub> environment within the 24 hour exposure. Among the cells that contained the 5HRE

promoter, only those that produced Bcl-2 $\Delta$  showed an increase in fluorescence as a function of time. Thus, without the enhancement of Bcl-2 $\Delta$ , the induction of the 5HRE promoter was not enough to overcome the detriment of hypoxia over a 24 hour period.

### *3.3.3 Bcl-2 $\Delta$ Protection of Cells under Hypoxic Stress*

In order to truly gauge the applicability of producing Bcl-2 $\Delta$  for protecting encapsulated cells, which face extended periods of hypoxia, it was important to not only examine the level of protein production, but also the levels of cell viability and apoptosis in treated cultures. These parameters will give a better measure of the long-term health and metabolic productivity of the cells. To accomplish this, cells transfected with the hypoxia inducible promoter vectors were placed under five different oxygen conditions and analyzed for their viability as well as their apoptotic levels. As hypothesized, the cells that produced Bcl-2 $\Delta$  had a consistently higher level of viability than those that were without the anti-apoptotic protein. Furthermore, these cells had lower levels of apoptosis (Figure 3.8). Thus, the production of Bcl-2 $\Delta$  was not only able to enhance the immediate protein productivity of its host, but also provided long term protection by reducing hypoxia induced necrosis and apoptosis.

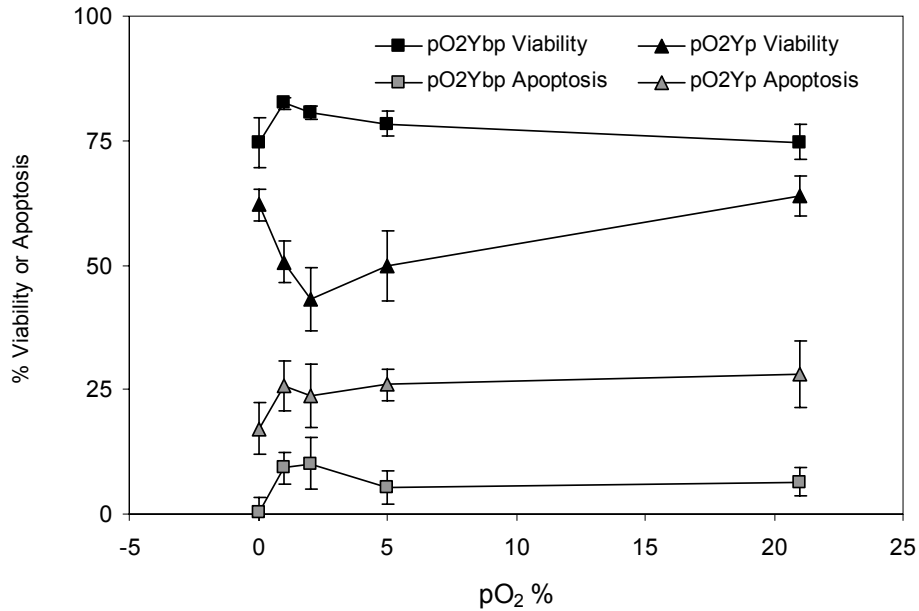


**Figure 3.8** The protective nature of Bcl-2 $\Delta$  against hypoxia can be more accurately accessed through measurements of necrosis and apoptosis in the host. C2C12 cells that were transfected with either pO2Ybp and pO2Yp were exposed to five hypoxic environments (0.0, 0.5, 1.0, 2.0, 5.0, or 21.0 % O<sub>2</sub> plus 5% CO<sub>2</sub>, balance N<sub>2</sub>) for 30 hours beginning at 24 hpt. Myoblasts that were able to express Bcl-2 $\Delta$  were able to sustain both a higher level of viability, as well as lowered levels of apoptosis. Thus, Bcl-2 $\Delta$  was successful in not only enhancing protein production, but also the long term health of the host cells under hypoxic stress.

### 3.4 Conclusions

C2C12 mouse myoblasts transfected with pO2Ybp were compared to those transfected with the original plasmid vector, p5HRE-d2EGFP, in order to verify the sensitivity of the hypoxia inducible construct. Both transfectants show a similar trend for upregulation of fluorescence protein production as the oxygen level dropped from 21% to 0%. The induction was exponential in nature, showing a dramatic rise below the 5% O<sub>2</sub> level. Three additional vectors were constructed in order to compare the efficacy of Bcl-2 $\Delta$ , as well as the hypoxia inducible promoters. When cells were



placed under the various oxygen conditions (0.0, 0.5, 1.0, 2.0, 5.0, or 21.0 %), those that contained the vectors with CMV promoters (pCYbp, pCYp) produced significantly more fluorescence than those with the 5HRE promoters (pO2Ybp, and pO2Yp). However, cells that contained the hypoxia sensitive promoters were able to produce more protein as the oxygen levels decreased, whereas those with the constitutive CMV promoters declined in protein expression. Within each type of promoter construct, cells that were able to manufacture Bcl-2 $\Delta$  were always able to out-produce EYFP as compared to those that were unable. This indicated that Bcl-2 $\Delta$  was crucial for helping the cell's metabolic functions despite the promoter system used. An examination of the transient expression of EYFP by these four plasmids also indicated the same effects of Bcl-2 $\Delta$  and 5HRE. In order to prove the utility of Bcl-2 $\Delta$  in counteracting hypoxia in an encapsulation environment, it was necessary to examine the long-term health of the transfected cells. Cells transfected with pO2Ybp not only indicated a higher viability when compared to those transfected with pO2Yp, but also a lower level of apoptosis at every oxygen level tested. Thus, the differential expression of Bcl-2 $\Delta$  using the 5HRE promoter has been shown to enhance not only protein productivity under hypoxic conditions, but also resistance to necrosis and apoptosis.

### **3.5 Acknowledgements**

Sincere thanks to Michael J. Betenbaugh and Bruno Figueroa (Johns Hopkins University) for their donation of the *EYFP-bcl-2 $\Delta$*  fusion gene, J. Martin Brown (Stanford University) for his donation of the 5HRE-hCMVmp hypoxia-inducible

promoter, and David M. Mosser (University of Maryland, College Park) for providing the usage of the FACSCalibur flow cytometer.

## **4. Biocompatible Cellular Scaffold for Encapsulating Cells**

### **4.1 Introduction**

In the field of tissue engineering there is great interest in designing cellular scaffolds that are not only biocompatible, but also physically and biochemically robust. Hydrogels made from thermally cooled gelatin are one of the most commonly used support matrices for mammalian cell growth [12]. The prevalence of gelatin hydrogels is due mainly to their ability to closely simulate the native environment of mammalian cells since gelatin is the basic building block of collagen, a major component of the extracellular matrix (ECM) [12-14]. The employment of these natural biopolymers thus offers a growth medium that is highly biocompatible with encapsulated cells, as well as host tissues. Nevertheless, these physical gelatin hydrogels are prone to premature degradation by proteolytic enzymes, such as gelatinase and collagenases or by simply melting [12]. Many researchers have sought to create more permanent hydrogels by using either uv-light or chemical crosslinkers (*e.g.* glutaraldehyde, carbodiimide, diphenylphosphoryl azide) [13, 20, 117]. Despite the improved mechanical strength and proteolytic stability of these hydrogels, the crosslinkers often elicit either cytotoxic side-effects or immunological responses from the host [15-20]. These effects in turn diminish their overall applicability as crosslinking agents. Thus, there is a need to develop cellular scaffolds that do not make concessions for either the biocompatibility or the physical and biochemical stabilities of the hydrogel.

To overcome the need to compromise either property, a naturally occurring protein crosslinking enzyme, transglutaminase, was used in this part of the work to

form thermally stable hydrogels from gelatin. Transglutaminase functions by catalyzing the formation of covalent N  $\epsilon$ -( $\gamma$ -glutamyl) lysine peptide bonds between individual gelatin strands in order to form a permanent network of polypeptides [21, 22]. This enzyme is ubiquitous in nature, being found among many species of the plant and animal kingdoms (*e.g.* peas, oysters, shrimps, tunas, chickens, cows, and humans) [23]. Microbial transglutaminase (mTG) is one form of the protein that is also innocuous [23]. This enzyme is commonly used in food manufacturing processes that are approved for human consumption by the US Food and Drug Administration [21]. The functional independence of mTG with respect to proenzymes or calcium ions, and its high level of activity over a wide range of temperatures ( $\sim$ 50% at 37°C, max at 50°C) and pH values ( $\sim$ 90% between 5 to 8), makes the enzyme amenable to a wide variety of gel formation and cell encapsulation techniques and conditions [132-134]. The improved mechanical strength and short amount of time ( $<$  30 min for 4% gelatin at 37 °C) that mTG needs to form a permanent gelatin network also makes this type of hydrogel appropriate for live surgery procedures, as well as injectable tissue engineering applications [135]. To advance the usage of mTG towards these applications, the work here seeks to (1) demonstrate the biocompatibility of mTG crosslinked gelatin hydrogels as 3D cellular scaffolding media, and (2) to characterize the tuneable degradability of these hydrogels. Biocompatible cellular scaffolds with customizable degradation rates can potentially be utilized in a wide variety of applications, ranging from the immunosolative encapsulation of cells to time-released delivery of cells for regenerative medicine.

## 4.2 Materials and Methods

### 4.2.1 Maintenance of Cell Cultures

The attachment dependent human embryonic kidney cell line, HEK293 (Flp-In™-293, Invitrogen) was cultured in Dulbecco's Modified Eagle's Media containing high glucose (4.5 g/L), GlutMAX™ I (3.97 mM) (DMEM, Invitrogen), with added fetal bovine serum (10%, FBS, Sigma), and zeocin (100 mM, Invitrogen) (complete media). Cells were cultured in 75 cm<sup>2</sup>-tissue culture flasks (Costar) and subcultured every two to three days as the population approached 80-90% confluency. Cells were passaged by first aspirating the spent media and then rinsing with Dulbecco's Phosphate Buffer Solution without Ca<sup>2+</sup> or Mg<sup>2+</sup> (DPBS-cm, Invitrogen). Rinsed cells were then incubated in 2 mL of a 0.25% Trypsin with 0.03% EDTA solution (Sigma) for 5 minutes under their normal growth environment (37 °C, 8% CO<sub>2</sub> incubator). Cells were passaged with a 1:10 split ratio and supplemented with fresh complete media up to 12 mL for further growth.

### 4.2.2 Cell Encapsulation and Culture

Three dimensional cell encapsulates were formed by mixing HEK293 cells with 4% gelatin and mTG solutions. Both gelatin and mTG stock solutions were sterile filtered and equilibrated in a 37 °C water bath for 20 min prior to mixing with cells in order to prevent heat shock. Encapsulates were formed in white-wall, clear-bottom, 96-well tissue culture plates (Costar) with 60 µL/well. HEK293 cells were used at a density of 2,000 cells per 60 µL. Mixtures of cells and gel were immediately aliquoted into well plates in order to avoid thermal cooling. The cell

encapsulates were incubated under normal cell culture conditions (37 °C, 8% CO<sub>2</sub>) with an overlay of 100 µL of complete media.

#### 4.2.3 *In Situ Cell Proliferation Assay*

The proliferation of encapsulated HEK293 cells was monitored with two membrane-permeable nucleic acid dyes, SYTO-16 and Hoechst 33342 (Molecular Probes; Invitrogen). Although both dyes can bind DNA, SYTO-16 can also stain RNA, cytoplasm, and mitochondria. Both dyes have the property of fluorescing only when bound to nucleic material, but not while they are free nor simply interacting with proteins such as gelatin. Cell encapsulates were stained within the 96-well plates by first aspirating the media overlays and then incubating each well with 60 µL of either dye at 2x concentrations (SYTO-16 = 2 µM, max Ex/Em = 489/520 nm; Hoechst 33342 = 20 µg/mL, max Ex/Em = 350/460 nm). Stock reagents were made with Dulbecco's Phosphate Buffer Solution (DPBS, Invitrogen), and stored in the dark at 4 °C until needed. The fluorescence of stained cells was measured with a LS55 fluorescence microplate reader (Perkin Elmer). Since fluorescence intensity measurements were found to vary with incubation time (data not shown), an arbitrary incubation period of 4 hr was fixed for all *in situ* assays. Calibration curves between cell number and fluorescence intensity within each well were developed for both SYTO-16 and Hoechst 33342 stains. SYTO-16 staining produced a nonlinear correlation between cell number and fluorescence, presumably due to saturation (Figure 4.1). This was less suitable as a calibration curve as compared to Hoechst 33342 staining, which yielded a linear fit between 0 to 40,000 cells/well.

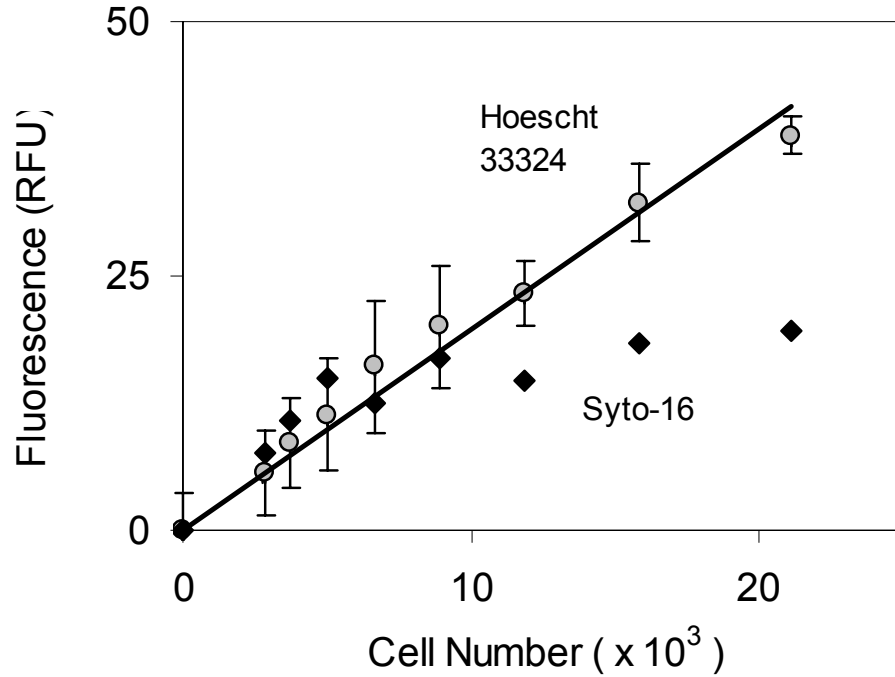


**Figure 4.1** In situ monitoring of proliferation for gelatin encapsulated cells was attempted with both SYTO-16 and Hoechst 33342 nucleic acid dyes. SYTO-16 staining produced a non-linear relationship, while Hoechst 33342 staining generated a linear correlation of  $5.05 \times 10^5$  cells/RFU ( $r^2 = 0.98$ ). This calibration curve was generated from HEK293 cells encapsulated in 60  $\mu$ L of 4% mTG-Gel in 96-well plate using a 4 hr incubation period.

### 4.3 Results and Discussion

The proliferation of mTG-Gel encapsulated HEK293 cells, with an initial concentration of 2,000 cells/well, was monitored with Hoechst 33342 staining for a three week period. Negative controls using gelatin hydrogels without any cells were made for each sampling time point. Cell numbers were calculated by multiplying the normalized ratio of fluorescence intensity ( $RFU_{\text{sample}} / RFU_{\text{negative control}}$ ) by the initial cell concentration. A plot of these values indicated that HEK293 cells were indeed proliferating within the hydrogels at a linear growth rate of  $0.03 \text{ day}^{-1}$  (Figure 4.2).

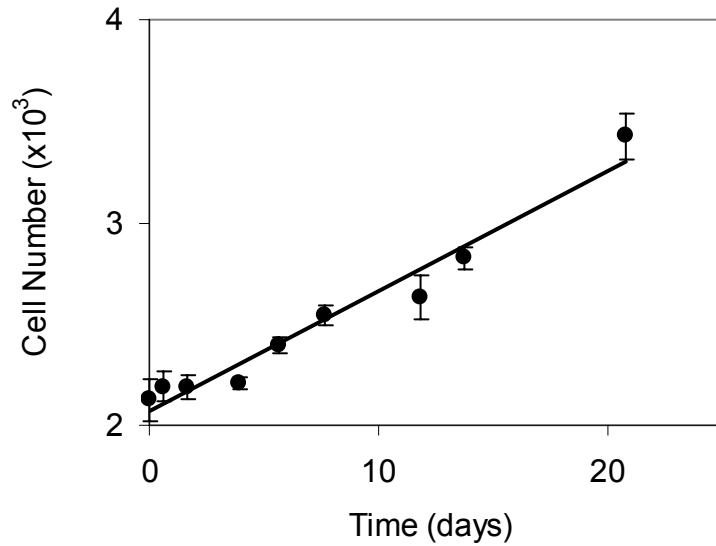


**Figure 4.2** HEK293 cells (2,000 cells/well) were encapsulated in the mTG crosslinked gelatin hydrogels (60  $\mu\text{L}$ /well) were initially seeded into 96-well plates with white walls and clear bottoms. Hoechst 33342 staining (4 hr incubation) showed that encapsulated cells were growing in clusters, and proliferating at a linear rate of approximately  $0.03 \text{ day}^{-1}$  ( $r^2 = 0.95$ ).

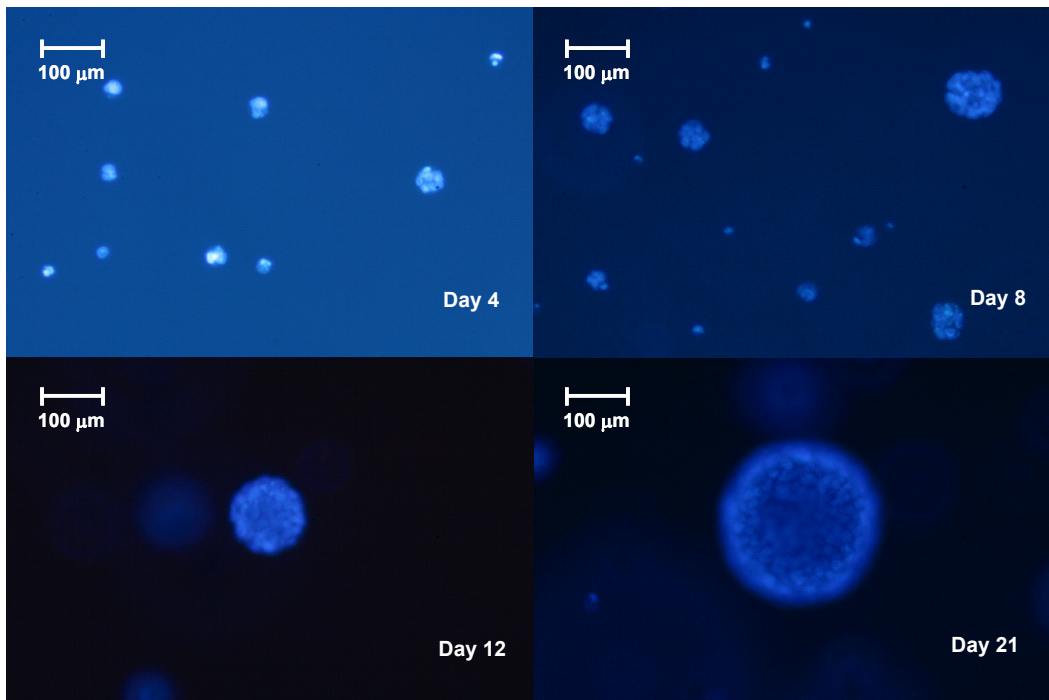


**Figure 4.3** HEK293 cells stained with Hoechst 33342 nuclear dye can be seen proliferating while they are encapsulated in mTG crosslinked gelatin hydrogels. Cells formed spherical clusters and proliferated linearly with time.



Images of the fluorescently stained cells (Figure 4.3) showed that singly encapsulated cells were replicating in place and forming cellular clusters within the hydrogels. Similarly, encapsulated HEK293 cells that were cast in 6-well tissue culture plates and grown for over one month were also observed to form clusters 1-2 mm in diameter. When the hydrogels were masticated and incubated in a 0.25% Trypsin + 0.03% EDTA solution at 37 °C for 20 minutes, the cell clusters were released. These clusters, when incubated under normal cell culturing conditions, were able to spread out and re-colonize plate surfaces (Figure 4.4A). Released cells that were of smaller cluster sizes or even singlets were also able to re-attach and propagate (Figure 4.4B). Since clusters could only have formed within the 3D environment of the hydrogels, these results definitively prove that HEK293 cells were indeed viable over a one month period while encapsulated in the mTG crosslinked gelatin hydrogels.

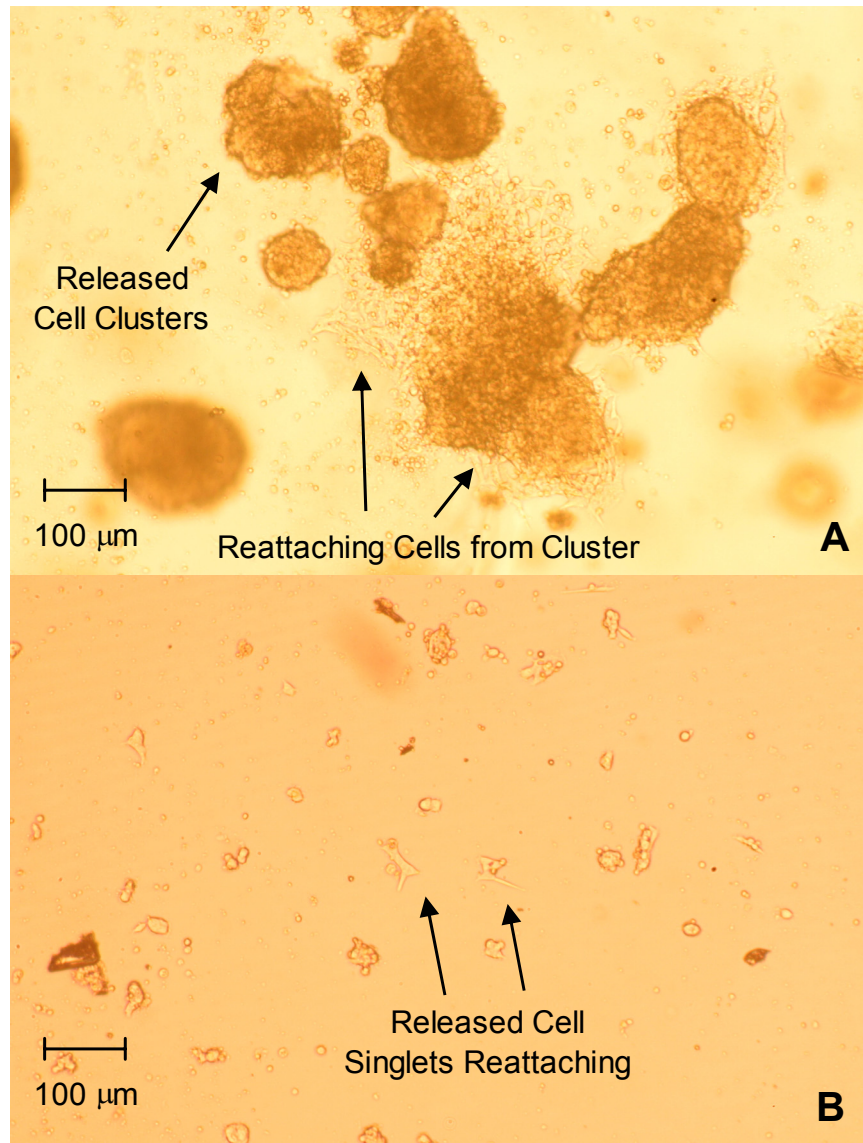


**Figure 4.4** Encapsulated HEK293 cells were released by masticating the mTG-Gels followed by a 20 minute incubation with a 0.25% Trypsin + 0.03% EDTA solution at 37 oC. Released cells appeared as clusters (A), as well as singlets (B). Both of these forms of released cells were able to re-attach to tissue culture plates under normal incubation conditions (37 oC, 8% CO<sub>2</sub>).

#### **4.4 Conclusions**

The objective of this portion of the work was to demonstrate that gelatin hydrogels, crosslinked by microbial transglutaminase (mTG), were biocompatible towards encapsulated cells, such that they may be used as a 3D cellular scaffold. The ability of HEK293 cells to proliferate within the hydrogel, as well as to re-attach to cell culture surfaces once released from encapsulation proved that mTG crosslinked hydrogels were indeed biocompatible.

## **5. Transglutaminase Crosslinked Gelatin Hydrogels as Tissue Engineering Scaffolds**

### **5.1 Introduction**

From previous work we have demonstrated that mTG-Gels are indeed compatible with encapsulated mammalian cells. To further extend the applicability of mTG-Gels, however, it is also important to demonstrate how well these hydrogels can withstand thermal and proteolytic degradation, which are major concerns for natural biopolymer-based hydrogels. It is also interesting to see how the degradation rate of mTG-Gels may be controlled to suit different applications. Hydrogels with slow degradation rates may serve well as an immuno-protective encapsulation material, whereas hydrogels with longer degradation rates, on the order of days or weeks, can be utilized for slow delivery of cells in regenerative medicine. This portion of the work investigates how, and at what rate, mTG-Gels are degraded under simulated physiological conditions, as well as seeks a mean for controlling its degradability.

### **5.2 Material and Methods**

#### *5.2.1 Transglutaminase Crosslinked Gelatin Hydrogels*

Gelatin hydrogels were made by three different methods, giving rise to thermal hydrogels (T-Gels), mTG crosslinked hydrogels (mTG-Gels), and hydrogels that are initially cooled before crosslinking with mTG (HybriGels). T-Gels are common physical gels formed by first dissolving 300-bloom gelatin (Type A, Sigma) in DMEM+FBS at 70 °C for 10 min, followed by sterile filtration through 0.22 µm SteriFlip (Millipore) media filters before thermally setting at 4 °C for 24 hr. These

hydrogels are not permanent and are thermally reversible. Enzyme crosslinked mTG-Gels are made by mixing dissolved gelatin with a 10% (*m/v*) stock solution of mTG (Ajinomoto, Inc.). Stock mTG solution is made by first dissolving mTG powder in DMEM+FBS at 50 °C for 10 min and then sterile filtering through a 0.22µm Millex (Millipore) syringe filters. Dissolved gelatin and mTG solutions are mixed with a final mass ratio of 0.2 g-mTG/g-gelatin. The crosslinking reaction is allowed to take place in a cell culture incubator set at 37 °C for 24 hours. HybriGels were formed by first cooling a gelatin solution at 4 °C for 12 hours without mTG. Afterwards, an equal volume of a 10% mTG stock solution was overlaid on top of the thermal hydrogel to start the crosslinking. This reaction phase was allowed to take place within an incubator at 37 °C for another 12 hour.

### 5.2.2 *Thermal and Proteolytic Degradation of mTG Crosslinked Hydrogels*

The three types of gelatin hydrogel were tested for their ability to resist thermal and proteolytic degradation. Two milliliter volumes of each hydrogel were cast in individual 35mm Petri dishes (9.6 cm<sup>2</sup>) and allowed to set overnight before placing each into their respective treatments. Thermal stability was examined by incubating the hydrogels under a DPBS solution at 37 °C. Proteolytic stability was examined by incubating the hydrogels in a 200 mL bath of 0.25% Trypsin plus 0.03% EDTA at room temperature (RT). To elucidate the mechanism by which degradation occurred, mTG crosslinked hydrogels were examined for characteristics of either surface or bulk degradation. Surface dependence was examined by setting 10% HybriGels in Petri dishes with variable surface areas (9.6, 28.3, and 78.5 cm<sup>2</sup>) while maintaining a fixed height (0.2 cm). Bulk degradation was studied by setting the

same gel in dishes with variable volumes (1, 3, and 4 mL), while maintaining a fixed surface area (9.6 cm<sup>2</sup>). All treatments were performed on an orbital shaker (75 rpm). Petri dishes were weighed on an analytical balance (Mettler Toledo AE50) before gels were cast and every 30 min after formation until the gel has fully degraded.

### 5.3 Results and Discussion

#### 5.3.1 Thermal and Proteolytic Stability of mTG-Gels

Beyond exploring the biocompatibility of mTG crosslinked hydrogels, it was also important to characterize the thermal and proteolytic stability of this novel cellular scaffold. Four percent T-Gels placed in a DPBS bath, equilibrated at 37 °C, were found to degrade within 30 min (Figure 5.1).

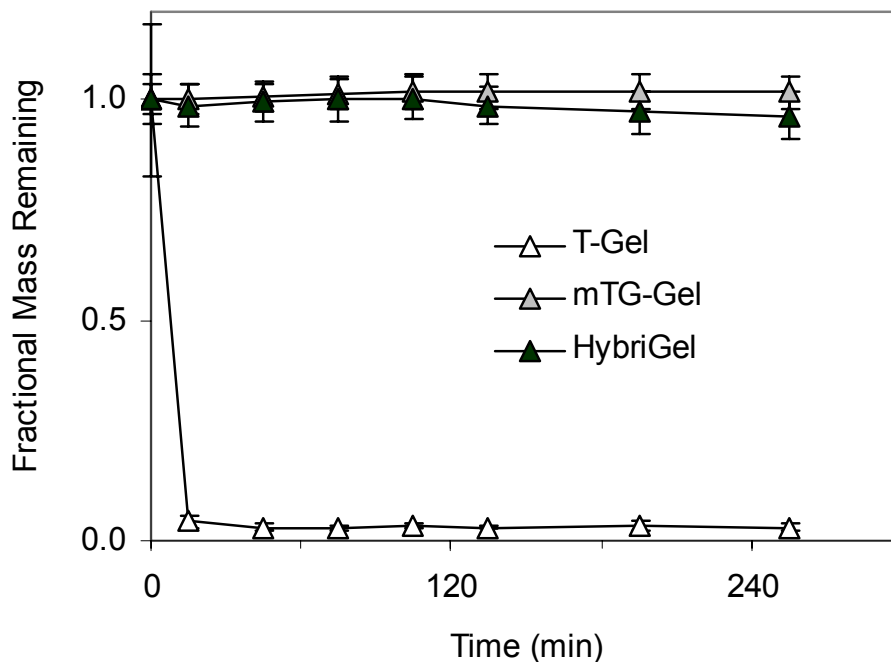


**Figure 5.1** Exposure of the three hydrogels (T-Gel, mTG-Gel, and HybriGel) in a 37 °C bath of DPBS showed that only the uncrosslinked T-Gel was susceptible to thermal degradation.

The same 4% gelatin hydrogels that were crosslinked with mTG (4% mTG-Gel), however, were extremely stable at 37 °C. The mass of these hydrogels was essentially unchanged over a 4 hr period. On the basis of these results, it was predicted that the mTG-Gel would also be more resistant to degradation by the model proteolytic enzyme, trypsin. However, the mTG-Gel was slightly less stable as compared to the thermally formed T-Gel, resulting in respective degradation rates of 19.0  $\mu\text{g}/\text{min}$  and 16.5  $\mu\text{g}/\text{min}$  (Figure 5.2).

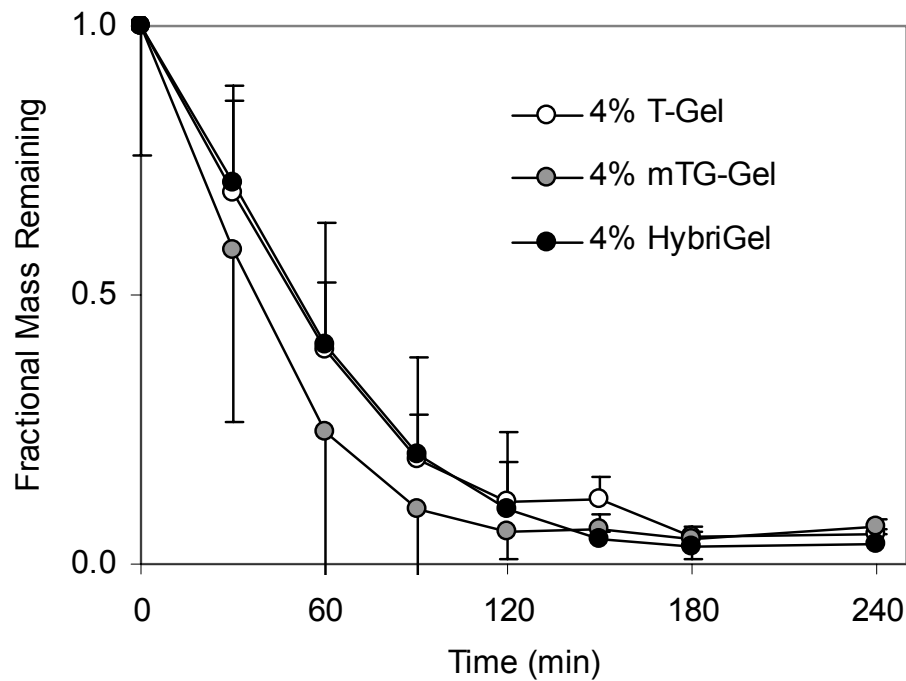


**Figure 5.2** Although 4% mTG-Gels were thermally stable, they were slightly less resistant to proteolysis by trypsin. HybriGels were developed by first thermally cooling gelatin and then crosslinking with a 10% mTG overlay. The resultant hydrogel was both thermally stable and as proteolytically resistant as the T-Gels.

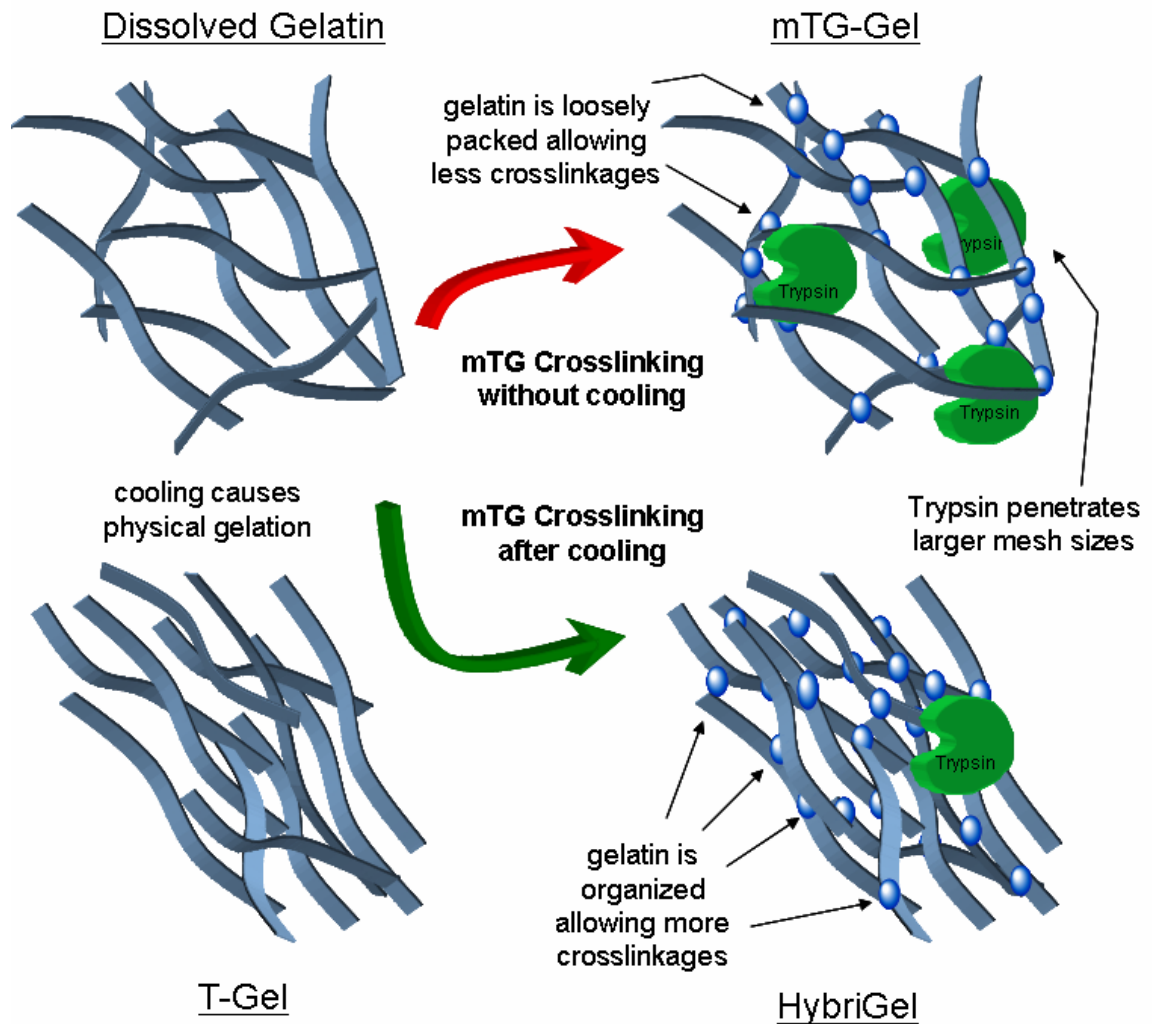


**Figure 5.3** Gelatin hydrogels formed with initial cooling, to create a physical gel, before crosslinking with mTG were found to be consistently more resistant to proteolysis as compared to hydrogels that were crosslinked before cooling (mTG-Gels). An explanation may be that thermal cooling allows gelatin to first self-organize into a tight network of polypeptides through hydrogen bonding. Once gelatin has formed this network, there are more potential junction points where crosslinking can occur, creating a denser permanent hydrogel. mTG-Gels, however, were unable to form this tight network since mTG is immediately crosslinking gelatin polypeptides. The result is a less tightly packed hydrogel with a larger mesh size, which may be more susceptible to proteolytic attack



Given the same finding upon multiple replications of the experiment, it was hypothesized that mTG-Gels may be more susceptible to degradation because the mTG is creating crosslinks before the gelatin polypeptides have a chance to form a tight network (Figure 5.3). Thus, mTG-Gels would have a higher mesh size than T-Gels, allowing them to be even more susceptible to proteolytic attack despite being thermally stable. To challenge this hypothesis, 4% gelatin solutions were allowed to cool completely, for 12 hr, before adding an overlay of an equal volume of a 10% mTG enzyme solution. The mTG overlay was allowed to incubate with the thermal gel for another 12 hr at 37 °C, creating a hydrogel that would theoretically have the same mesh size as a thermally cooled hydrogel along with the proteolytic stability of crosslinked mTG-Gels. When these new hybrid hydrogels (dubbed HybriGels) were subjected to the same trypsin bath as before, they were found to be consistently more resistant to proteolytic degradation. The rate of degradation was in fact similar to T-Gels (Figure 5.4). To confirm that these gels were thermally stable they were exposed to a 37 °C DPBS solution. These HybriGels proved to be resistant to thermal degradation, as no mass was lost over a 4 hr period.

### *5.3.2 Tuneable Degradability of HybriGels*

Since degradation rates of hydrogels can typically be influenced by polymer and crosslinking densities (mesh size), increasing gelatin concentration may be a simple method of retarding gel degradation rates. Four concentrations of HybriGels (4, 10, 15, and 25% gelatin) were tested for their resistance to proteolytic degradation by trypsin. Measurements of fractional mass remaining in the hydrogels showed that degradation rates decreased as a function of increasing gelatin concentration, as

expected (Table 5.1). The reduction in degradation rate, however, was not linear with respect to gelatin concentration, where a sharp deceleration in proteolysis was observed between the 4% and 10% HybriGels (Figure 5.5).

**Table 5.1** Thermal and enzymatic degradation rates for various forms of hydrogels

Hydrogel Form	Degradation Rates ( $\mu\text{g}/\text{min}$ )				
	37°C DPBS	0.25% Trypsin + 0.03% EDTA			
Gelatin ( $m/v$ %)	4	4	10	15	25
T-Gel	43.30	16.47	--	--	--
mTG-Gel	-0.15	19.00	--	--	--
HybriGels	0.22	17.41	3.03	2.12	0.92
Pre-Soaked HybriGels	--	--	6.32	3.28	--

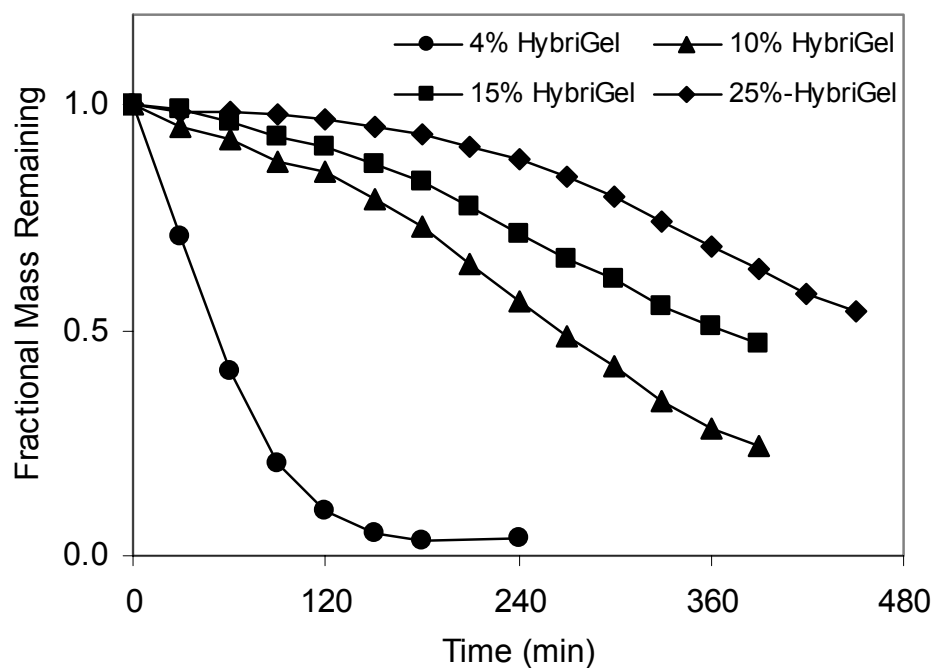


**Figure 5.4** The proteolytic degradation rate of HybriGels was found to be adjustable based on the amount of gelatin in the hydrogel (4, 10, 15, and 25%). A disproportionate drop in degradation rate between 4% and 10% HybriGels may indicate that below a critical mesh size the trypsin may be limited to the surface of denser gels.

This disproportionate decrease in the degradation rate may reflect a critical mesh size necessary for trypsin to penetrate the hydrogel beyond the surface. To investigate whether or not proteolysis was occurring mainly due to surface or bulk mechanisms, 10% HybriGels were set in Petri dishes with either fixed gel height and variable surface areas or fixed area and variable volumes. Indeed, the degradation rate was strongly affected by the change in surface area and then by the change in volume of the hydrogel (Figure 5.5). This indicates that the degradation of 10% HybriGels is dominated by surface erosion, but there is still slight bulk erosion. This phenomenon would likely apply to the HybriGels of higher concentrations, whereby

further increasing the gelatin content only serves to linearly decrease the rate of proteolytic degradation at the surface of the hydrogels.

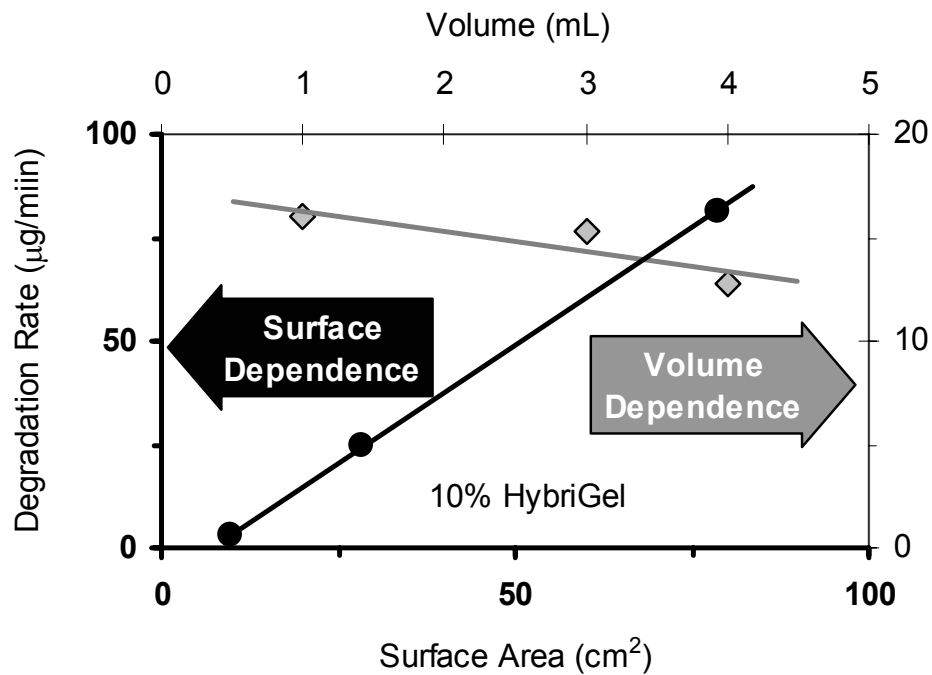


**Figure 5.5** A study to elucidate the mechanism by which trypsin degrades 10% HybriGels. Proteolysis occurs mainly by surface erosion.

To extend the applicability of using mTG crosslinked hydrogels as cellular scaffolds *in vivo*, it was interesting to see how degradation rates may be affected by hydration content. To examine this factor, 10% and 15% HybriGels were formed as before and with pre-soaking in DPBS overnight before performing degradation experiments with trypsin. As Figure 5.6 shows, the pre-soaking in DPBS tended to swell the hydrogels, making them more susceptible to proteolytic degradation in both

gelatin concentrations. This result indicates that HybriGels may have slightly higher degradation rates once implanted due to hydration of the scaffold by the host.

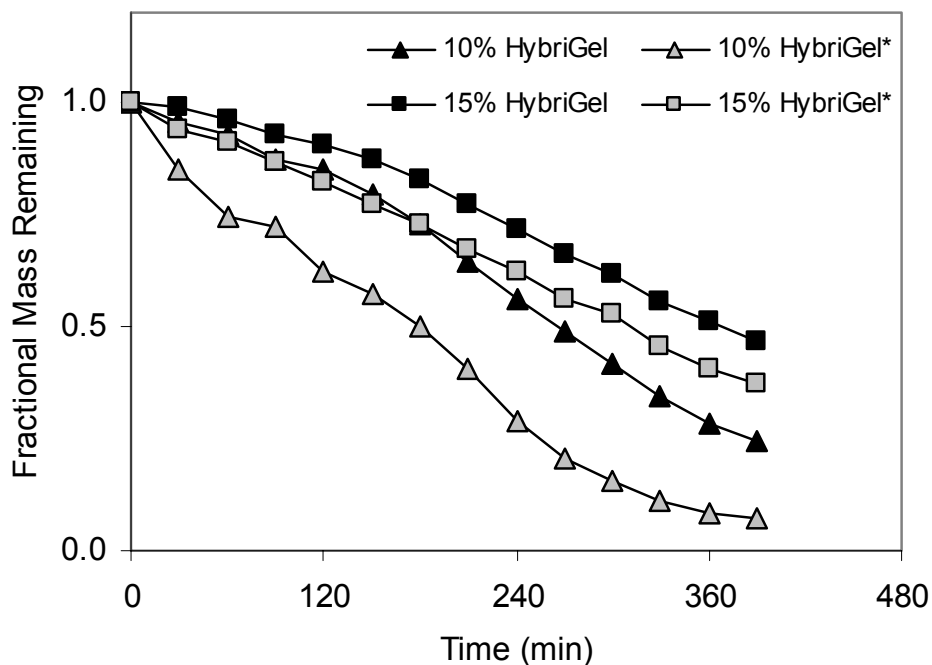


**Figure 5.6** Swelling studies were done to determine how proteolytic degradation rates would be affected by water content. 10% and 15% HybriGels that were pre-soaked in DPBS overnight (\*) were found to be more susceptible than their non-soaked counterparts.

#### 5.4 Conclusions

The discovery of a process to first thermally set a gelatin solution followed by enzymatic crosslinking with mTG (HybriGels), resulted in a hydrogel that was both thermally stable and slightly more resistant to proteolytic attack than hydrogels formed by concurrently mixing mTG with dissolved gelatin (mTG-Gels).

Measurement of degradation rates under conditions of either variable surface areas or volumes of 10% HybriGels indicated that degradation occurred mainly through

surface-dependant mechanisms. This demonstrated that encapsulated cells would be well insulated from proteolysis should they be implanted into a host body.

Furthermore, degradation rates of HybriGels were found to be customizable based on the level of gelatin used to form the hydrogel. Gelatin concentrations above 10% were found to be much more resistant to degradation compared to the 4% hydrogels. Although the ability of cells to survive direct encapsulation by these denser hydrogels was not examined, they may serve as an outer protective coating for cells that are encapsulated by 4% mTG-Gels. Thus, successive layers of hydrogels with different densities can serve as either a cellular scaffold (4%) or a protective encapsulation (25%) biomaterial. Utilizing mTG-Gels with customizable degradation rates may also provide a method of delivering regenerative cells in a controlled manner.

## **6. Diffusion of hIL2 from Encapsulated Cells**

### **6.1 Introduction**

To develop a biomaterial that is suitable for encapsulating cells, it is not only important to provide biocompatibility, but also functionality. One such functionality is the ability of the biomaterial to retain engineered cells while maintaining a low level of diffusion barrier. This functionality is important with respect to facilitating nutrient and oxygen transport, as well as diffusion of therapeutic proteins that engineered cells are secreting. As shown previously, mTG-Gels made by enzymatically crosslinking gelatin with transglutaminase, appear to have high biocompatibility, as well as tunable resistance to proteolytic degradation. In this portion of the work, the diffusivity of human interleukin 2 from engineered cells through 4% mTG-Gels was examined in order to characterize its protein transport capabilities. To accomplish this, HEK293 cells were transfected with either one of two plasmids. The first is pF2, which encodes a secretable hIL2 gene along with a bicistronically expressed destabilized DsRed-Express fluorescent marker. The second, pF3, is an analogous plasmid, having the additionally ability to induce the production of an anti-apoptotic protein, Bcl-2 $\Delta$ , based on increasing degrees of hypoxia. Diffusion cells containing three different thicknesses of mTG-Gels were used to determine the diffusion coefficient of hIL2 for comparison to that obtained from the encapsulated cells. A mathematical model was also developed to describe both the transient and steady state hIL2 transport behavior through the hydrogel membrane.

## 6.2 Materials and Methods

### 6.2.1 Maintenance of Cell Cultures

The attachment-dependent human embryonic kidney cell line, HEK293 (Flp-In™-293, Invitrogen), was cultured in Dulbecco's Modified Eagle's Media containing high glucose (4.5 g/L), GlutMAX™ I (3.97 mM) (DMEM, Invitrogen), with added fetal bovine serum (10%, FBS, Sigma), and zeocin (100 mM, Invitrogen) (complete media). Cells were cultured in 75 cm<sup>2</sup>-tissue culture flasks (Costar) and subcultured every two to three days as the population approached 80-90% confluency. Cells were passaged by first aspirating the spent media and then rinsing with Dulbecco's Phosphate Buffer Solution without Ca<sup>2+</sup> or Mg<sup>2+</sup> (DPBS-cm, Invitrogen). Rinsed cells were incubated in 2 mL of a 0.25% Trypsin with 0.03% EDTA solution (Sigma) for 5 minutes under their normal growth environment (37 °C, 8% CO<sub>2</sub> incubator). Cells were passaged with a 1:10 split ratio, and supplemented with fresh complete media up to 12 mL for further growth.

### 6.2.2 mTG-Gel Formation

Enzyme crosslinked gelatin hydrogels (mTG-Gels) as both cell overlays and diffusion cell membranes were formed by mixing 300-bloom gelatin (Type A, Sigma) and microbial transglutaminase (mTG, lot # 97.12.04, Ajinomoto) dissolved in complete media. Each solution was heated to 50 °C for 10 min, and sterile filtered through 0.22 µm SteriFlip (Millipore) media filters. The mTG-Gels have a final gelatin concentration of 4% (g/mL) and an mTG mass ratio of 0.2 g-mTG/g-gelatin. The crosslinking reaction was performed in a cell culture incubator set at 37 °C for 24 hours.



### 6.2.3 *Plasmid Constructs*

The first expression vector used in this study, pF2, contains an assembly of four gene elements: the human interleukin-2 (hIL2) gene, its Ig- $\kappa$  secretion signal, an internal ribosome entry site (IRES), and a Destabilized DsRed-Express (DsExDR) fluorescent protein marker. The secretable hIL2 (ShIL2) fragment was first derived from a previously constructed vector called pSIEG. This vector was made by PCR extraction of the hIL2 gene from pBlueBacHis2-GFPuv/hIL2 [123], using the following primers: 5'- AAT GTC GAC AAA TGG CAC CTA CTT CAA GTT CTA CAA A -3' and 5'- ATT ACC GGT TTC TTG TCA TCG TCA TCT CAA GTT AGT GTT GAG ATG ATG CTT TG -3'. The first primer contained a Sal I restriction site and the second primer has enterokinase (EK) and Age I restriction sites. The blunt PCR fragment was first ligated to pCR-Blunt II-TOPO (pCR, Invitrogen) before digesting with Sal I and Age I restriction enzymes. The digested fragment was then ligated into the corresponding unique cloning sites of pEGFP1-N1 (Clontech). Hind III and Not I were then used to restrict the hIL2-EK-EGFP fusion gene for ligation into pSecTag2A/hygro (Invitrogen) in order to add on the Ig- $\kappa$  secretion signal. The following primers were used to extract ShIL2 from pSIEG: 5'- GAA GAT CTG CCG CCA CCA TGG AGA CAG ACA CAC TCC TGC TAT -3' and 5'- GGA TCC GCG TTA TCA AGT TAG TGT TGA GAT GAT GCT TTG ACA AAA -3'. The first primer contained a Bgl II restriction site and a Kozak consensus sequence, which was used to further increase translation efficiency in eukaryotic cells [51]. The second primer introduced a BamH I restriction site. The pCR plasmid was again used as an intermediary cloning vector. The secretable hIL2 gene was excised with Bgl II and

BamH I digestion and ligated into pIRES2-DsRed2 (Clontech) in order to add the IRES bicistronic element. The ShIL2-IRES fragment was then re-extracted via PCR and ligated to pDsRed-Express-DR (Clontech) in order to add on the red fluorescent protein marker gene. The following primers: 5'-GAA GAT CTG CCG CCA CCA TGG AGA CAG ACA CAC TCC TGC TAT -3' and 5'- TCC CCG CGG GGA TGT GGC CAT ATT ATC ATC GTG TTT TTC AAA G -3' were used. The first primer was the same as the one used in the previous cloning procedure. The second primer contained a Sac II restriction site. The pCR plasmid was used as an intermediary cloning vector. The final expression vector, pF2, was constructed by using PCR to extract the ShIL2-IRES-DsExDR fragment using the following primers: 5'- CGA CAA ATG GCA CCT ACT TCA A -3' and 5'- GTC GCG AAT TTT AAC AAA ATA TTA ACG C -3', and directly ligating it to the host vector, pSecTag/FRT/V5-His-TOPO (Invitrogen).

The second vector, pF3, contains all the same genetic elements of pF2, with the addition of an anti-apoptotic gene, *bcl-2Δ*, placed downstream of a hypoxia inducible promoter, 5HRE-hCMVmp (5HRE). A vector, dubbed pCYbn, which was generously donated by M.J. Betenbaugh (Johns Hopkins University), was digested with NheI and EcoRI restriction enzymes to obtain *bcl-2Δ*. This gene was then ligated downstream of a human cytomegalovirus (CMV) promoter in the pIRESpuro3 (Invitrogen) cloning vector, using the respective enzyme sites, forming the vector in pCYbp. The CMV promoter was subsequently replaced with the 5HRE promoter derived from the p5HRE-d2EGFP vector, generously provided by J.M. Brown (Stanford University). This promoter was originally constructed by fusing five

hypoxia responsive elements (HRE) in tandem upstream of a minimal CMV promoter. This promoter was extracted by PCR from p5HRE-d2EGFP using the following primers: 5'- TAA TTC GCG ACA TAT GGG TAC CGA GCT TTT CT -3' and 5'- GCA ATG CTA GCG AAT GCC AAG CTT CTA GT -3', which contained NruI and NheI restriction sites, respectively. The exchange of the promoters was mediated by digestion and ligation of the respective NruI and NheI sites on the PCR product and pCYbp, to form pO2Ybp. Since this vector contains an EYFP gene between the hypoxia inducible promoter and *bcl-2Δ*, it was removed by first using PCR to extract the *bcl-2Δ* gene with the following primers: (+Nhe I) 5'- TTG CTA GCA TGG CGC ACG CTG -3' and (+Not I) 5'- AAG CGG CCG CGG ATC CGA A -3' (+Not I) and re-ligating it back into pCYbp, which effectively deleted the EYFP gene. The 5HRE-*bcl-2Δ* fragment was then extracted by PCR using the following primers: (+NruI) 5'- TCG CGA TCG AGC CAC AGT G -3' and 5'- TCA CTT GTG GCC CAG ATA GG -3', and ligated into pSecTag/FRT/V5-His-TOPO (Invitrogen). A large gene segment upstream of 5HRE-*bcl-2Δ*, flanked by two NruI sites, was excised, and replaced with the respective fragment from pF2, which contained the CMV-ShIL2-IRES-DsExDR gene fragment. The resultant vector, pF3, thus contains all the elements of pF2 along with the capability to produce Bcl-2Δ in response to low oxygen conditions.

#### 6.2.4 Cell Transfection and Encapsulation

To study the diffusion of hIL2 from HEK293 cells transfected with the pF2 and pF3 vectors, 2D cell cultures were overlaid with various heights of 4% mTG-Gels (0, 0.16, 0.32, and 0.64 cm). Cells were seeded in black walled, clear bottom, 96-well

tissue culture plates (Costar), as shown in Figure 6.1, at a density of  $4 \times 10^4$  cells/well.

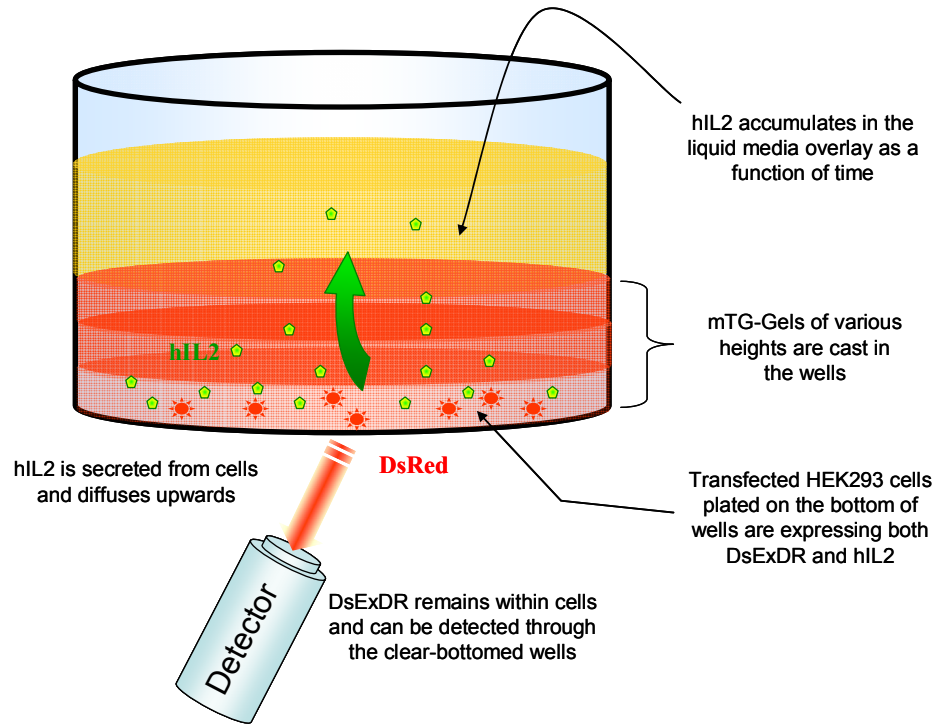


**Figure 6.1** To study the diffusion of hIL2, HEK293 cells were initially plated in 96-well tissue culture plates and transfected with either pF2 or pF3 expression vectors. The transfected cells were then overlaid with various heights of 4% mTG-Gels and a top layer of liquid media. Human IL2 secreted from the cell are then measured in the liquid overlay once it has diffused through the hydrogel. DsExDR fluorescence can be quantified photometrically through the clear-bottomed wells.

Since fluorescence measurements are to be taken from the cells, it was important to obtain an even distribution of cells. This was achieved by immediately centrifuging the 96-well plates after inoculation. The plates were spun at  $500 \times g$  (5810R, Eppendorf) using the slowest acceleration setting (# 9) and immediately

decelerated as slowly as possible (# 9). This centrifugation procedure quickly placed cells at the bottom surface of each well with a uniform distribution. Twenty-four hours after inoculation, HEK293 cells were transfected with either pF2 or pF3 vectors (0.2 µg/well) using LipofectAmine 2000 (0.5 µL/well, Invitrogen) and OptiMEMI (50 µL/well, Invitrogen). Thirty hours post-transfection, the spent media in each well were aspirated, and replaced with the appropriate volumes of 4% mTG-Gels (0, 50, 100, 200 µL/well, respectively). After a 6 hr gelation period, the hydrogels were overlaid with 100 µL/well of complete media. All gels and cells were incubated under normal cell culturing conditions.

#### *6.2.5 Fluorescence Microscopy and ELISA*

The transient expression of DsExDR by mTG-Gel overlaid cells was monitored with an inverted fluorescence microscope (IX71, Olympus) equipped with a TRITC filter cube (Ex: HQ545/30x, Dichroic: Q570LP, Em = HQ620/60m, Chroma). Images of fluorescing cells were captured by a monochrome digital camera (DP30, Olympus) set for a 3 s exposure. Fluorescence intensity was then analyzed with ImageJ (NIH Image) software. HEK293 cells that were not transfected but overlaid with various heights of mTG-Gel were used for background fluorescence intensities. Each vector transfection and gel height combination was reproduced in triplicates.

The detection of hIL2 secretion and diffusion through the hydrogels was examined by an Enzyme-Linked Immunosorbent Assay (ELISA). Supernatant samples containing secreted hIL2 were collected from the media overlays within each well (50 µL/well). Samples were stored in a -20°C freezer until the end of the

experiment and assayed immediately with an OptEIA Human IL-2 ELISA Kit II (BD Pharmingen). Human IL2 standards within the kit were diluted to eight concentrations, ranging from 0 to 500 pg/mL, producing a highly linear fit for the standards ( $r^2 > 0.98$ ). Standards were assayed in duplicates, as instructed by the manufacturer, while supernatant samples were always assayed in triplicates.

### 6.2.6 Diffusion Cell Experiments

Diffusion membranes were formed by casting 4% mTG-Gels of various thicknesses (0.20, 0.25, and 0.30 cm) in BD Falcon Cell Culture Inserts (BD Discovery Labware) as see in Figure 6.2.

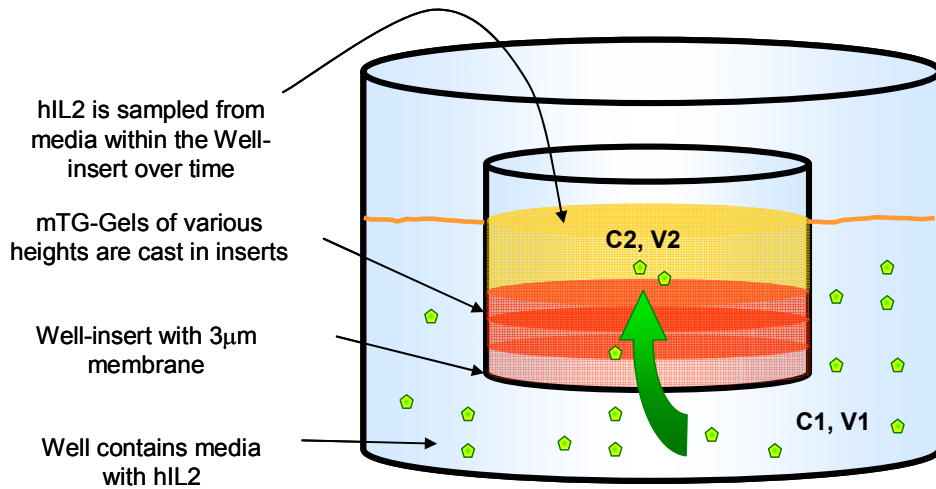


**Figure 6.2** A diffusion cells is composed of an outer well, which contains a stock solution of hIL2, and an inner well-insert, which contains mTG-Gels of various heights and a liquid overlay. The liquid overlay is sampled over time in order to determine the effective diffusion coefficient of hIL2.

Each insert has a polyethylene terephthalate (PET) membrane, which has a low protein binding affinity and high permeability. The membranes each have an area of 4.2 cm<sup>2</sup>, containing 3.0 μm pores at a density of 8 x 10<sup>5</sup> pores/cm<sup>2</sup>. Once the hydrogels have been crosslinked for 24 hr, the inserts were lightly rinsed with DPBS (2 x 3mL) and placed into individual wells of 6-well tissue culture plates. A 3 mL solution of hIL2 (10 ng/mL, Roche) was then add to the each well, while 3 mL of DMEM was added to the inserts. Supernatant samples (200 μL) were taken from the inserts every 4 hours, for 28 contiguous hours. Equal volumes of DMEM were used to replenish each well after each sampling time point.

The insert arrangement approximates a stirred diffusion cell provided the membrane is the controlling transport resistance. The change in concentration of hIL2 due to diffusion across the membrane can be simply described by the following mass balance:

$$[\text{Rate of hIL2 Leaving Well}] = [\text{Rate of hIL2 Transported Across Membrane}] \quad (6.2.2.1)$$

Quantitatively, this unsteady state mass balance can be expressed as:

$$-\frac{d(V_1 C_1)}{dt} = A_m N_m \quad (6.2.2.2)$$

Where:  $V_1$  is the volume of the well (cm<sup>3</sup>),  $C_1$  is the concentration of hIL2 in the well (ng cm<sup>-3</sup>),  $A_m$  is the area of the membrane (cm<sup>2</sup>), and  $N_m$  is the flux across the membrane (ng cm<sup>-2</sup> s<sup>-1</sup>) defined as:

$$N_m \equiv -D_m \frac{dC_m}{dx} \quad (6.2.2.3)$$

To solve this equation and relate the concentration of hIL2 that is within the membrane ( $C_m$ ) to measurable quantities, such as the concentration on both sides of

the membrane ( $C_1$  and  $C_2$ ), the diffusion equation across the membrane must first be

solved:

$$\frac{\partial C_m}{\partial t} = D_m \frac{\partial^2 C_m}{\partial x^2} \quad (6.2.2.4)$$

If the diffusion time scale across the membrane is assumed to be much smaller than the time scale for a concentration change within the wells, a Quasi Steady State Assumption (no accumulation within the membrane) can be applied, such that:

$$\frac{\partial C_m}{\partial t} \approx 0 \approx D_m \frac{\partial^2 C_m}{\partial x^2} \quad (6.2.2.5)$$

The solution of this second order ordinary differential equation with the boundary conditions ( $C_m = C_1 \Phi$  at  $x = 0$ ) and ( $C_m = C_2 \Phi$  at  $x = L$ ), where  $\Phi$  is the partition coefficient and  $L$  is the membrane thickness, is:

$$C_m = \frac{(C_1 \Phi - C_2 \Phi)}{L} x + C_m \Phi \quad (6.2.2.6)$$

Thus:

$$N_m \equiv -D_m \frac{dC_m}{dx} = \frac{D_m \Phi}{L} (C_1 - C_2) \quad (6.2.2.7)$$

Substituting the right hand side of Equation (6.2.2.7) for  $N_m$  in Equation (6.2.2.2) then gives the following mass balance:

$$-V_1 \frac{dC_1}{dt} = A_m D_m \Phi \frac{(C_1 - C_2)}{L} \quad (6.2.2.8)$$

Since it is assumed that there is no accumulation of hIL2 in the membrane, the concentration in the insert ( $C_2$ ) must be equal to the initial concentration of hIL2 in the well ( $C_0$ ) minus the insert well concentration ( $C_1$ ) for equal insert and well volumes. Using this relationship ( $C_2 = C_0 - C_1$ ), Equation (6.2.2.5) can be rewritten in terms of only  $C_1$ :



$$-V_1 \frac{dC_1}{dt} = A_m D_m \Phi \frac{(2C_1 - C_0)}{L_m} \quad (6.2.2.9)$$

Solving this differential equation, using an initial condition of ( $C_1 = C_0$  at  $t = 0$ ), generates the following equation:

$$\ln \left[ \frac{2C_1}{C_0} - 1 \right] \cdot \left[ \frac{-V_1 L_m}{2A_m} \right] = (D_m \Phi) \cdot t \quad (6.2.2.10)$$

After again using the relation ( $C_1 = C_0 - C_2$ ), the equation above can be expressed in terms of concentration of hIL2 in the insert ( $C_2$ ) as a function of time:

$$\ln \left[ \frac{2(C_0 - C_2)}{C_0} - 1 \right] \cdot \left[ \frac{-V_1 L_m}{2A_m} \right] = (D_m \Phi) \cdot t \quad (6.2.2.10)$$

Given the known values of  $A_m = 4.2 \text{ cm}^2$ ,  $V_1 = 3 \text{ cm}^3$ ,  $L_m = (0.20, 0.25, \text{ or } 0.30 \text{ cm})$ , and  $C_0 = 14 \text{ ng/cm}^3$ , and the measured concentrations of hIL2 in the insert ( $C_2$ ), the expression on the left can be plotted again time. A simple linear regression plot will then result in a slope that is equal to the effective diffusion coefficient ( $D_{\text{eff}} \equiv D_m \Phi$ ).

## 6.3 Results and Discussion

### 6.3.1 Therapeutic Protein Secretion by Encapsulated HEK293

Based on measurements of DsExDR fluorescence, transfected HEK293 cells that were not overlaid with any mTG-Gel were the least metabolically productive. This was true for cells transfected with both pF2 (Figure 6.3) and pF3 vectors (Figure 6.4).

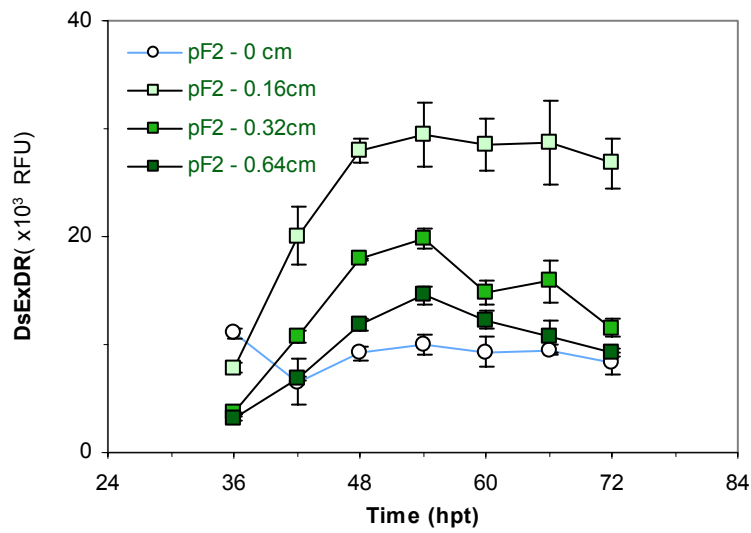


**Figure 6.3** Transient DsRed fluorescence in HEK293 cells transfected with the pF2 expression vector, and overlaid with three mTG-Gel thicknesses.

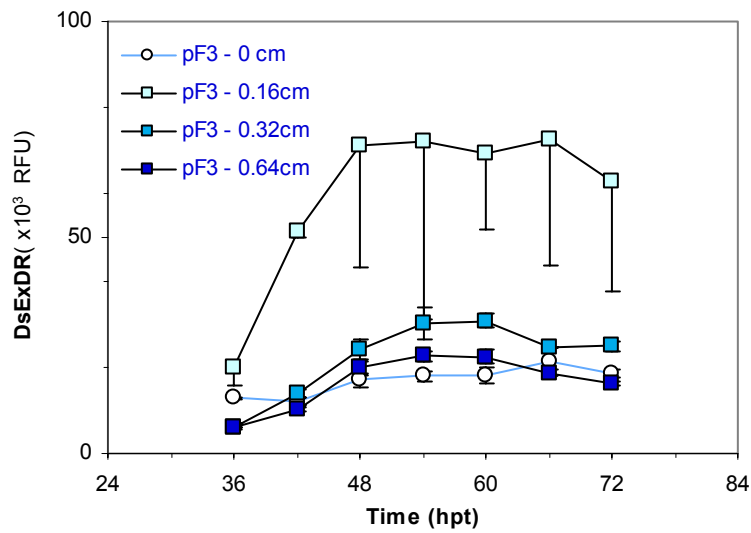


**Figure 6.4** Transient DsRed fluorescence in HEK293 cells transfected with the pF3 expression vector, and overlaid with three mTG-Gel thicknesses.

This phenomenon may be attributed to the ability of the gelatin hydrogels to simulate a growth environment that is closer in nature to the native conditions of the extracellular matrix. The advantage is of such significance that cells with any amount of gelatin were able to produce more fluorescent protein in comparison to cells that were simply cultured on a traditional tissue culture surface. However, as the gelatin layer increased in height, the level of fluorescence protein production began to decrease proportionally. This is reasonable given that the gelatin also serves as a diffusion barrier for oxygen and nutrients in the liquid media above the gel to reach the cells at the bottom of the wells. Invariably though, HEK293 cells that were transfected with pF3, and thus capable of expressing Bcl-2 $\Delta$ , always produced more fluorescence at each respective gel thickness. This finding is consistent with previous portions of this work, which showed that Bcl-2 $\Delta$  not only lessened necrosis and apoptosis, but also increased protein production levels in several mammalian cell lines. It is also noteworthy that cells that were either not overlaid or overlaid with only a thin layer of mTG-Gel (0.16 cm) were able to sustain an even level of fluorescence protein production as time progressed. Cells that were overlaid with more gelatin (0.32 and 0.64 cm) showed a slight decrease in production levels for both pF2 and pF3 transfections. This trend also indicated the effects of either nutrient or oxygen deprivation in the thicker overlays.

With respect to hIL2 secretion and subsequent diffusion, HEK293 cells that were not encapsulated had the highest level of protein accumulation (Figures 6.5 – 5.8). As the thickness of the gelatin overlay is increased, the amount of hIL2 accumulation begins to dramatically decrease. This result is expected since the

accumulation rate of a diffusing species is classically proportional to  $1/L^2$ , where L is the thickness of the overlay. Consistent with the fluorescence data, cells that were transfected with pF3 were able to consistently secrete and accumulate higher levels of hIL2 as compared to their pF2 counterparts at each overlay thickness.

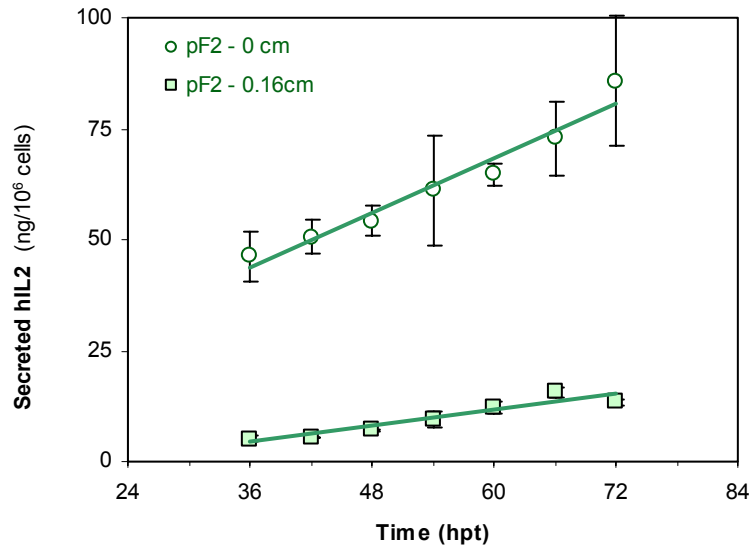


**Figure 6.5** HEK293 cells were transfected with the pF2 expression vector, and overlaid with three mTG-Gel thicknesses. hIL2 was measured in the media that was covering the mTG-Gel overlays. Rates have units of ng/hr-10<sup>6</sup> cells.

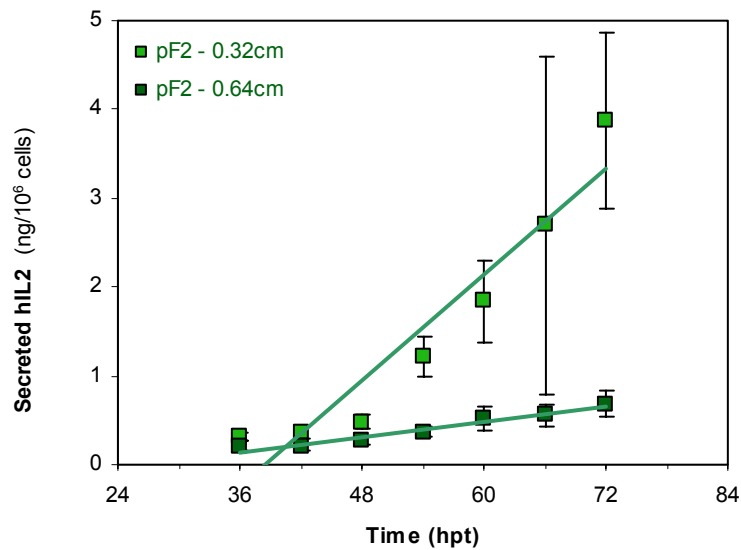


**Figure 6.6** HEK293 cells were transfected with the pF2 expression vector, and overlaid with three mTG-Gel thicknesses. hIL2 was measured in the media that was covering the mTG-Gel overlays. Rates have units of ng/hr-10<sup>6</sup> cells.

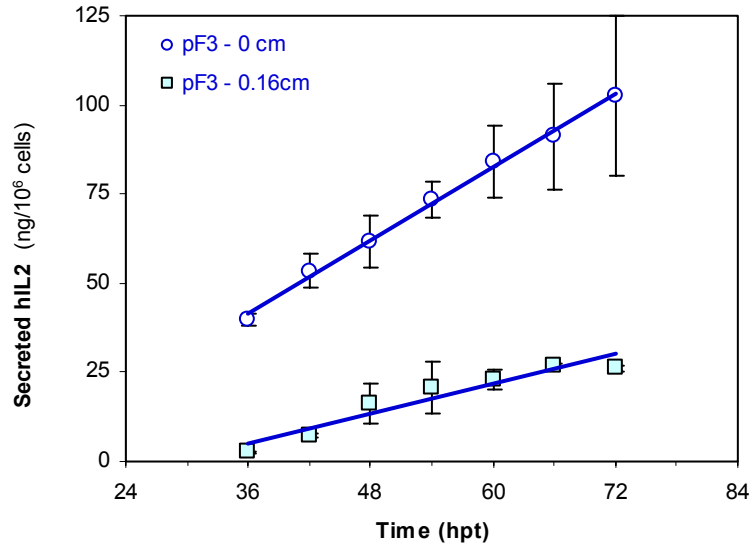


**Figure 6.7** HEK293 cells were transfected with the pF3 expression vector, and overlaid with three mTG-Gel thicknesses. HIL2 was measured in the media that was covering the mTG-Gel overlays. Rates have units of ng/hr-10<sup>6</sup> cells.

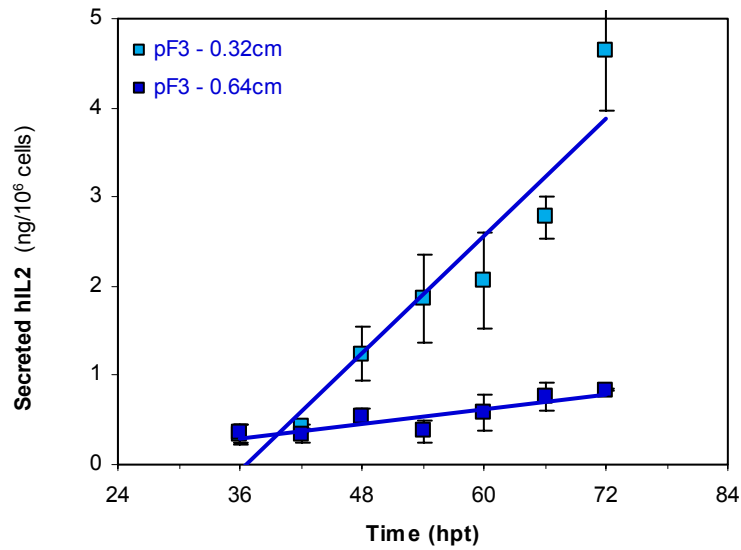


**Figure 6.8** HEK293 cells were transfected with the pF3 expression vector, and overlaid with three mTG-Gel thicknesses. HIL2 was measured in the media that was covering the mTG-Gel overlays. Rates have units of ng/hr-10<sup>6</sup> cells.

### 6.3.2 Mathematical Modeling of hIL2 Release

The diffusion of hIL2 from the bottom of the well ( $z = 0$ ), to the top of the mTG-Gel overlay ( $z = L$ ) can be described by the following partial differential equation (PDE):

$$\frac{\partial C_m}{\partial t} = D_m \frac{\partial^2 C_m}{\partial z^2} \quad (6.3.2.1)$$

with these initial and boundary conditions:

$$C_m(z,0) = 0 \quad C_m(L,t) = 0 \quad -D_m \frac{\partial C_m}{\partial z}(0,t) = N_o \quad \text{IC, BC1, BC2}$$

The first boundary condition ( $z = L$ ) assumes that the volume of media above the overlay is very large relative to the volume of gel and the second boundary condition ( $z = 0$ ) assumes that the cells produce hIL2 at a constant rate, as shown in Figures 6.3 and 6.4 for no overlays. By introducing the following dimensionless variables:

$$\theta \equiv \frac{C_m D_m}{N_o L} \quad \tau \equiv \frac{D_m t}{L^2} \quad \eta \equiv \frac{z}{L} \quad (6.3.2.1a, b, c)$$

Equation (6.3.2.1) can be non-dimensionalized to the form:

$$\frac{\partial \theta(\eta, \tau)}{\partial \tau} = \frac{\partial^2 \theta(\eta, \tau)}{\partial \eta^2} \quad (6.3.2.2)$$

with these new dimensionless initial and boundary conditions:

$$\theta(\eta, 0) = 0 \quad \theta(1, \tau) = 0 \quad \frac{\partial \theta}{\partial \eta}(0, \tau) = -1 \quad \text{IC', BC1', BC2'}$$

To solve the PDE of (6.3.2.2), the Finite Fourier Transform (FFT) method can be

used, where:

$$\theta(\eta, \tau) \equiv \sum_{n=0}^{\infty} \chi_n(\tau) \cdot \phi_n(\eta) \quad (6.3.2.3)$$

$$\chi_n(\tau) \equiv \int_0^1 \phi_n(\eta) \cdot \theta(\eta, \tau) d\eta \quad (6.3.2.4)$$

$$\phi_n(\eta) \equiv \sqrt{2} \cdot \cos(\lambda_n \eta) \quad \text{and} \quad \lambda_n \equiv \frac{2n+1}{n} \pi \quad (6.3.2.5)$$

First, the FFT is applied to the left side of Equation (6.3.2.2):

$$\int_0^1 \phi_n(\eta) \frac{\partial \theta(\eta, \tau)}{\partial \tau} d\eta = \frac{\partial \chi_n}{\partial \tau} \quad (6.3.2.6)$$

Then, the FFT is applied to the right side of Equation (6.3.2.2):

$$\begin{aligned} \int_0^1 \phi_n(\eta) \frac{\partial^2 \theta(\eta, \tau)}{\partial \eta^2} d\eta &= \left[ \phi_n(\eta) \frac{\partial \theta(\eta, \tau)}{\partial \eta} - \theta(\eta, \tau) \frac{\partial \phi_n(\tau)}{\partial \eta} \right]_{\eta=0}^{\eta=1} \\ &+ \int_0^1 \theta(\eta, \tau) \frac{\partial^2 \phi_n(\tau)}{\partial \eta^2} d\eta \end{aligned} \quad (6.3.2.7a)$$

$$\begin{aligned} &= \phi_n(1) \frac{\partial \theta_n(1, \tau)}{\partial \eta} - \theta(1, \tau) \frac{\partial \phi_n(\tau)}{\partial \eta} - \phi_n(0) \frac{\partial \theta(0, \tau)}{\partial \eta} + \theta(0, \tau) \frac{\partial \phi_n(\tau)}{\partial \eta} \\ &+ \int_0^1 \theta(\eta, \tau) \frac{\partial^2 \phi_n(\tau)}{\partial \eta^2} d\eta \end{aligned} \quad (6.3.2.7b)$$

By utilizing Equation (6.3.2.5), BC1' and BC2', respectively, the 1<sup>st</sup>, 2<sup>nd</sup>, and 4<sup>th</sup> terms are reduced to zeros, leaving the remaining terms:

$$= -\phi_n(0) \frac{\partial \theta(0, \tau)}{\partial \tau} + \int_0^1 \theta(\eta, \tau) \frac{\partial^2 \phi_n(\tau)}{\partial \tau^2} d\eta \quad (6.3.2.7c)$$

which are further reduced by again applying Equation (6.3.2.5) for  $\eta = 1$ :

$$= -\sqrt{2}(-1) - \lambda_n^2 \int_0^1 \theta(\eta, \tau) [\sqrt{2} \cos(\lambda_n^2 \eta)] d\eta \quad (6.3.2.7d)$$

$$= \sqrt{2} - \lambda_n^2 \cdot \chi_n \quad (6.3.2.7e)$$

The final transformed equation becomes:

$$\frac{\partial \chi_n}{\partial \tau} = \sqrt{2} - \lambda_n^2 \cdot \chi_n \quad (6.3.2.8)$$



The general solution of this non-homogeneous first-order ordinary differential

equation is then: 
$$\chi_n = C_n \cdot e^{\lambda_n^2 \tau} + \frac{\sqrt{2}}{\lambda_n^2} \quad (6.3.2.9)$$

To obtain an expression for the constant of integration,  $C_n$ , a transformed initial condition based on IC'  $\theta(\eta, 0) = 0$  must be applied using Equation (6.3.2.4):

$$\chi_n(0) = \int_0^1 \phi_n(\eta) \cdot \theta(\eta, 0) d\eta = 0 \quad \text{IC''}$$

yielding 
$$C_n = -\frac{\sqrt{2}}{\lambda_n^2} \quad (6.3.2.10)$$

and 
$$\chi_n(\tau) = \frac{-\sqrt{2}}{\lambda_n^2} e^{\lambda_n^2 \tau} + \frac{\sqrt{2}}{\lambda_n^2} \quad (6.3.2.11)$$

The solutions obtained for  $\phi_n(\eta)$  in (6.3.2.5) and  $\chi_n(\tau)$  in (6.3.2.11) can be substituted into the Fourier Series in (6.3.2.3) to obtain an expression for  $\theta(\eta, \tau)$ :

$$\theta(\eta, \tau) = \sum_{n=0}^{\infty} \frac{\sqrt{2}}{\lambda_n^2} \left[ 1 - e^{\lambda_n^2 \tau} \right] \cdot \sqrt{2} \cdot \cos(\lambda_n \eta), \quad \lambda_n = \frac{2n+1}{n} \pi \quad (6.3.2.12)$$

$\theta(\eta, \tau)$  can be reverted to the dimensional concentration, expressed as  $C_m$ , by reapplying the dimensionless quantities (6.3.2.1a, b, c):

$$\frac{C_m D_m}{N_o L} = \frac{8}{\pi^2} \cdot \sum_{n=0}^{\infty} \left[ \left( 1 - e^{-\left(\frac{2n+1}{2}\pi\right)^2 \frac{D \cdot t}{L^2}} \right) \frac{\cos\left(\frac{2n+1}{2}\pi \cdot \frac{z}{L}\right)}{(2n+1)^2} \right] \quad (6.3.2.13)$$

To apply this equation to the experimental data, one must obtain an expression for the accumulation, or  $Q(t)$ , defined as:

$$Q(t) = \int -D_m \frac{\partial C_m}{\partial z} \Big|_{z=L} dt \quad (6.3.2.14)$$

Taking the derivative of  $C_m$  with respect to  $z$ , and utilizing the simplification of

$\sin\left(\frac{2n+1}{2}\pi\right) = (-1)^n$ , Equation (6.3.2.14) becomes:

$$Q(t) = \int -D_m \frac{\partial C_m}{\partial z} \Big|_{z=L} dt = \int_0^t -D_m \frac{4N_o}{\pi^2} \cdot \sum_{n=0}^{\infty} \left[ \left( 1 - e^{-\left(\frac{2n+1}{2}\pi\right)^2 \frac{D \cdot t}{L^2}} \right) \frac{(-1)^n}{(2n+1)} \right] \cdot dt \quad (6.3.2.15)$$

Through algebraic simplification and two series approximations:

$$\sum_{n=0}^{\infty} \frac{(-1)^n}{2n+1} = \frac{\pi}{4} \quad \text{and} \quad \sum_{n=0}^{\infty} \frac{(-1)^n}{(2n+1)^3} = \frac{\pi}{32} \quad (6.3.2.15a, b)$$

Equation (6.3.2.12) can be reduced to:

$$Q(t) = N_o t - \frac{N_o L^2}{2D_m} + \frac{16N_o L^2}{\pi^3 D_m} \sum_{n=0}^{\infty} \left[ \frac{(-1)^n}{(2n+1)^3} e^{-\left(\frac{2n+1}{2}\pi\right)^2 \frac{D \cdot t}{L^2}} \right] \quad (6.3.2.16)$$

A dimensionless form of this equation may be written by rearranging several

variables: 
$$\frac{Q(t)D_m}{N_o L^2} = \frac{D_m t}{L^2} - \frac{1}{2} + \frac{16}{\pi^3} \sum_{n=0}^{\infty} \left[ \frac{(-1)^n}{(2n+1)^3} e^{-\left(\frac{2n+1}{2}\pi\right)^2 \frac{D \cdot t}{L^2}} \right] \quad (6.3.2.17)$$

The steady state form ( $t \rightarrow \infty$ ) of Equation (6.3.2.16) can be expressed as:

$$Q_{ss}(t) = N_o \left( t - \frac{L^2}{2D_m} \right) \quad (6.3.2.18)$$

### 6.3.3 Obtaining the Fluxes and Diffusion Coefficient of hIL2 Secreted by HEK293

As indicated by the positive x-intercepts of all regression lines in Figures 6.5 to 6.8, the accumulation of hIL2 in the liquid overlay was marked by an initial lag period where no protein was detected. This lag period can be attributed to both non-steady state diffusion, as well as a delay in protein expression, since proteins are not

immediately produced upon transfection ( $t = 0$ ). This expression time lag ( $t_{\text{expr}}$ ) is not related to the molecular transport resistance that this study hopes to elucidate, and must first be subtracted from all time values in order to obtain data that are representative of only diffusional characteristics of the system. The expression time lag can be readily determined by calculating the x-intercepts of regression lines in Figures 6.5 and 6.7 for samples that were not overlaid with gelatin, which is approximately 11 hr.

Utilizing the transformed data, which now has no expression time lag, the fluxes of hIL2 from transfected cells were determined from samples with the thinnest overlays (0.16 cm) presented in Figures 6.5 and 6.7 by applying the steady state model expressed in equation (6.5.3.18). First, the level of hIL2 accumulation,  $Q$ , was calculated by normalizing all hIL2 (ng/ $10^6$  cells) values by the unit area of the wells ( $0.3156 \text{ cm}^2$ ). The data for the two thicker gels were rescaled by the ratio  $L_1^2/L_2^2$ , where  $L_1$  is the thickness of the thinnest gel (0.16 cm) and  $L_2$  is the thickness of the other two. A plot of  $Q$  versus  $t$  is displayed in Figure 6.9 and 6.10 for all three gels.

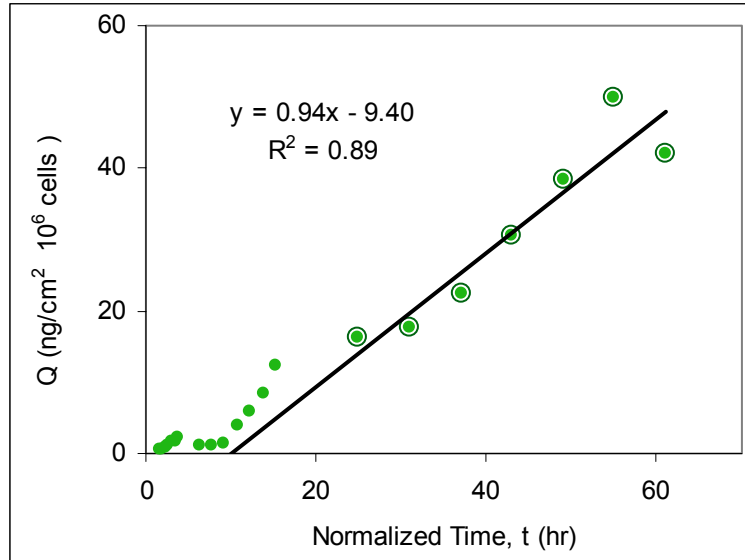


**Figure 6.9** Normalized hIL2 accumulation and time were plotted to reveal a transition from transient to steady state diffusion of hIL2. An analysis of the steady state flux, indicated by the linear regression (circled points) shows that HEK293 transfected with pF2 were producing hIL2 at a rate of 0.94 pg/cm<sup>2</sup> hr.

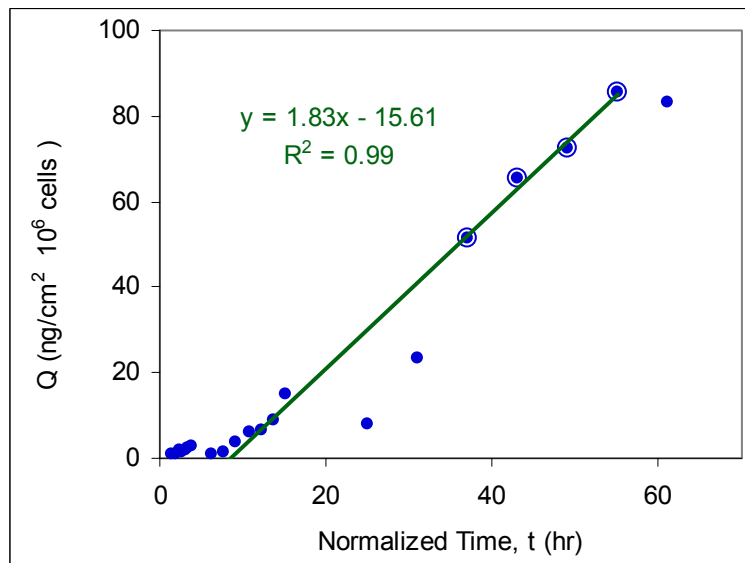


**Figure 6.10** Analysis of the steady state flux (circled points), show that HEK293 cells transfected with pF3 were producing hIL2 at double the rate (1.83 pg/cm<sup>2</sup> hr) of cells transfected with pF<sup>2</sup>.

The linear trend in  $Q$  at longer times indicates a steady state rate of hIL2 accumulation. Based on equation (6.5.3.18), the slope of the line regressed through these data is the flux ( $N_o$ ). HEK293 cells transfected with pF2 had a hIL2 flux of 0.94 ng/cm<sup>2</sup>-hr-10<sup>6</sup> cells. Cells transfected with pF3 had nearly twice the flux of 1.83 ng/cm<sup>2</sup>-hr-10<sup>6</sup> cells. To obtain the diffusion coefficient, Equation (6.5.3.18) can be rearranged after setting  $Q_{ss}(t) = 0$ :

$$D_m = \frac{L^2}{2t_{ss}} \quad (6.5.3.19)$$

Where  $L$  is the thickness of the thinnest gel (0.16 cm), from which the steady state assumption was applied and  $t_{ss}$  is diffusional time lag, represented by the x-intercept from the regression lines. Using equation 6.5.3.19, the diffusion coefficients of hIL2 ( $D_m$ ) were  $3.5 \times 10^{-7}$  cm<sup>2</sup>/s (for pF2 transfections) and  $4.1 \times 10^{-7}$  cm<sup>2</sup>/s (for pF3 transfections), which agree well with each other, as would be expected.

To demonstrate the validity of the steady state analysis, the diffusion coefficients can be plugged into Equation (6.5.3.17) to see how closely it can simulate the non-steady state data represented by the two thicker overlays. As seen in Figures 6.3 and 6.4, however, the level of DsExDR fluorescence is attenuated as the overlay thickness increases, indicating lowered overall level of protein expression. Thus, the fluxes obtained from the thinnest gel cases were rescaled by the level of DsExDR fluorescence in each gel thickness with respect to the thinnest gel, as shown in Table 6.1.

**Table 6.1** hIL2 flux determined from the thinnest overlay (0.16 cm) must be rescaled by the level of DsExDR fluorescence found in the thicker overlays.

	pF2	pF3
Flux (ng/cm <sup>2</sup> -hr-10 <sup>6</sup> cells)	0.94	1.83
L (cm)	Scaling Factor	
0.16	1	1
0.32	0.56	0.39
0.62	0.41	0.29

Utilizing the rescaled fluxes and the diffusion coefficients found from the steady state analysis, the simulated hIL2 accumulation can be compared to the data.

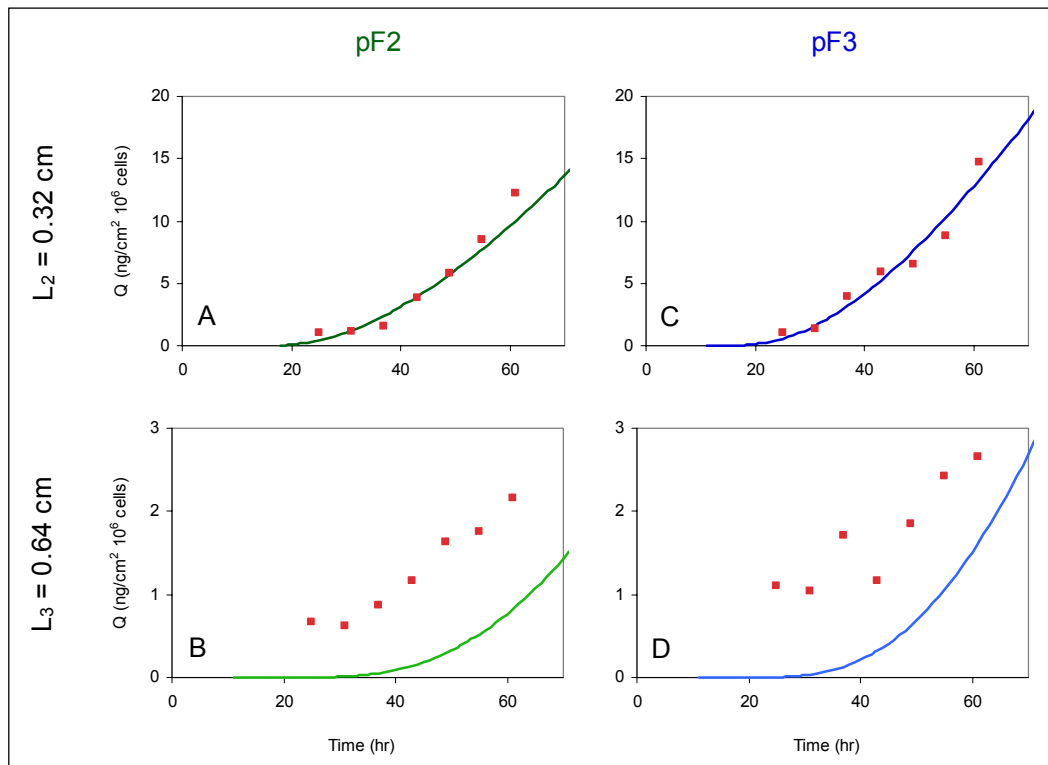


**Figure 6.11** Comparison of data with simulated hIL2 accumulation using diffusion coefficients obtained from steady state analysis and fluxes scaled by DsExDR fluorescence for each overlay thickness.

As shown in Figure 6.11, the simulated curve fits closely with data obtained from the 0.32 cm-overlay, but not from with the 0.64 cm-overlay.

#### 6.3.4 *Measuring Diffusion Coefficient of hIL2 in mTG-Gel*

To better characterize the transport characteristics of the mTG-Gels, diffusion cells based on cell culture inserts were modified to measure the effective diffusion coefficient of hIL2. As shown in Figure 6.12, the amount of hIL2 detected on the insert-side ( $C_2$ ) was plotted against time in accordance to Equation (6.4.2.10). The initial concentration of hIL2 on the well-side ( $C_0$ ) was also measured by ELISA, and found to be 14,518 pg/mL. The remaining parameters necessary for calculating Equation (6.4.2.10) are as follows:  $A_m=4.2 \text{ cm}^2$ ,  $V_1 = 3 \text{ cm}^3$ ,  $L_m = (0.20, 0.25, \text{ and } 0.30 \text{ cm})$ . As expected, the data expressed as the left-hand side of (6.4.2.10) for all the gelatin thicknesses fell along the same linear regression line. The slope of this regression is the effective diffusion coefficient,  $D_m\Phi = 3.2 \times 10^{-7} \text{ cm}^2/\text{s}$ . This value is well within the expected range of proteins that have similar molecular weights as hIL2 (~15 kDa). The ratio of this effective diffusion coefficient and the  $D_m$  value determined from the previous gelatin-overlay experiments reveal that the partition coefficient,  $\Phi$ , for hIL2 between a 4% mTG-Gel and DMEM media is 0.84, which is very reasonable for a hydrogel that is approximately 96% water in weight.

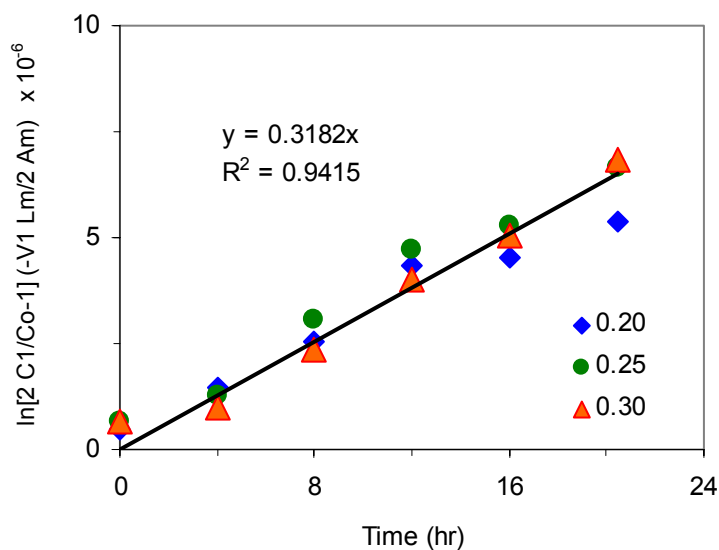


**Figure 6.12** Well inserts filled with three thicknesses of 4% mTG-Gels were used as diffusion cells to measure the diffusion coefficient of hIL2.

## 6.4 Conclusions

Various methods were used to calculate the diffusion coefficient of hIL2 in 4% mTG-Gels. Utilizing a steady state analysis of hIL2 diffusion from HEK293 cells overlaid with 0.16 cm of gelatin, average diffusion coefficient of  $3.8 \times 10^{-7} \text{ cm}^2/\text{s}$  was obtained. Simulations of the non-steady state data was found to be very consistent 0.32 cm overlays, but not with 0.64 cm overlays. This may simply be due to an insensitivity in measuring hIL2 diffusion in thick gels, or that cell metabolism is affected in a way that is not accountable by scaling the flux by the  $D_s \text{ExDR}$  fluorescence. Diffusion cells made from well inserts, however, independently showed a very similar effective diffusion coefficient of hIL2 is  $D_m \Phi = 3.2 \times 10^{-7} \text{ cm}^2/\text{s}$ . Using the results from these two experiments, the partition coefficient is 0.84, which is very consistent with a highly hydrated hydrogel (~96% water).



## 7. Summary

### 7.1 Integrated Non-Invasive System for Quantifying Secreted Human Therapeutic hIL2

Cell encapsulation has been used to treat diabetes, amyotrophic lateral sclerosis, and other chronic ailments by the secretion of therapeutic proteins *in vivo*. Detection of these proteins typically requires invasive procedures such as blood sampling or device extraction, however. In this paper, a non-invasive means of measuring secreted protein concentration using a co-expressed red fluorescent protein marker is developed. A bicistronic expression vector was constructed for the intracellular production of a red fluorescent protein marker and the secreted production of human interleukin-2 (hIL2). The destabilized red fluorescent protein, DsExDR, was selected for its rapid turnover, as well as its ability to emit red light, which is readily transmitted through mammalian tissue. Transfections of this bicistronic vector into three cell lines C2C12, HEK293, and Jurkat showed linear correlations between the expressed proteins, DsExDR (intracellular) and hIL2 (secreted), with transfection DNA concentration. Correspondingly, there was a linear correlation between secreted product (hIL2) and intracellular marker (DsExDR). As transfection DNA was increased, Jurkat cells were found to increase secreted hIL2 in direct proportion to the accumulated DsExDR. HEK293 and C2C12 cells expressed and secreted significantly more hIL2 than the Jurkat cells, while still maintaining a linear relationship. Thus, all three cell lines were suitable hosts for the bicistronic expression of DsExDR and expression and secretion of therapeutic hIL2. This reporting strategy may find the greatest use in cell encapsulation therapy.

## **7.2 Counteracting Apoptosis and Necrosis with Hypoxia Responsive Expression of Bcl-2 $\Delta$**

In the encapsulated environment of a biohybrid artificial organ, cells often encounter a deficiency in the availability of oxygen. This hypoxic condition leads to necrosis and apoptosis, and is a fundamental challenge to designing a viable device. Several strategies such as inducing vascularization around the implant, electrochemically generating oxygen by decomposing water, as well as using synthetic oxygen carriers have already been taken to mitigate the detrimental effects of hypoxia. These methods seek to change the environment rather than adapt to it. An alternative method is to genetically engineer cells to withstand hypoxia induced apoptosis and necrosis. Specifically, four plasmid vectors were constructed to investigate the efficacy of cells producing the anti-apoptotic protein, Bcl-2 $\Delta$ . The first two plasmids contained a constitutive CMV promoter and were either able to produce Bcl-2 $\Delta$  plus a yellow fluorescent marker protein (EYFP) (pCYbp) or simply the just EYFP without Bcl-2 $\Delta$  (pCYp). Two analogous vectors with hypoxia responsive promoters in lieu of the CMV promoters were also constructed (pO2Ybp, pO2Yp). Although these last two vectors showed lower level of EYFP protein production at the all oxygen levels (0.0, 0.5, 1.0, 2.0, 5.0, or 21.0 %), they were able to increase expression as the oxygen decreased. The vectors with the CMV promoters showed an attenuated level of expression as oxygen levels dropped. In both promoter systems, the presence of Bcl-2 $\Delta$  enhanced protein production. When examining the amount of protection offered by Bcl-2 $\Delta$ , cells transfected with pO2Ybp showed a significantly higher viability and lowered apoptosis as compared to those

transfected with pO2Yp. In summary, Bcl-2 $\Delta$  was effective at prolonging cell viability. Also, while not a specific objective of our work, we found that Bcl-2 $\Delta$  increased production of hIL2.

### **7.3 Biocompatible Cellular Scaffold for Encapsulating Cells**

Gelatin is one of the most commonly used biomaterials for creating cellular scaffolds due to its innocuous nature. In order to create permanent hydrogels, however, harmful crosslinking agents are typically used. To circumvent this problem, and create cellular scaffolds that are both physiologically robust and biocompatible, a recombinant microbial transglutaminase (mTG) was used as an enzymatic crosslinker of gelatin. The biocompatibility of mTG crosslinked hydrogels (mTG-Gels) was demonstrated by observing the proliferation of encapsulated HEK293 cell for over a three week period ( $0.03 \text{ day}^{-1}$ ). Released cells were then also able to re-colonized tissue culture flasks.

### **7.4 Transglutaminase Crosslinked Gelatin Hydrogels as Tissue Engineering Scaffolds**

The thermal and proteolytic stabilities of mTG-Gels were challenged by submersion in a 37 °C saline solution or a 0.25% trypsin + EDTA enzyme bath at RT. mTG-Gels were found to be resistant to both forms of degradation. A novel technique for creating gelatin hydrogels, by first cooling dissolved gelatin followed by crosslinking with a 10% mTG overlay, produced hydrogels (HybriGels) that are consistently even more resistant to proteolysis. Further investigation showed that degradation occurred mainly through surface-dependent mechanisms. Degradation

rates were found to be adjustable based on gelatin content, such that HybriGels may be used for permanent cell encapsulation or time-released regenerative cell delivery.

## **7.5 Diffusion of hIL2 from Encapsulated Cells**

Fluorescence measurements of DsExDR from transiently transfected HEK293 cells showed that 0.16-cm mTG-Gel overlays were more conducive to protein production than cells without overlays. This indicated that the cells may benefit from being surrounded by a natural cellular scaffolding biomaterial. Further increasing the gel height led to relatively less fluorescence, most likely due to increased diffusional resistances for nutrients and oxygen to the cells. The increased diffusion barrier was readily noted by drastically decreased hIL2 accumulation in the media as the gel thickness increased. For either measurements, intracellular DsExDR fluorescence or secreted hIL2 accumulation, it was clear that cells that were able to express Bcl-2 $\Delta$  had a higher level of protein production. This phenomenon was also observed in the rate of hIL2 production from layer of cells without gel overlay: 0.94 pg/cm<sup>2</sup>-s for pF2 and 1.83 pg/cm<sup>2</sup>-s for pF3. From diffusion cell experiments, the effective diffusion coefficient of hIL2 in a 4% mTG-Gel was  $3.2 \times 10^{-7}$  cm<sup>2</sup>/s. This value agrees well with the diffusion coefficient of  $3.9 \times 10^{-7}$  cm<sup>2</sup>/s, which was determined from a steady state model of protein diffusion from the cell layer through the gel overlay. The ratio of these values represents the partition coefficient, which is equal to 0.82. The diffusion coefficient regressed from the steady state hIL2 data was used to calculate values for the unsteady state accumulation, which compared favorably with data scaled in time.

## 8. Bibliography

- [1] Aebischer, P., E. Buchser, J.M. Joseph, J. Favre, N. de Tribolet, M. Lysaght, S. Rudnick, and M. Goddard, Transplantation in humans of encapsulated xenogeneic cells without immunosuppression. A preliminary report. *Transplantation*, 1994. 58;11: p. 1275-7.
- [2] Aebischer, P., N.A. Pochon, B. Heyd, N. Deglon, J.M. Joseph, A.D. Zurn, E.E. Baetge, J.P. Hammang, M. Goddard, M. Lysaght, F. Kaplan, A.C. Kato, M. Schlupe, L. Hirt, F. Regli, F. Porchet, and N. De Tribolet, Gene therapy for amyotrophic lateral sclerosis (ALS) using a polymer encapsulated xenogenic cell line engineered to secrete hCNTF. *Hum Gene Ther*, 1996. 7;7: p. 851-60.
- [3] Clark, H., T.A. Barbari, K. Stump, and G. Rao, Histologic evaluation of the inflammatory response around implanted hollow fiber membranes. *Journal of Biomedical Materials Research*, 2000. 52;1: p. 183-192.
- [4] Wu, H., E.S. Avgoustiniatos, L. Swette, S. Bonner-Weir, G.C. Weir, and C.K. Colton, In situ electrochemical oxygen generation with an immunoisolation device. *Ann N Y Acad Sci*, 1999. 875:105-25.
- [5] Mathy-Hartert, M., M.P. Krafft, C. Deby, G. Deby-Dupont, M. Meurisse, M. Lamy, and J.G. Riess, Effects of perfluorocarbon emulsions on cultured human endothelial cells. *Artif Cells Blood Substit Immobil Biotechnol*, 1997. 25;6: p. 563-75.
- [6] Patton, J.N. and A.F. Palmer, Engineering temperature-sensitive hydrogel nanoparticles entrapping hemoglobin as a novel type of oxygen carrier. *Biomacromolecules*, 2005. 6;4: p. 2204-2212.
- [7] Banasiak, K.J., T. Cronin, and G.G. Haddad, bcl-2 Prolongs neuronal survival during hypoxia-induced apoptosis. *Molecular Brain Research*, 1999. 72;2: p. 214-225.
- [8] Oehler, M.K., C. Norbury, S. Hague, M.C.P. Rees, and R. Bicknell, Adrenomedullin inhibits hypoxic cell death by upregulation of Bcl-2 in endometrial cancer cells: a possible promotion mechanism for tumour growth. *Oncogene*, 2001. 20;23: p. 2937-2945.
- [9] Figueroa, B.J., T.M. Sauerwald, A.J. Mastrangelo, J.M. Hardwick, and M.J. Betenbaugh, Comparison of Bcl-2 to a Bcl-2 deletion mutant for mammalian cells exposed to culture insults. *Biotechnol Bioeng*, 2001. 73;3: p. 211-22.
- [10] Shibata, T., A.J. Giaccia, and J.M. Brown, Development of a hypoxia-responsive vector for tumor-specific gene therapy. *Gene Ther*, 2000. 7;6: p. 493-8.
- [11] Cao, Y.J., T. Shibata, and N.G. Rainov, Hypoxia-inducible transgene expression in differentiated human NT2N neurons - a cell culture model for gene therapy of postischemic neuronal loss. *Gene Therapy*, 2001. 8;17: p. 1357-1362.
- [12] Lee, K.Y. and D.J. Mooney, Hydrogels for tissue engineering. *Chem Rev*, 2001. 101;7: p. 1869-79.
- [13] Drury, J.L. and D.J. Mooney, Hydrogels for tissue engineering: scaffold design variables and applications. *Biomaterials*, 2003. 24;24: p. 4337-51.
- [14] Bruce Alberts, D.B., Julian Lewis, Martin Raff, James D. Watson, *Molecular biology of the cell*. 1994, New York: Garland Science.
- [15] Williams, C.G., A.N. Malik, T.K. Kim, P.N. Manson, and J.H. Elisseeff, Variable cytocompatibility of six cell lines with photoinitiators used for polymerizing hydrogels and cell encapsulation. *Biomaterials*, 2005. 26;11: p. 1211-8.
- [16] Gendler, E., S. Gendler, and M.E. Nimni, Toxic reactions evoked by glutaraldehyde-fixed pericardium and cardiac valve tissue bioprosthesis. *J Biomed Mater Res*, 1984. 18;7: p. 727-36.
- [17] Liang, H.C., W.H. Chang, K.J. Lin, and H.W. Sung, Genipin-crosslinked gelatin microspheres as a drug carrier for intramuscular administration: in vitro and in vivo studies. *J Biomed Mater Res A*, 2003. 65;2: p. 271-82.
- [18] Barker, H., R. Oliver, R. Grant, and L. Stephen, Formaldehyde as a pre-treatment for dermal collagen heterografts. *Biochimica et Biophysica Acta (BBA) - General Subjects*, 1980. 632;4: p. 589-597.

- [19] Choi, Y.S., S.R. Hong, Y.M. Lee, K.W. Song, M.H. Park, and Y.S. Nam, Study on gelatin-containing artificial skin: I. Preparation and characteristics of novel gelatin-alginate sponge. *Biomaterials*, 1999. 20;5: p. 409-17.
- [20] Choi, Y.S., S.R. Hong, Y.M. Lee, K.W. Song, M.H. Park, and Y.S. Nam, Studies on gelatin-containing artificial skin: II. Preparation and characterization of cross-linked gelatin-hyaluronate sponge. *J Biomed Mater Res*, 1999. 48;5: p. 631-9.
- [21] Yokoyama, K., N. Nio, and Y. Kikuchi, Properties and applications of microbial transglutaminase. *Appl Microbiol Biotechnol*, 2004. 64;4: p. 447-54.
- [22] Yokoyama, K., Y. Kikuchi, and H. Yasueda, Overproduction of DnaJ in *Escherichia coli* improves in vivo solubility of the recombinant fish-derived transglutaminase. *Biosci Biotechnol Biochem*, 1998. 62;6: p. 1205-10.
- [23] Kobayashi, K., K. Hashiguchi, K. Yokozeki, and S. Yamanaka, Molecular cloning of the transglutaminase gene from *Bacillus subtilis* and its expression in *Escherichia coli*. *Biosci Biotechnol Biochem*, 1998. 62;6: p. 1109-14.
- [24] Henis-Korenblit, S., N.L. Strumpf, D. Goldstaub, and A. Kimchi, A novel form of DAP5 protein accumulates in apoptotic cells as a result of caspase cleavage and internal ribosome entry site-mediated translation. *Mol Cell Biol*, 2000. 20;2: p. 496-506.
- [25] Holcik, M. and R.G. Korneluk, Functional characterization of the X-linked inhibitor of apoptosis (XIAP) internal ribosome entry site element: role of La autoantigen in XIAP translation. *Mol Cell Biol*, 2000. 20;13: p. 4648-57.
- [26] Stoneley, M., S.A. Chappell, C.L. Jopling, M. Dickens, M. MacFarlane, and A.E. Willis, c-Myc protein synthesis is initiated from the internal ribosome entry segment during apoptosis. *Mol Cell Biol*, 2000. 20;4: p. 1162-9.
- [27] Cornelis, S., Y. Bruynooghe, G. Denecker, S. Van Huffel, S. Tinton, and R. Beyaert, Identification and characterization of a novel cell cycle-regulated internal ribosome entry site. *Mol Cell*, 2000. 5;4: p. 597-605.
- [28] Pyronnet, S., L. Pradayrol, and N. Sonenberg, A cell cycle-dependent internal ribosome entry site. *Mol Cell*, 2000. 5;4: p. 607-16.
- [29] Creancier, L., P. Mercier, A.C. Prats, and D. Morello, c-myc Internal ribosome entry site activity is developmentally controlled and subjected to a strong translational repression in adult transgenic mice. *Mol Cell Biol*, 2001. 21;5: p. 1833-40.
- [30] Vazquez, D., Inhibitors of protein synthesis. *FEBS Lett*, 1974. 40;0: p. suppl:S63-84.
- [31] Blobel, G., P. Walter, C.N. Chang, B.M. Goldman, A.H. Erickson, and V.R. Lingappa, Translocation of proteins across membranes: the signal hypothesis and beyond. *Symp Soc Exp Biol*, 1979. 339-36.
- [32] Deshaies, R.J. and R. Schekman, A yeast mutant defective at an early stage in import of secretory protein precursors into the endoplasmic reticulum. *J Cell Biol*, 1987. 105;2: p. 633-45.
- [33] Garoff, H., Using recombinant DNA techniques to study protein targeting in the eucaryotic cell. *Annu Rev Cell Biol*, 1985. 1403-45.
- [34] Oliver, D.B. and J. Beckwith, *E. coli* mutant pleiotropically defective in the export of secreted proteins. *Cell*, 1981. 25;3: p. 765-72.
- [35] von Heijne, G., Protein targeting signals. *Curr Opin Cell Biol*, 1990. 2;4: p. 604-8.
- [36] Alberts, B., D. Bray, J. Lewis, M. Raff, K. Roberts, and J.D. Watson, *Proteins Can Move Between Compartments in Different Ways Signal Peptides and Signal Patches Direct Proteins to the Correct Cellular Address*, in *Molecular Biology of The Cell*, M. Robertson and S.M. Cobert, Editors. 1994, Garland Publishing, Inc.: New York. p. 556-558.
- [37] Coloma, M.J., A. Hastings, L.A. Wims, and S.L. Morrison, Novel vectors for the expression of antibody molecules using variable regions generated by polymerase chain reaction. *J Immunol Methods*, 1992. 152;1: p. 89-104.
- [38] Harvey, E.N., A General Survey of Bioluminescence - Introduction. *Annals of the New York Academy of Sciences*, 1948. 49;3: p. 329-336.
- [39] Herring, P.J., *Bioluminescence in Action*. 1978, New York: Academic.
- [40] Hastings, J.W. and J.G. Morin, *Bioluminescence. In Neural and Integrative Animal Physiology*, ed. C.L. Prosser. 1991, New York: Wiley-Interscience. 131-170.

- [41] Hastings, J.W., Biological diversity, chemical mechanisms, and the evolutionary origins of bioluminescent systems. *J Mol Evol*, 1983. 19;5: p. 309-21.
- [42] Prasher, D.C., V.K. Eckenrode, W.W. Ward, F.G. Prendergast, and M.J. Cormier, Primary structure of the *Aequorea victoria* green-fluorescent protein. *Gene*, 1992. 111;2: p. 229-33.
- [43] Chalfie, M., Y. Tu, G. Euskirchen, W.W. Ward, and D.C. Prasher, Green fluorescent protein as a marker for gene expression. *Science*, 1994. 263;5148: p. 802-5.
- [44] Davenport, D. and J.A.C. Nichol, Luminescence in Hydromedusae. *Proceedings of the Royal Society, Series B*, 1955. 144399-411.
- [45] Shimomura, O., F.H. Johnson, and Y. Saiga, Extraction, purification and properties of aequorin, a bioluminescent protein from the luminous hydromedusan, *Aequorea*. *J Cell Comp Physiol*, 1962. 59223-39.
- [46] Cutler, M.W., Characterization and energy transfer mechanism of the green-fluorescent protein from *Aequorea victoria*. Rutgers University: New Brunswick, NJ.
- [47] Yang, F., L.G. Moss, and G.N. Phillips, Jr., The molecular structure of green fluorescent protein. *Nat Biotechnol*, 1996. 14;10: p. 1246-51.
- [48] Ward, W.W., *In Bioluminescence and Chemiluminescence: Basic Chemistry and Analytical Applications*, in *Properties of the coelenterate green-fluorescent protein.*, M. DeLuca and D.W. McElroy, Editors. 1981, Academic: New York.
- [49] Morise, J.G., *Coelenterate bioluminescence*, in *Coelenterate Biology: Reviews and New Perspectives*, L. Muscatine and H. Lenhoff, Editors. 1974, Academic: New York. p. 396-438.
- [50] Heim, R., A.B. Cubitt, and R.Y. Tsien, Improved green fluorescence. *Nature*, 1995. 373;6516: p. 663-4.
- [51] Kozak, M., An analysis of 5'-noncoding sequences from 699 vertebrate messenger RNAs. *Nucleic Acids Res*, 1987. 15;20: p. 8125-48.
- [52] Haas, J., E.C. Park, and B. Seed, Codon usage limitation in the expression of HIV-1 envelope glycoprotein. *Curr Biol*, 1996. 6;3: p. 315-24.
- [53] Cormack, B.P., R.H. Valdivia, and S. Falkow, FACS-optimized mutants of the green fluorescent protein (GFP). *Gene*, 1996. 173;1 Spec No: p. 33-8.
- [54] Yang, T.T., L. Cheng, and S.R. Kain, Optimized codon usage and chromophore mutations provide enhanced sensitivity with the green fluorescent protein. *Nucleic Acids Res*, 1996. 24;22: p. 4592-3.
- [55] Olson, K.R., J.R. McIntosh, and J.B. Olmsted, Analysis of MAP 4 function in living cells using green fluorescent protein (GFP) chimeras. *J Cell Biol*, 1995. 130;3: p. 639-50.
- [56] Rizzuto, R., M. Brini, F. De Giorgi, R. Rossi, R. Heim, R.Y. Tsien, and T. Pozzan, Double labelling of subcellular structures with organelle-targeted GFP mutants in vivo. *Curr Biol*, 1996. 6;2: p. 183-8.
- [57] Cole, N.B., C.L. Smith, N. Sciaky, M. Terasaki, M. Edidin, and J. Lippincott-Schwartz, Diffusional mobility of Golgi proteins in membranes of living cells. *Science*, 1996. 273;5276: p. 797-801.
- [58] Ogawa, H., S. Inouye, F.I. Tsuji, K. Yasuda, and K. Umesono, Localization, trafficking, and temperature-dependence of the *Aequorea* green fluorescent protein in cultured vertebrate cells. *Proc Natl Acad Sci U S A*, 1995. 92;25: p. 11899-903.
- [59] Kaether, C. and H.H. Gerdes, Visualization of protein transport along the secretory pathway using green fluorescent protein. *FEBS Lett*, 1995. 369;2-3: p. 267-71.
- [60] Dodds, E., M.G. Dunckley, K. Naujoks, U. Michaelis, and G. Dickson, Lipofection of cultured mouse muscle cells: a direct comparison of Lipofectamine and DOSPER. *Gene Ther*, 1998. 5;4: p. 542-51.
- [61] Chiu, W., Y. Niwa, W. Zeng, T. Hirano, H. Kobayashi, and J. Sheen, Engineered GFP as a vital reporter in plants. *Curr Biol*, 1996. 6;3: p. 325-30.
- [62] Cramer, A., E.A. Whitehorn, E. Tate, and W.P. Stemmer, Improved green fluorescent protein by molecular evolution using DNA shuffling. *Nat Biotechnol*, 1996. 14;3: p. 315-9.
- [63] Elowitz, M.B., M.G. Surette, P.E. Wolf, J. Stock, and S. Leibler, Photoactivation turns green fluorescent protein red. *Current Biology*, 1997. 7;10: p. 809-812.
- [64] Sawin, K.E. and P. Nurse, Photoactivation of green fluorescent protein. *Current Biology*, 1997. 7;10: p. R606-R607.

- [65] Matz, M.V., A.F. Fradkov, Y.A. Labas, A.P. Savitsky, A.G. Zarausky, M.L. Markelov, and S.A. Lukyanov, Fluorescent proteins from nonbioluminescent Anthozoa species. *Nat Biotechnol*, 1999. 17;10: p. 969-73.
- [66] Wall, M.A., M. Socolich, and R. Ranganathan, The structural basis for red fluorescence in the tetrameric GFP homolog DsRed. *Nat Struct Biol*, 2000. 7;12: p. 1133-8.
- [67] Yarbrough, D., R.M. Wachter, K. Kallio, M.V. Matz, and S.J. Remington, Refined crystal structure of DsRed, a red fluorescent protein from coral, at 2.0-Å resolution. *Proc Natl Acad Sci U S A*, 2001. 98;2: p. 462-7.
- [68] Baird, G.S., D.A. Zacharias, and R.Y. Tsien, Biochemistry, mutagenesis, and oligomerization of DsRed, a red fluorescent protein from coral. *Proc Natl Acad Sci U S A*, 2000. 97;22: p. 11984-9.
- [69] Colton, C.K., Engineering challenges in cell-encapsulation technology. *Trends in Biotechnology*, 1996. 14;5: p. 158-162.
- [70] Bevis, B.J. and B.S. Glick, Rapidly maturing variants of the *Discosoma* red fluorescent protein (DsRed). *Nat Biotechnol*, 2002. 20;1: p. 83-7.
- [71] Clontech, B.B., *BD Living Colors User Manual Volume II: Reef Coral Fluorescent Proteins*. July 2003.
- [72] Colton, C.K., Implantable Biohybrid Artificial Organs. *Cell Transplantation*, 1995. 4;4: p. 415-436.
- [73] Dionne, K.E., C.K. Colton, and M.L. Yarmush, Effect of Hypoxia on Insulin-Secretion by Isolated Rat and Canine Islets of Langerhans. *Diabetes*, 1993. 42;1: p. 12-21.
- [74] Monaco, A.P., T. Maki, H. Ozato, M. Carretta, S.J. Sullivan, K.M. Borland, M.D. Mahoney, W.L. Chick, T.E. Muller, J. Wolfrum, and et al., Transplantation of islet allografts and xenografts in totally pancreatectomized diabetic dogs using the hybrid artificial pancreas. *Ann Surg*, 1991. 214;3: p. 339-60; discussion 361-2.
- [75] Sullivan, S.J., T. Maki, K.M. Borland, M.D. Mahoney, B.A. Solomon, T.E. Muller, A.P. Monaco, and W.L. Chick, Biohybrid artificial pancreas: long-term implantation studies in diabetic, pancreatectomized dogs. *Science*, 1991. 252;5006: p. 718-21.
- [76] Lanza, R.P., A.M. Beyer, J.E. Staruk, and W.L. Chick, Biohybrid artificial pancreas. Long-term function of discordant islet xenografts in streptozotocin diabetic rats. *Transplantation*, 1993. 56;5: p. 1067-72.
- [77] Acker, H., Mechanisms and Meaning of Cellular Oxygen Sensing in the Organism. *Respiration Physiology*, 1994. 95;1: p. 1-10.
- [78] Rolfs, A., I. Kvietikova, M. Gassmann, and R.H. Wenger, Oxygen-regulated transferrin expression is mediated by hypoxia-inducible factor-1. *Journal of Biological Chemistry*, 1997. 272;32: p. 20055-20062.
- [79] Shweiki, D., A. Itin, D. Soffer, and E. Keshet, Vascular endothelial growth factor induced by hypoxia may mediate hypoxia-initiated angiogenesis. *Nature*, 1992. 359;6398: p. 843-5.
- [80] Melillo, G., T. Musso, A. Sica, L.S. Taylor, G.W. Cox, and L. Varesio, A Hypoxia-Responsive Element Mediates a Novel Pathway of Activation of the Inducible Nitric-Oxide Synthase Promoter. *Journal of Experimental Medicine*, 1995. 182;6: p. 1683-1693.
- [81] Lee, P.J., B.H. Jiang, B.Y. Chin, N.V. Iyer, J. Alam, G.L. Semenza, and A.M. Choi, Hypoxia-inducible factor-1 mediates transcriptional activation of the heme oxygenase-1 gene in response to hypoxia. *J Biol Chem*, 1997. 272;9: p. 5375-81.
- [82] Wang, G.L. and G.L. Semenza, Purification and characterization of hypoxia-inducible factor 1. *J Biol Chem*, 1995. 270;3: p. 1230-7.
- [83] Semenza, G.L., Perspectives on oxygen sensing. *Cell*, 1999. 98;3: p. 281-4.
- [84] Chandel, N.S., E. Maltepe, E. Goldwasser, C.E. Mathieu, M.C. Simon, and P.T. Schumacker, Mitochondrial reactive oxygen species trigger hypoxia-induced transcription. *Proc Natl Acad Sci U S A*, 1998. 95;20: p. 11715-20.
- [85] Chandel, N.S., D.S. McClintock, C.E. Feliciano, T.M. Wood, J.A. Melendez, A.M. Rodriguez, and P.T. Schumacker, Reactive oxygen species generated at mitochondrial complex III stabilize hypoxia-inducible factor-1  $\alpha$  during hypoxia - A mechanism of O<sub>2</sub> sensing. *Journal of Biological Chemistry*, 2000. 275;33: p. 25130-25138.
- [86] Semenza, G.L., Regulation of mammalian O<sub>2</sub> homeostasis by hypoxia-inducible factor 1. *Annu Rev Cell Dev Biol*, 1999. 15:551-78.



- [87] Agani, F.H., P. Pichiule, J.C. Chavez, and J.C. LaManna, The role of mitochondria in the regulation of hypoxia-inducible factor 1 expression during hypoxia. *Journal of Biological Chemistry*, 2000. 275;46: p. 35863-35867.
- [88] Haddad, J.J.E., R.E. Olver, and S.C. Land, Antioxidant/pro-oxidant equilibrium regulates HIF-1 alpha and NF-kappa B redox sensitivity - Evidence for inhibition by glutathione oxidation in alveolar epithelial cells. *Journal of Biological Chemistry*, 2000. 275;28: p. 21130-21139.
- [89] Shimizu, S., Y. Eguchi, W. Kamiike, Y. Itoh, J. Hasegawa, K. Yamabe, Y. Otsuki, H. Matsuda, and Y. Tsujimoto, Induction of apoptosis as well as necrosis by hypoxia and predominant prevention of apoptosis by Bcl-2 and Bcl-XL. *Cancer Res*, 1996. 56;9: p. 2161-6.
- [90] Vaux, D.L., S. Cory, and J.M. Adams, Bcl-2 gene promotes haemopoietic cell survival and cooperates with c-myc to immortalize pre-B cells. *Nature*, 1988. 335;6189: p. 440-2.
- [91] Tsujimoto, Y., Stress-resistance conferred by high level of bcl-2 alpha protein in human B lymphoblastoid cell. *Oncogene*, 1989. 4;11: p. 1331-6.
- [92] Shimizu, S., Y. Eguchi, H. Kosaka, W. Kamiike, H. Matsuda, and Y. Tsujimoto, Prevention of hypoxia-induced cell death by Bcl-2 and Bcl-xL. *Nature*, 1995. 374;6525: p. 811-3.
- [93] Shimizu, S., Y. Eguchi, W. Kamiike, S. Waguri, Y. Uchiyama, H. Matsuda, and Y. Tsujimoto, Retardation of chemical hypoxia-induced necrotic cell death by Bcl-2 and ICE inhibitors: possible involvement of common mediators in apoptotic and necrotic signal transductions. *Oncogene*, 1996. 12;10: p. 2045-50.
- [94] Shimizu, S., Y. Eguchi, W. Kamiike, S. Waguri, Y. Uchiyama, H. Matsuda, and Y. Tsujimoto, Bcl-2 blocks loss of mitochondrial membrane potential while ICE inhibitors act at a different step during inhibition of death induced by respiratory chain inhibitors. *Oncogene*, 1996. 13;1: p. 21-9.
- [95] Kane, D.J., T. Ord, R. Anton, and D.E. Bredesen, Expression of bcl-2 inhibits necrotic neural cell death. *J Neurosci Res*, 1995. 40;2: p. 269-75.
- [96] Hunter, J.J., B.L. Bond, and T.G. Parslow, Functional dissection of the human Bcl2 protein: sequence requirements for inhibition of apoptosis. *Mol Cell Biol*, 1996. 16;3: p. 877-83.
- [97] Huang, D.C., J.M. Adams, and S. Cory, The conserved N-terminal BH4 domain of Bcl-2 homologues is essential for inhibition of apoptosis and interaction with CED-4. *Embo J*, 1998. 17;4: p. 1029-39.
- [98] Borner, C., Diminished cell proliferation associated with the death-protective activity of Bcl-2. *J Biol Chem*, 1996. 271;22: p. 12695-8.
- [99] Chang, B.S., A.J. Minn, S.W. Muchmore, S.W. Fesik, and C.B. Thompson, Identification of a novel regulatory domain in Bcl-X(L) and Bcl-2. *EMBO J*, 1997. 16;5: p. 968-77.
- [100] Hillman, G.G., G.P. Haas, W.H. Wahl, and D.M. Callewaert, Adoptive Immunotherapy of Cancer - Biological Response Modifiers and Cytotoxic-Cell Therapy. *Biotherapy*, 1992. 5;2: p. 119-129.
- [101] Kaplan, G., Z.A. Cohn, and K.A. Smith, Rational immunotherapy with interleukin 2. *Biotechnology (N Y)*, 1992. 10;2: p. 157-62.
- [102] Waldmann, T.A., The IL-2/IL-2 receptor system: a target for rational immune intervention. *Immunol Today*, 1993. 14;6: p. 264-70.
- [103] Smith, K.A., The interleukin 2 receptor. *Annu Rev Cell Biol*, 1989. 5397-425.
- [104] Graham, F.L., J. Smiley, W.C. Russell, and R. Nairn, Characteristics of a human cell line transformed by DNA from human adenovirus type 5. *J Gen Virol*, 1977. 36;1: p. 59-74.
- [105] O'Gorman, S., D.T. Fox, and G.M. Wahl, Recombinase-mediated gene activation and site-specific integration in mammalian cells. *Science*, 1991. 251;4999: p. 1351-5.
- [106] Sauer, B., Site-specific recombination: developments and applications. *Curr Opin Biotechnol*, 1994. 5;5: p. 521-7.
- [107] Craig, N.L., The mechanism of conservative site-specific recombination. *Annu Rev Genet*, 1988. 2277-105.
- [108] Weiss, A., R.L. Wiskocil, and J.D. Stobo, The role of T3 surface molecules in the activation of human T cells: a two-stimulus requirement for IL 2 production reflects events occurring at a pre-translational level. *J Immunol*, 1984. 133;1: p. 123-8.

- [109] Robb, R.J. and K.A. Smith, Heterogeneity of human T-cell growth factor(s) due to variable glycosylation. *Mol Immunol*, 1981. 18;12: p. 1087-94.
- [110] Trinchieri, G., M. Matsumoto-Kobayashi, S.C. Clark, J. Seehra, L. London, and B. Perussia, Response of resting human peripheral blood natural killer cells to interleukin 2. *J Exp Med*, 1984. 160;4: p. 1147-69.
- [111] Rosenstein, M., I. Yron, Y. Kaufmann, and S.A. Rosenberg, Lymphokine-activated killer cells: lysis of fresh syngeneic natural killer-resistant murine tumor cells by lymphocytes cultured in interleukin 2. *Cancer Res*, 1984. 44;5: p. 1946-53.
- [112] Grimm, E.A., A. Mazumder, H.Z. Zhang, and S.A. Rosenberg, Lymphokine-activated killer cell phenomenon. Lysis of natural killer-resistant fresh solid tumor cells by interleukin 2-activated autologous human peripheral blood lymphocytes. *J Exp Med*, 1982. 155;6: p. 1823-41.
- [113] Ritz, J., R.E. Schmidt, J. Michon, T. Hercend, and S.F. Schlossman, Characterization of functional surface structures on human natural killer cells. *Adv Immunol*, 1988. 42:181-211.
- [114] Smith, K.A., E.L. Jacobson, R. Emert, M. Giordano, E. Kovacs, N. Mumneh, F. Pilaro, T. Sohn, and D. Warren, Restoration of immunity with interleukin-2 therapy. *AIDS Read*, 1999. 9;8: p. 563-72.
- [115] Jacobson, E.L., F. Pilaro, and K.A. Smith, Rational interleukin 2 therapy for HIV positive individuals: daily low doses enhance immune function without toxicity. *Proc Natl Acad Sci U S A*, 1996. 93;19: p. 10405-10.
- [116] Petite, H., I. Rault, A. Huc, P. Menasche, and D. Herbage, Use of the acyl azide method for cross-linking collagen-rich tissues such as pericardium. *J Biomed Mater Res*, 1990. 24;2: p. 179-87.
- [117] Elisseeff, J., K. Anseth, D. Sims, W. McIntosh, M. Randolph, and R. Langer, Transdermal photopolymerization for minimally invasive implantation. *Proc Natl Acad Sci U S A*, 1999. 96;6: p. 3104-7.
- [118] de Kock, J.P., K.J. Reynolds, L. Tarassenko, and J.T. Moyle, The effect of varying LED intensity on pulse oximeter accuracy. *J Med Eng Technol*, 1991. 15;3: p. 111-5.
- [119] Severinghaus, J.W. and P.B. Astrup, History of blood gas analysis. VI. Oximetry. *J Clin Monit*, 1986. 2;4: p. 270-88.
- [120] Cirone, P., J.M. Bourgeois, F. Shen, and P.L. Chang, Combined immunotherapy and antiangiogenic therapy of cancer with microencapsulated cells. *Hum Gene Ther*, 2004. 15;10: p. 945-59.
- [121] Valentina Ciccarone, Y.C., Kevin Schifferli, and P.H.-N. Jean-Pierre Pichet, Krista Evans, Linda Roy, Shelley Bennett, LIPOFECTAMINE™ 2000 Reagent: For Rapid, Efficient Transfection of Eukaryotic Cells. *Focus*, 1999. 21;2: p. 54-55.
- [122] Cha, H.J., N.G. Dalal, V.N. Vakharia, and W.E. Bentley, Expression and purification of human interleukin-2 simplified as a fusion with green fluorescent protein in suspended Sf-9 insect cells. *J Biotechnol*, 1999. 69;1: p. 9-17.
- [123] Cha, H.J., N.G. Dalal, M.Q. Pham, and W.E. Bentley, Purification of human interleukin-2 fusion protein produced in insect larvae is facilitated by fusion with green fluorescent protein and metal affinity ligand. *Biotechnol Prog*, 1999. 15;2: p. 283-6.
- [124] Gelman, M.S., E.S. Kannegaard, and R.R. Kopito, A principal role for the proteasome in endoplasmic reticulum-associated degradation of misfolded intracellular cystic fibrosis transmembrane conductance regulator. *J Biol Chem*, 2002. 277;14: p. 11709-14.
- [125] Zhuang, X., T. Ha, H.D. Kim, T. Centner, S. Labeit, and S. Chu, Fluorescence quenching: A tool for single-molecule protein-folding study. *Proc Natl Acad Sci U S A*, 2000. 97;26: p. 14241-4.
- [126] Cha, H.J., T. Gotoh, and W.E. Bentley, Simplification of titer determination for recombinant baculovirus by green fluorescent protein marker. *Biotechniques*, 1997. 23;5: p. 782-4, 786.
- [127] Leach, R.M. and D.F. Treacher, Oxygen transport-2. Tissue hypoxia. *Bmj*, 1998. 317;7169: p. 1370-3.
- [128] Shibata, T., A.J. Giaccia, and J.M. Brown, Hypoxia-inducible regulation of a prodrug-activating enzyme for tumor-specific gene therapy. *Neoplasia*, 2002. 4;1: p. 40-8.

- [129] Beidler, D.R. and Y.C. Cheng, Camptothecin Induction of a Time-Dependent and Concentration-Dependent Decrease of Topoisomerase-I and Its Implication in Camptothecin Activity. *Molecular Pharmacology*, 1995. 47;5: p. 907-914.
- [130] Haddad, H., D. Windgassen, C.G. Ramsborg, C.J. Paredes, and E.T. Papoutsakis, Molecular understanding of oxygen-tension and patient-variability effects on ex vivo expanded T cells. *Biotechnol Bioeng*, 2004. 87;4: p. 437-50.
- [131] Treacher, D.F. and R.M. Leach, Oxygen transport-1. Basic principles. *Bmj*, 1998. 317;7168: p. 1302-6.
- [132] McDermott, M.K., T. Chen, C.M. Williams, K.M. Markley, and G.F. Payne, Mechanical properties of biomimetic tissue adhesive based on the microbial transglutaminase-catalyzed crosslinking of gelatin. *Biomacromolecules*, 2004. 5;4: p. 1270-9.
- [133] Elisseeff, J., Injectable cartilage tissue engineering. *Expert Opin Biol Ther*, 2004. 4;12: p. 1849-59.
- [134] Broderick, E.P., D.M. O'Halloran, Y.A. Rochev, M. Griffin, R.J. Collighan, and A.S. Pandit, Enzymatic stabilization of gelatin-based scaffolds. *J Biomed Mater Res B Appl Biomater*, 2005. 72;1: p. 37-42.
- [135] Truskey, G.Y., F; Katz, DF, *Transport Phenomena in Biological Systems*. 2004, Upper Saddle River, NJ 07458: Prentice Hall.

# Curriculum Vitae

# Chong Wing Yung

## US Citizen

3421 Tulane Dr. #13, Hyattsville, MD 20783  
Telephone: (240) 620-8766 Email: [cyung@umd.edu](mailto:cyung@umd.edu)

---

### EDUCATION

- Post-doctoral Fellow in Chemical Engineering 2005-Present  
University of Maryland, College Park (UMCP)
- Ph.D. in Chemical Engineering 2005  
University of Maryland, College Park (UMCP)
- BS in Chemical Engineering 1996  
University of California, Irvine

### ACADEMIC & INDUSTRIAL RESEARCH EXPERIENCES

Post-doctoral Fellow 2005-Present

Department of Chemical and Biomolecular Engineering, UMCP

- Develop RNAi metabolic engineering techniques
- Develop smart-protein separation membranes
- Lead and train graduate students in individual research projects

Graduate Research Assistant 2000-2005

Department of Chemical and Biomolecular Engineering, UMCP

- Develop cell lines for tissue engineering and biohybrid artificial organ applications
- Construct expression vectors for constitutive and inductive mammalian protein expression
- Create transient and stable mammalian cell lines (*e.g.* C2C12, HEK293, Jurkat)
- Design hydrogels with tuneable degradation characteristics for cellular scaffolds and encapsulation
- Proficient with flow cytometer, uv, visible and fluorescence spectrometry, confocal microscopy, ELISA, apoptosis and proliferation assays, Western-Blotting, etc.

Pilot Plant Biochemical Technician 1996-1999

Genentech, Inc., South San Francisco, CA

- GMP-certified mammalian cell culture techniques
- Leader for technical training
- Operate and troubleshoot bioreactors (2-1000-L scales) for process optimization research
- Conduct research development of novel media sterilization process (High Temperature Short Time; flash sterilization)

Undergraduate Researcher 1992-1995

Department of Chemical and Biochemical Engineering, UC Irvine

- Design and built functional packed bed bioreactor from all custom parts
- Assist in the writing of grant proposals
- Develop skills in aseptic and bacterial cell culture techniques

## AWARDS AND HONORS

- Merck Award for Best Student Poster March, 2004  
Engineering Conferences International (ECI),  
Cell Culture Engineering IX Conference, Cancun, Mexico
- Featured Article on Research and Patent 2002  
A New Dish for the Laboratory, *Maryland Research Journal, Fall 2002 Vol III, No.1*
- Albertus Magnus Award for Excellence in Teaching (1<sup>st</sup> Runner-up) 1999-2000  
Department of Chemistry, University of Maryland, College Park
- Undergraduate Research and Creative Project Grant 1993  
Department of Chemical Engineering, University of California, Irvine
- NSF Research Experience for Undergraduates Award 1992  
Department of Chemical Engineering, University of California, Irvine

## PUBLICATIONS

- Yung CW, Barbari TA, and Bentley WE; Utilizing intracellular red fluorescence protein markers to quantify therapeutic protein secretions for applications in biohybrid artificial organs (*In Review at: Biotechnology and Bioengineering*)
- Yung CW, Barbari TA, and Bentley WE; Counteracting hypoxia-induced apoptosis, prevalent in biohybrid artificial organs, with the oxygen sensitive expression of Bcl-2 $\Delta$  (*In Submission to: Metabolic Engineering*)
- Yung CW, Wu LQ, Payne GF, Bentley WE, and Barbari TA; Transglutaminase crosslinked gelatin hydrogels for tissue engineering (*In Submission to: Biomaterials*)
- Yung CW, "Tissues and Metabolic Engineering of Biohybrid Artificial Organs", PhD Thesis, University of Maryland, College Park, 2005.
- Yung CW, Bentley WE, and Barbari TA; Metabolic Engineering of Biohybrid Artificial Organs, (*In Preparation for: Tissue Engineering*)
- Yung CW, and Bentley WE; Metabolic Engineering Review, (*Invited review, in submission to: Biotechnology*)
- Luu PP, Yung CW, Sun AK, and Wood TK: Monitoring trichloroethylene mineralization by *Pseudomonas cepacia* G4 PR1. *Appl. Microbiol. Biotechnol.* 1995, 44:259-264.

## PATENTS

- Patent for Recessed Petri Dish Lid (Filed) – The recessed lid permits fluorescence imaging of mammalian cells attached to bottoms of a Petri Dish using a standard Upright microscope rather than a specialized inverted fluorescence microscope.

## PROFESSIONAL MEMBERSHIPS

- American Chemical Society (ACS) - Student Member Since 2002
- American Institute of Chemical Engineers (AIChE) - Student Member Since 2002
- Biomedical Engineering Society - Student Member Since 2005

## PRESENTATIONS

- American Institute of Chemical Engineers Fall 2005  
Food, Pharmaceutical & Bioengineering Division  
Tissue Engineering Area (15D12), Cincinnati, OH  
Oral Presentation: Traceable hIL2 secretion from enzyme crosslinked gelatin cellular scaffolds
- American Chemical Society Spring 2005  
Division of Biochemical Technology  
Tissue Engineering/Biomaterials Session, San Diego, CA  
Oral Presentation: Engineering “smart” cells to produce non-invasively traceable human therapeutic proteins in a hypoxic environment for biohybrid artificial organs
- Engineering Conferences International (ECI) March, 2004  
Cell Culture Engineering IX Conference, Cancun, Mexico  
Poster Title: Counteracting hypoxia-induced apoptosis in biohybrid artificial organs
- American Chemical Society Spring 2003  
Division of Biochemical Technology, New Orleans, LA  
Poster Title: Applications of HcRed fluorescence for measuring hIL2 secretion levels and pericellular oxygen concentrations
- Bioscience Research & Technology Review Day, UMCP  
Poster Title: Counteracting hypoxia-induced apoptosis in biohybrid artificial organs 2003  
Poster Title: Applications of HcRed fluorescence for measuring hIL2 secretion levels and pericellular oxygen concentrations 2002
- Mid-Atlantic Biochemical Engineering Consortium (MABEC) Mar 22, 2002  
Drexel University, 15th Annual Meeting  
Poster Title: Utilizing EGFP to model oxygen and drug release profiles in encapsulated murine myoblasts

## TEACHING EXPERIENCES

- Graduate Mentor Summer 2003 - 2005  
Research for Undergraduates (REU) Program  
Department of Chemical Engineering, UMCP
  - Guide four students in conducting various research projects and experiments.
  - Two students have moved on to graduate programs in Chemical Engineering
  - A third student will enter a Biomedical Engr. graduate program in the Fall of 2006
- Substitute Lecturer Fall 2001 & 2002  
ENCH 648B - Advanced Biochemical Engineering  
Department of Chemical Engineering, UMCP
  - Design my own lectures for mammalian cell culture research and industrial applications.
- Teaching Assistant 1999-2000  
CHEM 103 - General Chemistry I  
Department of Chemistry & Biochemistry, UMCP

## REFERENCES

**Timothy A. Barbari** (Ph.D. Advisor)

Professor of Chemical Engineering  
University of Maryland, College Park  
2113 Chemical & Nuclear Engineering  
College Park, MD 20742-2111

Email: [barbari@umd.edu](mailto:barbari@umd.edu)

Phone: (301) 405-2983

Fax: (301) 405-0523

**William E. Bentley** (Ph.D. Advisor)

Herbert Rabin Distinguished Professor of  
Chemical Engineering & Director, Bioengineering  
University of Maryland, College Park & Center for Biosystems Research  
University of Maryland Biotechnology Institute  
5115 Plant Science Bldg.  
College Park, MD 20742

Email: [bentley@umd.edu](mailto:bentley@umd.edu)

Phone: (301) 405-4321

Fax: (301) 314-9075

**Dewey Ryu**

Professor of Chemical Engineering & Material Science  
Director of Biochemical Engineering Program  
University of California, Davis  
125 Everson Hall

Email: [ddyryu@ucdavis.edu](mailto:ddyryu@ucdavis.edu)

Phone: (530)752-8954

Fax: (530) 752-3112;